Universidad Técnica Federico Santa María
Departamento de Ingeniería Eléctrica
Valparaíso, Chile

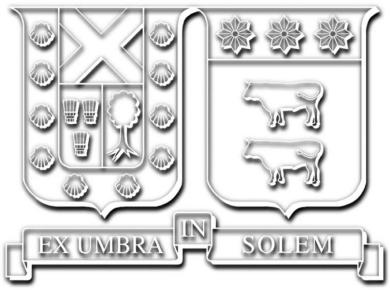

Resilient Scheduling of Automatic Generation Control Units via Corrective Transmission Switching under an N-1-1 Security Criterion

Mauricio Xavier Aguirre Velasco

2025

Tesis para optar al grado de:
Magíster en Ciencias de la Ingeniería Eléctrica

Comisión de Evaluación:

Director de Tesis:
Dr. Víctor Hinojosa Mateus
Universidad Técnica Federico Santa María - Chile

Presidente de la Comisión:
Dr. Esteban Pulido Venegas
Universidad Técnica Federico Santa María - Chile

Correferentes Externos:
Dr. Francisco Gonzalez Longatt
University of South-Eastern Norway - Norway

Dr. José Manuel Arroyo
Universidad de Castilla-La Mancha - España

Valparaíso, septiembre del 2025.

Universidad Técnica Federico Santa María
Departamento de Ingeniería Eléctrica
Valparaíso, Chile

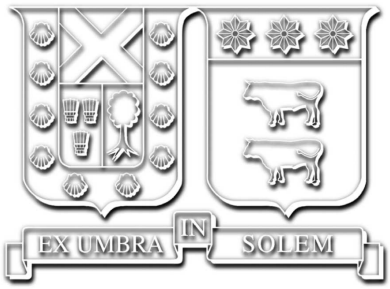

Resilient Scheduling of Automatic Generation Control Units via Corrective Transmission Switching under an N-1-1 Security Criterion

Mauricio Xavier Aguirre Velasco

2025

CONSTANCIA DE VALIDACIÓN Y CONFIDENCIALIDAD DE MONOGRAFÍA A REPOSITORIO ACADÉMICO

1.- IDENTIFICACIÓN DEL TRABAJO ACADÉMICO

Tipo de monografía (marcar una opción): ☐ Memoria o trabajo de título ☒ Tesis de Postgrado

Título del trabajo: _Resilient Scheduling of Automatic Generation Control Units via Corrective Transmission Switching under an N-1-1 Security Criterion_____

Nombre del candidato(a): _Mauricio Xavier Aguirre Velasco_____

Carrera / Grado: _Magíster en Ciencias de la Ingeniería Eléctrica_____

Campus: _Casa Central Valparaíso_____ **Departamento:** _Departamento de Ingeniería Eléctrica_____

2.- VALIDACIÓN DEL PROFESOR GUÍA/DIRECTOR DE TESIS

Yo, _Víctor Hugo Hinojosa Mateus _, en mi calidad de profesor(a) guía/director(a) del trabajo académico mencionado anteriormente **DEJO CONSTANCIA** que:

- He revisado esta versión del documento y corresponde a la versión final aprobada del trabajo.
- El trabajo cumple con los requisitos académicos y de formato establecidos por la institución.

3.- EVALUACIÓN DE CONFIDENCIALIDAD POR PROPIEDAD INDUSTRIAL (marcar una opción)

☒ El trabajo **NO contiene** información que amerite confidencialidad y puede ser publicado de inmediato en repositorio con acceso abierto.

☐ El trabajo **CONTIENE** información con potenciales implicancias de propiedad industrial o intelectual y requiere un periodo de confidencialidad (**embargo**) por **(marcar una opción)**:

☐ 6 meses ☐ 12 meses ☐ 2 años ☐ 3 años ☐ 5 años ☐ 10 años

Fundamentación de la necesidad de confidencialidad (obligatorio si se solicita embargo):

_____

_____

_____

4.- FIRMAS

Profesor(a) guía o director(a) de memoria o tesis:

Fecha: _____20/10/2025_____ **Firma:** _____

Estudiante o Candidato(a):

Fecha: _____20/10/2025_____ **Firma:** _____

Este formulario debe ser insertado como página 2 de la memoria o tesis, completado y firmado por estudiante y profesor(a) antes de la entrega en portal PRISMA de Biblioteca USM.

"Somewhere, something incredible is waiting to be known"
— Carl Sagan

Acknowledgements

First, I would like to thank my parents, Jorge and Katia, for their sacrifice, affection, and, above all, the values they instilled in me. To my dear siblings, Gaby and Kevin, who, although we are far apart today, I always carry close to my heart. To my aunts, Myriam and Mónica, for always encouraging me to pursue my goals. To all of you, thank you; your voices have guided my path and have resonated deep within me.

To my beloved Karlita, for all your love, your spontaneity, and, above all, the calm you have given me, not only along this journey but in everything we have built together. You are and will always be the engine that drives me to seek excellence and to dare to take on the greatest challenges. Thank you for being that source of inspiration and admiration, my beautiful woman. This thesis is not only the result of my effort but also of your companionship and understanding.

To my dear friends Andrés and Miguel, for all the good and difficult moments we have gone through together and that have led us to surpass ourselves at this point in life. To my friends Jorge and Israel, for always being there and for offering a word of encouragement when needed. To all of you, thank you for your sincere friendship and for the stories we have shared.

To the Universidad Técnica Federico Santa María and the Department of Electrical Engineering, for giving me the opportunity to live this experience. Most especially, many thanks to my thesis supervisor, Dr. Víctor Hinojosa, who, beyond guiding me academically, has been a role model and a source of inspiration. Thank you for your advice, the knowledge you imparted, and your patience. I appreciate the opportunity to have learned from you.

To the one who, from another place, continues to illuminate my path and give me strength at every step of this achievement through their eternal love.

Contents

List of Figures

List of Tables

Acronyms

ac	Alternating current.
ACE	Area Control Error.
AGC	Automatic generation control.
CCUC	Contingency-constrained unit commitment.
dc	Direct current.
DSL	DIgSILENT Simulation Language.
ED	Economic dispatch.
ISO	Independent system operator.
MILP	Mixed-integer linear programming.
OPF	Optimal power flow.
PFC	Primary frequency control.
PI	Proportional-integral.
PJM	Pennsylvania-New Jersey-Maryland.
RMS	Root-Mean-Square.
SACE	Smooth Area Control Error.
SCUC	Security-constrained unit commitment.
SFC	Secondary frequency control.
TFC	Tertiary frequency control.
TS	Transmission switching.
U.S.	United States.
UC	Unit commitment.

Nomenclature

Indices:

b	Index for buses.
g	Index for generating units.
j	Index for blocks of the piecewise linear approximations of transmission losses.
k	Index for operating conditions.
l, l', l''	Index for branches.
s	Index for contingency states.
$fr(l)$, $to(l)$	Indices of the sending and receiving buses of branch l.

Sets:

$\mathcal{B}$	Index sets of buses.
$\mathcal{G}$	Index sets of all generating units.
$\mathcal{G}_b$	Index sets of all generating units connected to bus b.
$\mathcal{G}^{\text{AGC}}$	Index sets of AGC candidate generating units.
$\mathcal{G}_b^{\text{AGC}}$	Index sets of AGC candidate generating units connected to bus b.
$\mathcal{J}$	Index sets of blocks of the piecewise linear approximations of transmission losses.
$\mathcal{K}$	Index sets of operating conditions.
$\mathcal{L}$	Index sets of branches.
$\mathcal{L}^{\text{TS}}$	Index sets of candidate branches for switching.
$\mathcal{S}$	Index sets of contingency states.

Parameters:

$A_{l,s,k}$	Availability parameter equal to 0 if branch l is unavailable under contingency state s and operating condition k; being 1 otherwise.
B_l, G_l	Susceptance and conductance of branch l [p.u.].
C_g^{Fuel}	Fuel cost coefficient of generating unit g [\$/MWh].
C^{L}, C^{Ue}	Penalty cost coefficients for transmission losses and unserved energy [\$/MWh].
C_g^{SFC}	Secondary frequency control cost coefficient of generating unit g [\$].
C^{TS}	Switching cost coefficient [\$].
$D_{b,s,k}^{\text{PFC}}$	Load demand at bus b at the end of the primary frequency control under contingency state s and operating condition k [MW].
$D_{b,k}^{\text{Pre}}$	Pre-contingency load demand at bus b under operating condition k [MW].
F_l^{Max}	Capacity of branch l [MW].
M	Sufficiently large constant.
N^{Max}	Maximum number of branches allowed to be switched off.

$P_g^{\text{Max}}, P_g^{\text{Min}}$	Maximum and minimum production limits of generating unit g [MW].
$P_{b,s,k}^{\text{Out}}$	Lost generation at bus b under contingency state s and operating condition k [MW].
$P_{g,s,k}^{\text{PFC}}$	Power output of generating unit g at the end of the primary frequency control under contingency state s and operating condition k [MW].
$P_{g,k}^{\text{Pre}}$	Pre-contingency power output of generating unit g under operating condition k [MW].
$\text{PL}_{l,k}^{\text{Pre}}$	Pre-contingency resistive losses on branch l under operating condition k [MW].
RD_g, RU_g	Ramp-down and ramp-up rate limits of generating unit g [MW/min].
$\text{SF}_{l,b,s}$	Lossy shift factor for branch l with respect to bus b under contingency state s [p.u.].
T^{SFC}	Time range used to obtain an adequate dynamic AGC operation [min].
$\pi_{s,k}$	Probability of occurrence of contingency state s under operating condition k [p.u.].

Variables:

Csfc	AGC scheduling cost for secondary frequency control [$].
$\text{Cop}_{s,k}$, $\text{Cpl}_{s,k}$	Operating and transmission losses costs for contingency state s and operating condition k [$].
$\text{Cts}_{s,k}$, $\text{Cue}_{s,k}$	Corrective transmission switching and unserved energy costs for contingency state s and operating condition k [$].
$f_{l,s,k}$, $\widetilde{f}_{l,s,k}$	Variables used to model the non-uniform power flow and the virtual power flow on branch l under contingency state s and operating condition k [MW].
$f_{l,s,k}^{\text{Neg}}, f_{l,s,k}^{\text{Pos}}$	Auxiliary variables used to model the active power flow on branch l under contingency state s and operating condition k [MW].
$pl_{l,s,k}$	Resistive losses of branch l under contingency state s and operating condition k [MW].
$p_{b,s,k}^{\text{Ue}}$	Unserved energy at bus b under contingency state s and operating condition k [MW].
$v_g^{\text{Dn}}, v_g^{\text{Up}}$	Binary variables equal to 1 if generating unit g participates in the secondary frequency control by providing regulation down or regulation up, and 0 otherwise.
$z_{l,s,k}$	Binary variable equal to 1 if candidate branch l is switched on under contingency state s and operating condition k; being 0 otherwise.
$\Delta f_{j,l,s,k}$	Contribution of block j to the active power flow on branch l under contingency state s and operating condition k [MW].
$\Delta p_{g,s,k}^{\text{Dn}}, \Delta p_{g,s,k}^{\text{Up}}$	Regulation down and up adjustments of the power output of generating unit g under contingency state s and operating condition k [MW].

Others:

$\hat{P}_{s,k}^{\text{Out}}$	Corrected generation deficit for the contingency state s and operating condition k [MW].
$\gamma_{g,s,k}$	Participation factor of AGC candidate generating unit g under contingency state s and operating condition k [p.u.].
$\mathbf{P_N}$	Vector of net nodal injections.

Resumen

Los sistemas eléctricos modernos operan cada vez más con márgenes estrechos, por lo que una perturbación inicial puede dejar a la red vulnerable durante la ventana de recuperación. Una segunda contingencia creíble en ese intervalo puede desencadenar efectos en cascada que profundizan las desviaciones de frecuencia, alteran los programas de potencia en las interconexiones y sobrecargan corredores clave. En consecuencia, la seguridad del sistema se ve comprometida y los costos de operación aumentan.

Motivado por este riesgo, el presente estudio aborda el desafío de garantizar la seguridad del sistema y la operación económica durante la etapa de control secundario de frecuencia en presencia de contingencias en cascada inciertas. Con este fin, se propone un marco novedoso para la programación del control automático de generación (AGC) que integra una plataforma de simulación en el dominio del tiempo con un modelo estocástico de programación lineal entera mixta de dos etapas.

A diferencia de enfoques previos, la propuesta introduce dos innovaciones principales: (i) se adopta un criterio de seguridad $N-1-1$, en lugar del estándar tradicional $N-1$, para representar la pérdida de un generador seguida de la desconexión de una línea de transmisión durante la fase de recuperación de la frecuencia; y (ii) se incorporan acciones correctivas de transmisión switching (TS) en el contexto de la regulación de frecuencia.

La metodología propuesta determina, fuera de línea, el conjunto de unidades de generación que participarán en el AGC y sus factores de participación, así como las decisiones óptimas de TS correctivo. Además, el problema de optimización utiliza una formulación basada en factores de participación (conocidos también como factores de sensibidad del sistema de transmisión) que capturan eficazmente tanto las fallas de líneas como las acciones de TS. En esta formulación también se consideran las pérdidas de transmisión y la dependencia de voltaje de las cargas.

El desempeño del marco propuesto se valida mediante simulaciones dinámicas realizadas en un sistema de 50 barras en DIgSILENT PowerFactory. Los resultados muestran que habilitar TS mejora la eficiencia económica y refuerza la seguridad de la respuesta transitoria del AGC, lo que se traduce en una asignación más efectiva de la regulación entre las unidades candidatas al AGC. Además, los resultados muestran que adoptar el criterio $N-1-1$ conduce a una programación coordinada de las unidades participantes en AGC y de las acciones de TS más resiliente, capaz de enfrentar contingencias más severas que las contempladas bajo el estándar convencional $N-1$.

Abstract

Modern power systems increasingly operate under tight margins, so an initial disturbance can leave the grid vulnerable during the recovery stage. A second credible outage in that interval can trigger cascading effects that deepen frequency deviations, upset tie-line schedules, and overload key corridors. Consequently, system security is compromised and operating costs increased.

Motivated by this risk, the present study addresses the challenge of ensuring system security and economic operation during the secondary frequency control stage in the presence of uncertain cascading outages. In this study, a novel framework for automatic generation control (AGC) scheduling is formulated, incorporating a time-domain simulation platform with a two-stage stochastic mixed-integer linear programming model.

Unlike previous approaches, the proposal introduces two main innovations: (i) an $N-1-1$ security criterion is adopted, in place of the traditional $N-1$ standard, to represent a generator loss followed by a transmission line tripping during the frequency recovery phase; and (ii) corrective transmission switching (TS) actions are incorporated in the context of frequency regulation.

The introduced methodology determines, off-line, the set of generating units to be scheduled for AGC and their participation factors, along with the optimal corrective TS decisions. Also, the proposed optimization problem employs a shift factor-based formulation that effectively captures both line tripping and TS actions, while accounting for transmission losses and load-voltage dependency.

The performance of the proposed framework is validated through transient simulations conducted on a 50-bus power system using DIgSILENT PowerFactory. The results show that enabling TS improves economic efficiency and enhances the security of the AGC transient response, resulting in more effective scheduling of regulation among AGC candidate units. In addition, the results show that the adoption of the $N-1-1$ criterion leads to a more resilient, coordinated scheduling of AGC-participating units and corrective TS actions, capable of withstanding more severe contingencies than those contemplated under the conventional $N-1$ standard.

Chapter 1

Introduction

This introductory chapter provides the overall context for the thesis and frames the problem of AGC scheduling under cascading contingencies, emphasizing the role of corrective TS as a mechanism to support frequency control. The discussion is limited to background and motivation and does not introduce the analytical framework or detailed models.

The chapter is organized as follows: Section 1.1 presents the motivation and summarizes the key gaps that motivate this thesis. Section 1.2 states the main objective and the specific objectives that guide the subsequent chapters. Section 1.3 clarifies what is covered and what is out of scope, including assumptions on cascading failures and the focus on frequency control. Section 1.4 lists the software platforms, solvers, and simulation tools used in the thesis work. Section 1.5 describes how the remainder of the thesis is structured.

1.1 Motivation

Modern power systems operate with progressively tighter security and economic margins as renewable penetration rises and power transfers intensify across already congested corridors [5]. In this context, system operators must provide a continuous supply of electric power while maintaining strict operating and security standards in the most economical option. One mechanism used to support optimal system operation is AGC. This mechanism is responsible for restoring frequency after the primary response and maintaining scheduled inter-area exchanges [6]. However, typical implementations of this controller neither optimize the generation costs of participating units nor explicitly consider transmission network constraints. As a result, regulation schedules can be economically suboptimal or even operationally infeasible once real network effects are taken into account.

Another shortcoming lies in the treatment of security. While many studies evaluate AGC decisions under single-contingency (N–1) conditions, none consider cascading disturbances. In practice, a second credible outage can occur before the system has recovered from the first one. These events are captured by the $N-1-1$ criterion and can push stressed corridors into overloading conditions, escalating the risk of load shedding, cascading outages, and eventually, blackouts [7]. Thus, AGC schedules that appear adequate under $N-1$ conditions can therefore become unsafe under $N-1-1$ events because the second disturbance reshapes power flows and available regulation in ways the original schedules did not anticipate.

In addition, flexible mechanisms, such as TS, are largely absent as frequency support instruments. TS is an ISO-managed corrective action that reconfigures the network by opening or closing lines to relieve congestion and redirect transmission power flows. It is noteworthy that system operators have adopted technical operational procedures to identify corrective TS actions in order to decrease congestion effects. However, its potential to improve transient frequency performance and support AGC during and after contingencies remains unexplored. Ignoring TS in the AGC context overlooks a powerful source of network flexibility precisely when the system is most stressed.

Given the above gaps, this thesis proposes a novel AGC scheduling framework that integrates corrective TS actions to ensure both economic and security operation under $N-1-1$ events in the context of secondary frequency control. By integrating these elements, the thesis aims to provide system operators with an actionable tool that delivers more resilient AGC schedules, reduces the likelihood of load shedding under severe events, and lowers operating costs by aligning regulation provision with network flexibility.

1.2 Objectives

1.2.1 Main objective

To employ corrective TS as a network flexibility mechanism in order to enable a more resilient and economic scheduling of AGC units under $N-1-1$ contingency scenarios.

1.2.2 Specific objectives

To achieve the main objective, the following specific objectives must be accomplished:

1. Review specialized literature on AGC enhancement techniques, with a focus on economic and flexibility strategies, network-aware approaches, and security criteria.

2. Develop a framework based on Python–Gurobi–DIgSILENT PowerFactory that integrates corrective TS and explicitly models $N-1-1$ contingencies to achieve a more resilient scheduling of AGC units, ensuring secure operation in critical conditions.

3. Develop a dc-based power flow modeling approach that captures ac transmission characteristics to accurately represent transmission losses and assess corrective TS as a flexibility mechanism to improve the economic operation of the AGC.

4. Validate the proposed model through RMS-based simulations under various operating scenarios, including generation and transmission outages, assessing improvements in regulation performance.

1.3 Scope

The scope of this work is to develop and evaluate a framework for AGC scheduling that incorporates corrective TS actions to ensure both economic efficiency and system security under $N-1-1$ events in the context of secondary frequency control. In this work, an $N-1-1$ event corresponds to a critical failure of a generating unit followed by a transmission line outage, assuming that the second event occurs at the end of the primary frequency control.

The framework integrates an optimization problem and a time-domain simulation platform to determine, off-line, the optimal set of generating units to be scheduled in the AGC, along with their participation factors and corrective TS decisions. The optimization problem is formulated using a two-stage stochastic mixed-integer linear programming (MILP) approach. A shift factor-based formulation is employed to represent the transmission power flow problem, taking into account line tripping, switching, and transmission losses.

The framework is validated through Root-Mean-Square (RMS)-based simulations in DIgSILENT PowerFactory (PF) using a 50-bus system. The evaluation compares traditional AGC schedules based on the $N-1$ criterion with the proposed framework applied to $N-1-1$ scenarios, highlighting the economic and resilience benefits of incorporating corrective TS actions into AGC operation.

1.4 Modeling and Simulation Platforms

In this work, RMS-based simulations are performed in DIgSILENT PF 2023 [8] using the Python API [9]. The optimization problems are solved with Gurobi 12.0.1 [10], employing a branch-and-bound framework with a MILP gap tolerance of 1%. All computations are carried out on a Windows 11 Home computer with an AMD Ryzen 5 8645HS processor at 4.3 GHz and 16 GB RAM.

1.5 Organization of the Thesis

Chapter 1 presents the motivation for the study and states the thesis objectives and scope. It also describes the simulation and modeling tools used for dynamic studies and for formulating and solving the proposed optimization problem. The chapter ends with a brief synthesis of the document and a roadmap of the remaining chapters.

Chapter 2 presents the theoretical background of the thesis, starting with the main concepts of power system stability and emphasizing the fundamentals of frequency control. Particular attention is given to primary and secondary control, with detailed descriptions of generator, turbine, governor, load, and AGC models. The chapter concludes with a general AGC scheme that will be referenced in later chapters.

Chapter 3 reviews the technical literature relevant to this thesis, covering recent developments in AGC scheduling, the application of the $N-1-1$ criterion to account for sequential contingencies in the operational context, and an overview of TS applications. The chapter closes by showing that sequential contingencies and TS are largely absent from prior AGC scheduling studies and by positioning the main contributions of this work.

Chapter 4 details the proposed AGC scheduling framework, which incorporates corrective TS actions to address $N-1-1$ events. First, the assumptions behind the considered $N-1-1$ events and their impact on frequency stability are presented. Next, the AGC model implemented in the time-domain simulation platform is introduced. Subsequently, the proposed two-stage stochastic MILP model is developed in detail. The chapter concludes with a workflow description that specifies the information exchanged between the time-domain simulation platform and the MILP model.

Chapter 5 introduces the test system and experimental setup employed to validate the proposed framework, alongside the corresponding numerical results. The analysis encompasses an evaluation of model accuracy and an assessment of the technical and economic implications of the proposal. Additionally, the dynamic behavior of frequency restoration and the associated voltage effects provoked by $N-1-1$ events and TS actions are examined through RMS-based simulations.

Chapter 6 presents the relevant conclusions regarding the implementation of the proposed framework. Additionally, future avenues of research that could complement this proposal are suggested.

Chapter 2

Theoretical Background

This chapter develops and reviews the fundamental concepts of frequency control in electric power systems, with particular emphasis on AGC as the core topic of this thesis. The presentation provides essential background, notation, and modeling assumptions used later in the document.

The chapter is organized as follows: Section 2.1 introduces the time scales of power-system transient phenomena. Section 2.2 outlines the modern taxonomy of power system stability. Section 2.3 introduces the hierarchical structure of frequency control and reviews the primary, secondary, and tertiary layers. Section 2.4 provides a detailed description of primary control and integrates it into a compact block diagram representation. Section 2.5 describes the main principles of secondary control and AGC operation, first for an isolated system and then for a two-area interconnection, and concludes with a generalized AGC scheme.

2.1 Time Scales of Transient Power System Phenomena

Power system dynamics span several characteristic time bands in which different phenomena dominate. As illustrated in Fig. 2.1, these bands can be summarized as follows:

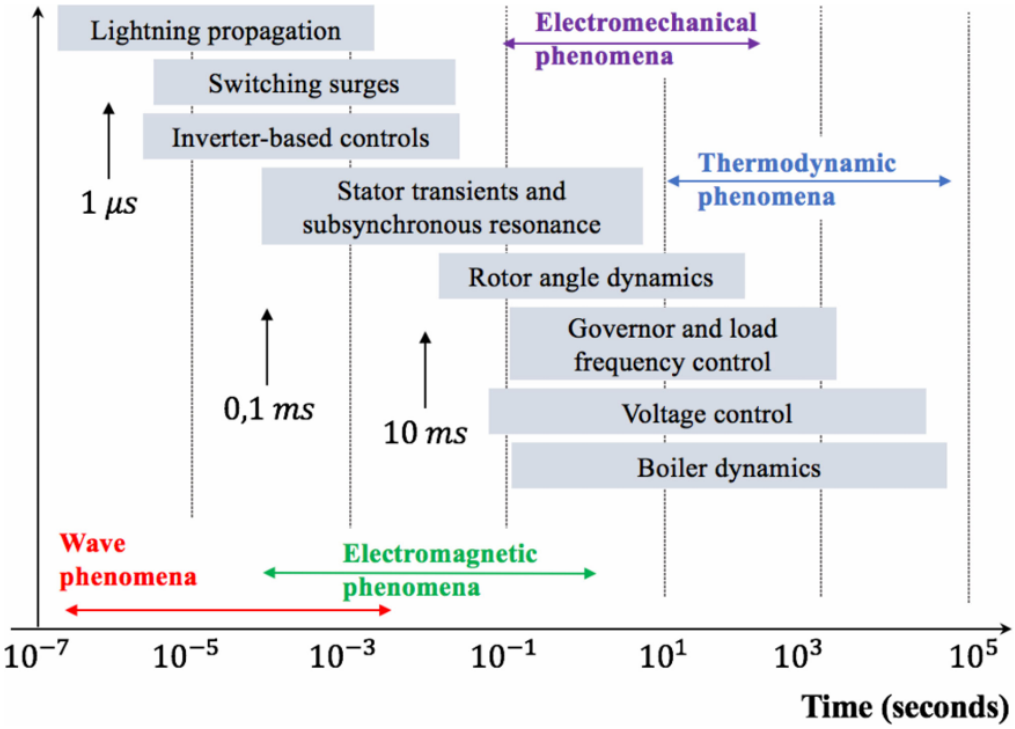

Figure 2.1. Power system times scales [1].

– *Electromagnetic phenomena:* This band encompasses very-fast processes in the network and equipment, including traveling-wave propagation (e.g., lightning), switching surges, apparatus transients, and stator subtransients. Controls and switching actions of inverter-based generating resources (IGBRs), flexible ac transmission systems (FACTS), and high-voltage direct current (HVDC) converters also operate in this band due to their kHz switching frequencies. These effects must be represented with electromagnetic-transient (EMT) models.

– *Electromechanical phenomena:* Arise from the exchange of kinetic energy among synchronous machines through the network and from temporary imbalances between mechanical input and electrical output power. This band covers transients related to rotor angle oscillations, the action of excitation/voltage regulators, and power system stabilizers (PSS), as well as the frequency control layers, which involve the governor and load response. These events are accurately represented with RMS time-domain models under the quasi-sinusoidal assumption at 50/60 Hz.

– *Thermodynamic phenomena:* These phenomena involve effects related to plant-level thermal processes, including boiler and turbine-reheater dynamics, fuel and combustion systems, and thermal limits, which evolve over minutes to hours. They arise on economic and operational time frames and are typically represented with simplified dynamic or steady-state models.

Given that this research is primarily concerned with frequency stability, the subsequent subsections provide a detailed discussion of power system stability.

2.2 Power System Stability

Power system stability refers to the ability of the system to maintain a state of equilibrium during normal operating conditions and to recover it following a disturbance [6]. This concept has traditionally been analyzed in terms of synchronous machine dynamics and electromechanical interactions. However, the classification of stability phenomena has evolved to capture a wider range of dynamic behaviors present in modern grids.

Figure 2.2 shows an updated classification of power system stability, which includes not only the classical categories of rotor angle, voltage, and frequency stability, but also two additional classes: resonance stability and converter-driven stability [1]. These additions extend the scope of analysis to capture the evolving dynamic behavior of electrical grids due to the increasing penetration of IBRs [1].

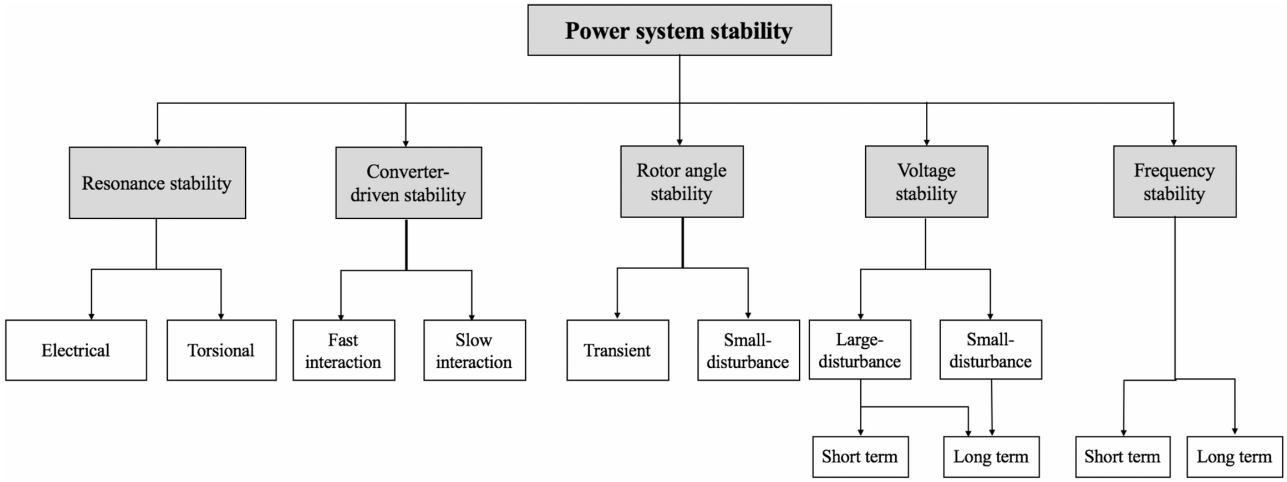

Figure 2.2. Classification of power system stability [1].

2.2.1 Resonance Stability

Resonance stability refers to the ability of the system to withstand oscillatory energy exchanges that may become unstable when damping is insufficient. These resonant oscillations can amplify cur-

rent, voltage, or torque, potentially damaging system components. Resonance phenomena are typically categorized into two types.

– *Torsional resonance*: Classically known as subsynchronous resonance, it arises from the interaction between series-compensated lines and the torsional shaft modes of synchronous turbine-generators. These oscillations may be exacerbated or mitigated by FACTS devices such as static var compensators (SVCs), static synchronous compensators (STATCOMs), or HVDC links, leading to what is termed device-dependent subsynchronous oscillations.

– *Electrical resonance*: Typically associated with induction-based generators such as doubly-fed induction generators. The combination of series compensation and converter controls can lead to self-excitation and large oscillations, known as subsynchronous control interaction.

2.2.2 Converter-driven Stability

Although initially not included in classical classifications, converter-driven stability has been recognized as a distinct category due to the presence of fast control loops of the IBRs and their interactions with the system. It can be divided into:

– *Fast interaction stability*: Related to high-frequency oscillations and control interactions between IBRs and the network, which can destabilize the system due to their rapid transient response.

– *Slow interaction stability*: Involves the coupling between IBRs and synchronous generators, affecting long-term behavior such as frequency and voltage stability, particularly in low-inertia systems.

2.2.3 Rotor Angle Stability

Rotor angle stability is the ability of synchronous machines to maintain synchronism after disturbances. It occurs when the electromagnetic torque matches the mechanical torque of the prime mover. Stability is divided into transient and small-disturbance stability.

– *Transient stability*: Refers to the system's ability to remain in synchronism after large disturbances such as short circuits. It involves significant rotor angle excursions, typically analyzed through time-domain simulations.

– *Small-signal stability*: Concerns the ability to maintain synchronism under small perturbations, typically involving poorly damped or growing oscillations around the equilibrium point. These oscillations are often mitigated with PSS and FACTS devices.

2.2.4 Voltage Stability

Voltage stability ensures that voltages at all buses remain stable post-disturbance. Instability can cause voltage collapse and cascading outages, especially when system components like generators lose synchronism. This category includes:

– *Short-term voltage stability*: Involves fast-acting components such as induction motors and IBRs, which can trigger instability within seconds, especially in weak ac networks.

– *Long-term voltage stability*: Involves slower mechanisms such as on-load tap changers, thermostatically controlled loads, and generator current limiters. Instability may manifest as a gradual decline in voltage over several minutes, leading to load disconnection, generator tripping, or cascading failures.

2.2.5 Frequency Stability

Frequency stability refers to the system's ability to maintain balance between generation and load following a disturbance. Instability can lead to frequency swings, tripping of generating units, or load shedding. Given that this research is primarily concerned with frequency stability, the subsequent analysis focuses on the main mechanisms involved in maintaining system frequency within acceptable bounds.

This thesis focuses on frequency stability (seconds to minutes). Moreover, the inclusion of IBRs and their dynamics is outside the scope of this work. Under these assumptions, the next section reviews in detail the frequency stability.

2.3 Frequency Control Fundamentals

Maintaining the frequency of an electric power system within acceptable bounds is fundamental for secure and stable operation, since frequency is a global variable common to the entire interconnected network. Deviations from the nominal value indicate an imbalance between generation and demand, which may result from disturbances such as generator outages, line trips, or sudden load variations. If not corrected in due time, these deviations can compromise system stability and even lead to cascading failures.

To address this issue, modern power systems rely on a hierarchical control structure composed of primary, secondary, and tertiary frequency control layers [6]. These layers are implemented through frequency controllers, which adjust the power output of conventional synchronous generators to restore the generation–demand balance and bring the frequency back to its nominal value. Figure 2.3 illustrates the operation of frequency control in an electrical system after a generation outage, showing control times, characteristics, and expected frequency behavior. The different stages of frequency control involved in this process are explained below.

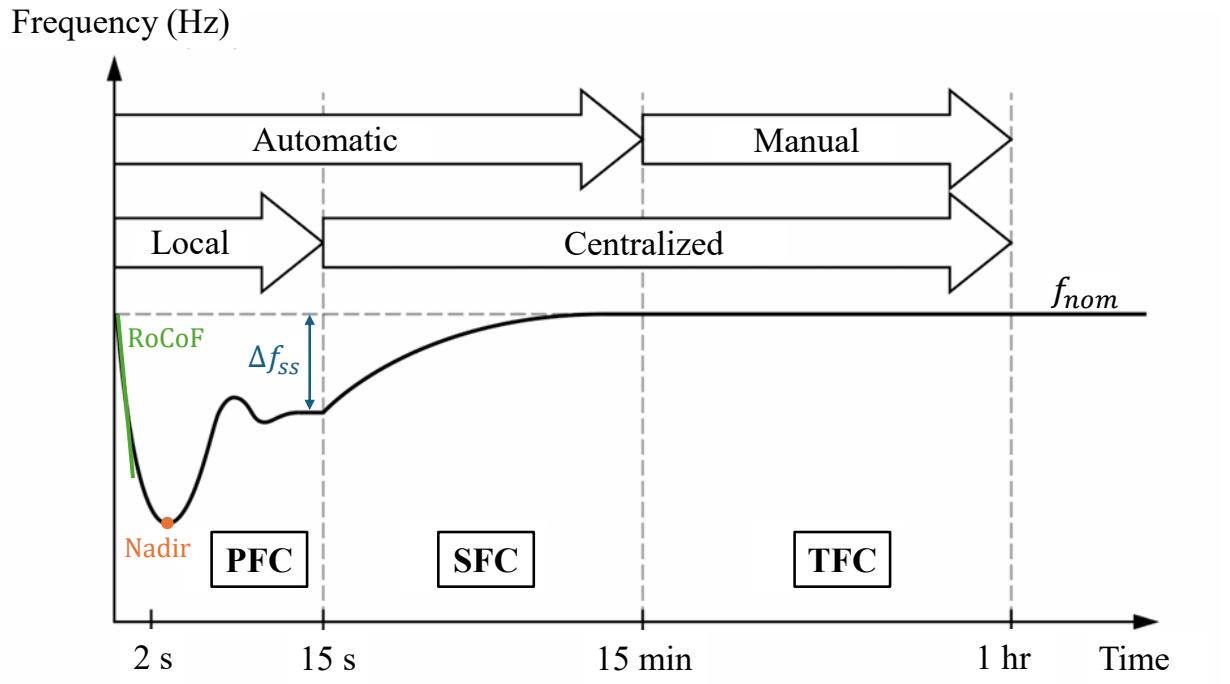

Figure 2.3. Stages of frequency control. Adapted from [2].

1. **Primary Frequency Control (PFC):** Following a generator outage, frequency drops with an initial rate of change (RoCoF) determined by system inertia, the power imbalance, and the load-damping factor. The inertial response arrests the fastest part of the drop. Then, PFC acts locally

and autonomously over roughly 2–15 seconds, rebalancing power by adjusting generator outputs according to the governor droop characteristic. The trajectory reaches a minimum, known as the frequency nadir, whose value is set by system inertia, the droop characteristic of generating units, and the load-damping factor.

Although PFC does not restore nominal frequency, it stabilizes the immediate post-disturbance response and drives the system to a new steady state that remains below the nominal target (Δf_{ss}). This steady-state deviation depends on the droop characteristic of the generating units and the load-damping factor.

2. **Secondary Frequency Control (SFC):** This stage operates between 15 seconds and 15 minutes, following the action of PFC. It is centrally coordinated and automatically executed through the AGC mechanism, which continuously adjusts generator setpoints to restore nominal frequency, eliminate steady-state frequency deviations, and maintain scheduled power exchanges between control areas. The AGC must perform this task both technically and economically.

3. **Tertiary Frequency Control (TFC):** Typically begins about 15 minutes after a disturbance and is executed by the system operator through a manual, centralized re-dispatch that optimizes generation allocation and restores the reserves used by power units during the SFC.

This study considers the timeframes associated with both primary and secondary control stages, with particular emphasis on the role of the AGC in restoring nominal frequency after a generation disturbance. The main aspects of these control stages are explained in the following subsections.

2.4 Primary Frequency Control - PFC

In this section, the dynamic models related to PFC are introduced. The aim is to provide a structured description of the main elements involved in this control layer. In particular, the following models are considered: the synchronous generator, the load–frequency dependency, a simplified turbine, and the governor or speed regulator. Each model is presented in a concise way, emphasizing its role within the primary control stage and its contribution to the system frequency response after a disturbance. Finally, these elements are integrated into a complete PFC model [6].

2.4.1 Synchronous Generator Model

The dynamics of a synchronous generator are regulated by the balance of two opposing torques: the mechanical torque T_m, provided by the prime mover, and the electromagnetic torque T_e, developed in the stator windings. This interaction determines the acceleration or deceleration of the rotor and can be expressed by Newton's second law given in equation (2.1).

$$J\frac{d\omega}{dt} = T_m - T_e \tag{2.1}$$

where J is the moment of turbine-generator inertia and ω is the rotor angular velocity.

For power system studies, it is convenient to rewrite equation (2.1) in per-unit form. Considering a base power S_{base}, a synchronous angular speed ω_{base}, and a torque base defined as $T_{base} = S_{base}/\omega_{base}$, the normalized form of equation (2.1) is given in equation (2.2).

$$2H\frac{d\omega}{dt} = T_m - T_e \tag{2.2}$$

where H is the inertia constant and represents the ratio between the kinetic energy stored at synchronous speed and the machine's rated power, as defined in equation (2.3).

$$H = \frac{\frac{1}{2} J \omega_{base}^2}{S_{base}} \tag{2.3}$$

In frequency analysis, it is more convenient to describe the power unit dynamics in terms of power rather than torque, since power variables directly reflect system operation and balance. Consequently, the instantaneous power of the machine is expressed in equation (2.4).

$$P = \omega T \tag{2.4}$$

To examine the response to small disturbances, deviations around the initial steady-state operating point (denoted by the subscript 0) are considered. This leads to the expression in equation (2.5), which follows directly from equation (2.4).

$$P_0 + \Delta P = (\omega_0 + \Delta\omega)(T_0 + \Delta T), \tag{2.5}$$

Neglecting second-order terms, equation (2.5) reduces to equation (2.6):

$$\Delta P = \omega_0 \Delta T + T_0 \Delta\omega. \tag{2.6}$$

By opposing the mechanical and electrical powers acting on the machine shaft, equation (2.6) can be written as equation (2.7):

$$\Delta P_m - \Delta P_e = \omega_0(\Delta T_m - \Delta T_e) + (T_{m0} - T_{e0})\Delta\omega \tag{2.7}$$

Taking into account that at steady state $T_{m0} = T_{e0}$ and $\omega_0 = 1$ p.u., equation (2.7) leads to equation (2.8).

$$\Delta P_m - \Delta P_e = \Delta T_m - \Delta T_e \tag{2.8}$$

Hence, by combining equation (2.8) with small deviations of the rotor angular velocity, equation (2.2) can be expressed in terms of incremental powers, leading to the well-known swing equation (2.9). This equation describes the electromechanical oscillations of the synchronous generator that arise from imbalances between mechanical input power and electrical output power. Its block diagram representation is shown in Figure 2.4.

$$2H\frac{d\Delta\omega}{dt} = \Delta P_m - \Delta P_e \tag{2.9}$$

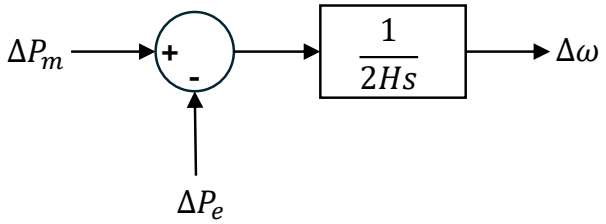

Figure 2.4. Block diagram of the synchronous generator swing equation. Own work.

2.4.2 Load–frequency Dependency Model

The aggregate demand of a power system is composed of a wide variety of devices, whose behavior with respect to frequency deviations can be classified into two main categories. On the one hand, purely resistive loads, such as incandescent lamps or heating elements, consume power that is practically independent of frequency. On the other hand, certain devices, such as motors, pumps, or fans, exhibit a

frequency-dependent demand, since their power consumption changes as the system frequency deviates from its nominal value.

Considering both types of loads, the total variation of the electrical power demanded by the system can be modeled according to equation (2.10).

$$\Delta P_e = \Delta P_L + D\Delta\omega, \tag{2.10}$$

where ΔP_L represents the variation of load that is independent of frequency, while $D\Delta\omega$ accounts for the frequency-dependent component. The parameter D is known as the load-damping constant and quantifies the sensitivity of the demand to frequency deviations. Typical values of D reported in the literature range between 1% and 2% of the load per 1% change in frequency [6].

If the load model expressed in equation (2.10) is incorporated into the generator dynamics given by equation (2.9), the resulting combined model is obtained as equation (2.11).

$$2H\frac{d\Delta\omega_r}{dt} = \Delta P_m - \Delta P_L - D\Delta\omega \tag{2.11}$$

This equation represents the combined dynamics of the generator and the frequency-dependent load. The block diagram corresponding to equation (2.11) is shown in Figure 2.5, while a simplified equivalent representation is depicted in Figure 2.6.

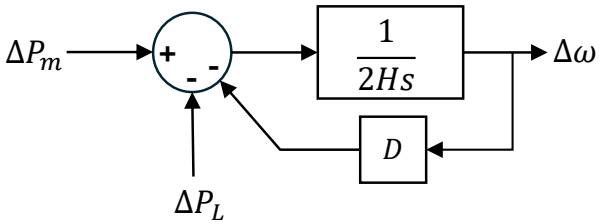

Figure 2.5. Block diagram of the synchronous generator and load model. Own work.

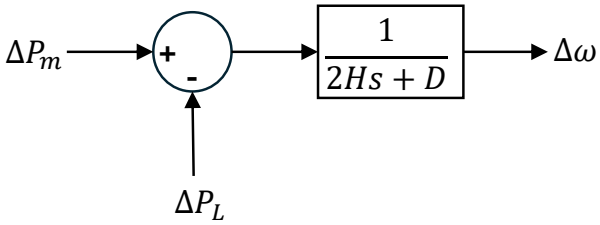

Figure 2.6. Reduced block diagram of the synchronous generator and load model. Own work.

2.4.3 Simplified Turbine Model

The mechanical power required by synchronous generators is provided by turbines, which can be driven by different primary energy sources such as water, steam, or gas. Although the dynamic behavior of each turbine type depends on its specific technology, for power system stability and frequency studies, it is common to adopt a simplified representation.

According to the literature [6], the turbine dynamics can be modeled by a first-order transfer function that relates variations in the mechanical power output ΔP_m to changes in the valve or gate position ΔY. This representation introduces a delay associated with the physical response of the turbine components, and it is expressed in equation (2.12), where τ_T is the turbine time constant.

$$G_T(s) = \frac{\Delta P_m}{\Delta Y} = \frac{1}{1 + \tau_T s} \tag{2.12}$$

The block diagram corresponding to equation (2.12) is shown in Figure 2.7, which illustrates the first-order relationship between the valve position and the mechanical power delivered to the generator shaft.

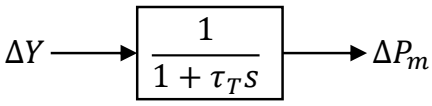

Figure 2.7. Block diagram of the simplified turbine model. Own work.

2.4.4 Speed Regulator Model

Sudden variations in system demand or generation outages create a power imbalance that is initially supplied by the kinetic energy stored in the rotating masses of generators and turbines. This transient exchange modifies the rotor speed and, consequently, the system frequency. The speed regulator, commonly referred to as the governor, is responsible for detecting these frequency deviations and issuing a control signal to adjust the turbine valve position. In this way, the mechanical power delivered to the generator shaft is modified to counteract the imbalance and partially restore the frequency toward its nominal value [6].

A key governor element is the droop characteristic, which defines the steady-state relationship between frequency deviation and power output. The droop ensures that multiple generators can participate in frequency control without instability, since each unit contributes proportionally to its rating capacity. The droop constant, denoted by R, is formally defined in equation (2.13) as the ratio between the steady-state frequency deviation and the change in turbine power, both expressed in per-unit.

$$R = \frac{\Delta\omega}{\Delta P} = \frac{\omega_{nl} - \omega_{fl}}{\omega_0}, \tag{2.13}$$

where ω_{nl} is the no-load frequency, ω_{fl} the full-load frequency, and ω_0 the nominal frequency.

Typical values of R for conventional synchronous units range between 4% and 7% [6]. The slope of the frequency–power curve in steady state is illustrated in Figure 2.8, where the droop characteristic is represented by the red line relating ΔP and $\Delta\omega$.

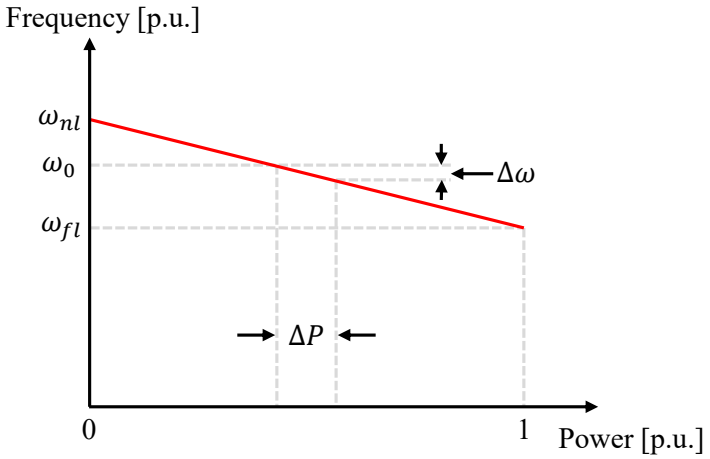

Figure 2.8. Steady-state frequency–power characteristic of the governor. Own work.

In addition to the droop characteristic R, the governor includes the dynamic response of the valve mechanism. Since this action involves mechanical and hydraulic components, it does not occur instantly and is typically represented by a first-order delay with a time constant τ_G. The block diagram in Figure 2.9 shows this simplified model, where the output ΔY denotes the change in valve position that modifies the mechanical power delivered to the generator shaft.

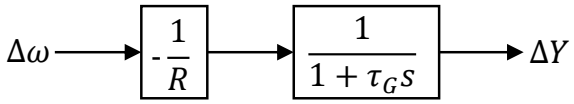

Figure 2.9. Simplified block diagram of the speed governor. Own work.

The governor also receives a power reference P_{ref}, which sets the scheduled operating point of the unit. As illustrated in Figure 2.10, this reference is combined with the droop response so that the valve command ΔY accounts for both the dispatch set-point and frequency deviations.

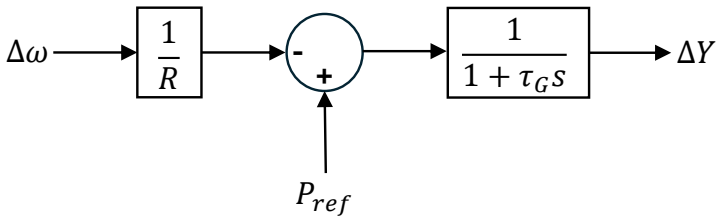

Figure 2.10. Simplified block diagram of the speed governor with a power reference. Own work.

Adding the power reference P_{ref} vertically shifts the generator's droop characteristic so that, at $\Delta\omega = 0$, the unit produces $P = P_{ref}$. By setting P_{ref} between the generator's minimum technical output P_{min} and maximum capacity P_{max}, the operator deliberately leaves upward and downward marginsR^{Up} and R^{Dn}. These margins, defined in (2.14) and (2.15), constitute the available primary reserve.

$$R^{\mathrm{Up}} = P_{max} - P_{ref} \tag{2.14}$$

$$R^{\mathrm{Dn}} = P_{ref} - P_{min} \tag{2.15}$$

Furthermore, the term $\frac{1}{R}\Delta\omega$ represents the required change in power proportional to the frequency deviation. Moreover, the output of the adder, $u = P_{ref} - \frac{1}{R}\Delta\omega$, is the instantaneous power request, which is then shaped by the governor dynamics to produce the valve-position change signal ΔY.

2.4.5 PFC Model

The PFC can be represented through an integrated model that combines the elements described in the previous subsections. Figure 2.11 presents the corresponding block diagram, which summarizes the overall dynamics of the control loop in a compact form and serves as a basis for subsequent analysis. Appendix A provides more detailed turbine and governor models used in electrical power systems.

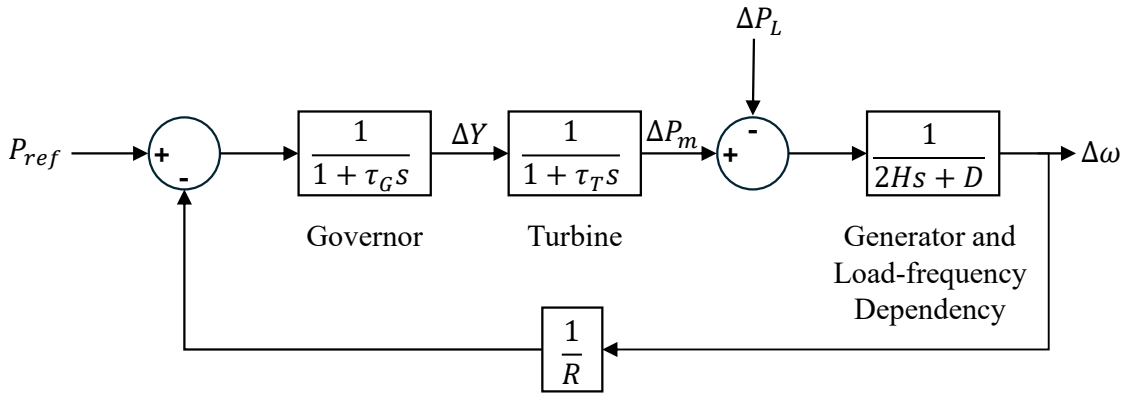

Figure 2.11. Simplified block diagram of the integrated PFC model. Own work.

2.5 Secondary Frequency Control - SFC

While PFC provides a rapid stabilization of system frequency after a disturbance, it does not fully restore frequency to its nominal value and may leave steady-state deviations. SFC addresses these residual errors with two main objectives: (i) to restore the system frequency to its nominal value, and (ii) to reestablish the scheduled power interchange between interconnected areas [6].

The implementation of SFC is carried out through the AGC, which continuously adjusts the set-points of selected generating units. To provide a clear understanding of its operation, two cases are considered in this section. First, the application of AGC in an isolated system is described, where the focus lies solely on frequency restoration. Then, the analysis is extended to a two-area system, in which AGC regulates both the frequency and the power flows across the interconnection. Finally, a generalized control scheme is presented, summarizing the essential structure of AGC.

2.5.1 AGC in an Isolated System

Figure 2.12 illustrates a simplified representation of frequency control mechanisms in power systems, distinguishing between generating units that participate only in the primary control and those that also participate in the secondary control.

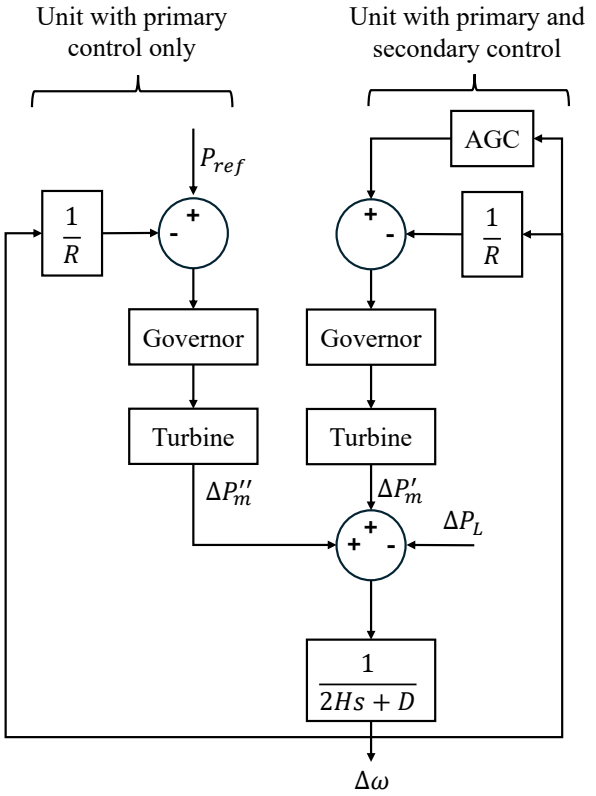

Figure 2.12. Control scheme for primary and secondary frequency control in an isolated system. Own work.

On the left side of the diagram, the unit with PFC only adjusts its power output based on local frequency measurements using the droop characteristic R. The error between the frequency deviation and the droop reference feeds the governor, which regulates the mechanical turbine output. This action results in a power variation $\Delta P_m''$, contributing to system stabilization immediately after a disturbance. A larger number of units participating in PFC leads to a smaller frequency deviation.

On the right side, a unit with both primary and secondary control includes the additional action of the AGC. This component, typically implemented as a proportional-integral (PI) or proportional-integral-derivative (PID) controller, adjusts the reference power setpoint to eliminate steady-state frequency errors. The AGC acts after the primary frequency response, and its output is integrated

into the droop mechanism, leading to a controlled variation in mechanical power $\Delta P'_m$. In practice, this secondary control is centrally coordinated by the system operator to ensure a stable and economic allocation of resources.

The *Governor* and *Turbine* blocks correspond to the simplified structures previously discussed for generating units, such as thermal or hydro plants. Although simplified, this structure reflects the fundamental roles of both primary and secondary control in preserving frequency stability after power system disturbances.

2.5.2 AGC in a Two-Area Interconnected System

Interconnected power systems are often divided into control areas, each consisting of generating units coordinated by a common AGC signal. The interaction between areas is essential for analyzing frequency dynamics and tie-line power exchanges. A two-area representation is therefore commonly adopted as a simplified yet effective framework for studying load–frequency control and the role of interconnections in maintaining stability [6].

The scheme in Figure 2.13a shows two areas linked through a tie-line of reactance X_l. For frequency analysis, each area can be reduced to an equivalent generator that captures the aggregated dynamics of all synchronous machines and their associated control systems. The equivalent electrical model is illustrated in Figure 2.13b, where each area is represented by a voltage source in series with a reactance.

The active power transferred through the tie-line is expressed in equation (2.16), where E_1 and E_2 denote the equivalent internal voltages of the areas, while δ_1 and δ_2 correspond to the respective phase angles of these voltages.

$$P_{12} = \frac{E_1 E_2}{X_T} \sin(\delta_1 - \delta_2), \tag{2.16}$$

By linearizing equation (2.16) around the initial operating point ($\delta_1 = \delta_{10}$, $\delta_2 = \delta_{20}$), the incremental tie-line power is obtained as described in equation (2.17).

$$\Delta P_{12} = T_0 \, \Delta\delta_{12}, \tag{2.17}$$

where $\Delta\delta_{12} = \Delta\delta_1 - \Delta\delta_2$, and T_0 denotes the synchronizing torque coefficient, as defined in equation (2.18).

$$T_0 = \frac{E_1 E_2}{X_T} \cos(\delta_{10} - \delta_{20}). \tag{2.18}$$

The complete block diagram of the two-area system is shown in Figure 2.14. This initial representation considers only PFC, where each area is modeled by an equivalent generator with inertia H, damping D, the turbine, and a governor with droop R. The tie-line power deviation ΔP_{12} results from the synchronizing torque acting on the angular difference between both areas, with a positive value indicating active power transfer from area 1 to area 2.

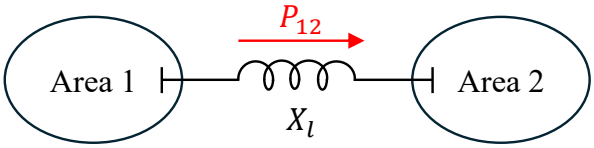

(a) Physical representation

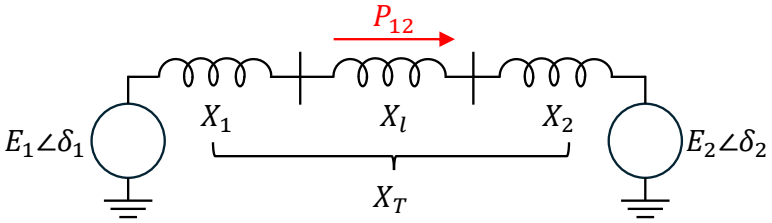

(b) Equivalent electrical representation

Figure 2.13. Two-area system. Own work.

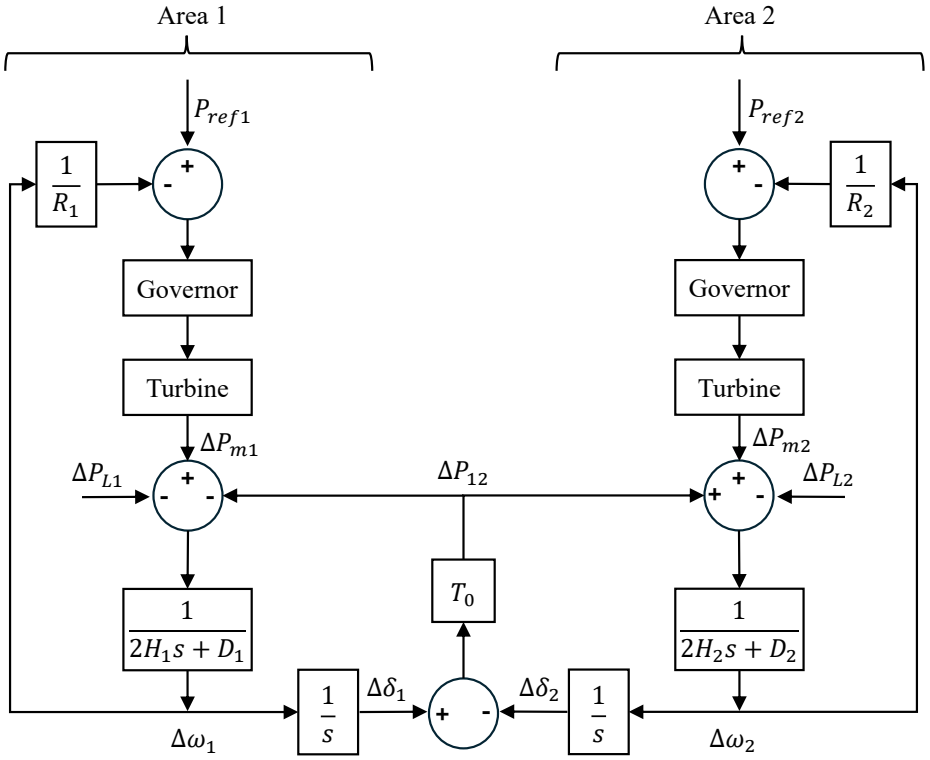

Figure 2.14. Two-area system control scheme with only primary frequency control. Own work.

At steady state, once the primary frequency response has settled, the deviations in both areas become identical, i.e., $\Delta\omega_1 = \Delta\omega_2 = \Delta\omega$. Under this condition, the incremental power balances in areas 1 and 2 are given by equations (2.19) and (2.20), respectively.

$$\Delta P_{m1} - \Delta P_{12} - \Delta P_{L1} = D_1\,\Delta\omega \tag{2.19}$$

$$\Delta P_{m2} + \Delta P_{12} - \Delta P_{L2} = D_2\,\Delta\omega \tag{2.20}$$

where ΔP_{m1} and ΔP_{m2} denote the mechanical power variations in each area, ΔP_{L1} and ΔP_{L2} represent the load variations, D_1 and D_2 are the load–damping factors, and $\Delta\omega$ is the common frequency deviation.

Considering the steady-state effect of only a load increase in area 1 (ΔP_{L1}), the power balances for each area are given by equations (2.21) and (2.22).

$$\Delta P_{m1} - \Delta P_{12} - \Delta P_{L1} = D_1 \, \Delta\omega \tag{2.21}$$
$$\Delta P_{m2} + \Delta P_{12} = D_2 \, \Delta\omega \tag{2.22}$$

At the end of PFC, the change in turbine mechanical power in each area is given by the governor droop equations (2.23) and (2.24).

$$\Delta P_{m1} = \frac{1}{R_1} \, \Delta\omega \tag{2.23}$$
$$\Delta P_{m2} = \frac{1}{R_2} \, \Delta\omega \tag{2.24}$$

Substituting equations (2.23) and (2.24) into equations (2.21) and (2.22) gives:

$$\Big(\frac{1}{R_1} + D_1\Big)\Delta\omega = -\Delta P_{12} - \Delta P_{L1} \tag{2.25}$$
$$\Big(\frac{1}{R_2} + D_2\Big)\Delta\omega = \Delta P_{12} \tag{2.26}$$

Solving equations (2.25) and (2.26) yields:

$$\Delta\omega = -\frac{\Delta P_{L1}}{\beta_1 + \beta_2} \tag{2.27}$$
$$\Delta P_{12} = -\frac{\beta_2}{\beta_1 + \beta_2} \, \Delta P_{L1} \tag{2.28}$$

where $\beta_1 = \frac{1}{R_1} + D_1$ and $\beta_2 = \frac{1}{R_2} + D_2$.

Analyzing equations (2.27) and (2.28) shows that a load change in area 1 produces a common frequency deviation in both areas and alters the active power interchange ΔP_{12}. In particular, $\Delta P_{L1} > 0$ implies a decrease in frequency and an increase in power interchange from area 1.

To eliminate the residual errors in frequency and tie-line power exchange after the primary response, the AGC introduces a supplementary control action. For this purpose, a signal is constructed that combines both components: the system frequency deviation and the deviation of tie-line power from its scheduled value. This composite signal, termed the area control error (ACE), quantifies the corrective power to be supplied by the AGC-participating units. For each area, the ACE is calculated according to equations (2.29) and (2.30).

$$\mathrm{ACE}_1 = \Delta P_{12} + B_1 \, \Delta\omega \tag{2.29}$$
$$\mathrm{ACE}_2 = -\Delta P_{12} + B_2 \, \Delta\omega \tag{2.30}$$

where B_1 and B_2 are the frequency-bias factors from area 1 and area 2, respectively.

The bias determines the relative weight assigned to the frequency deviation in the calculation of the ACE, thereby influencing how each area contributes to correcting both local frequency errors and tie-line power deviations. Accordingly to [6], a customary and effective choice for the bias is given in equation (2.31).

$$B_i = \frac{1}{R_i} + D_i = \beta_i, \tag{2.31}$$

where R_i is the governor droop of area i, D_i the load–damping coefficient, and β_i the composite frequency response characteristic of area i.

With this selection, the bias reflects the combined effect of generators participating in AGC and the natural load frequency sensitivity. Substituting equation (2.31) into equations (2.29) and (2.30), and considering a load change in area 1 (ΔP_{L1}), yields:

$$\mathrm{ACE}_1 = \Delta P_{12} + \beta_1 \Delta\omega = -\frac{\Delta P_{L1}\beta_1}{\beta_1+\beta_2} - \frac{\Delta P_{L1}\beta_2}{\beta_1+\beta_2} = -\Delta P_{L1}, \tag{2.32}$$

$$\mathrm{ACE}_2 = -\Delta P_{12} + \beta_2 \Delta\omega = \frac{\Delta P_{L1}\beta_2}{\beta_1+\beta_2} - \frac{\Delta P_{L1}\beta_2}{\beta_1+\beta_2} = 0. \tag{2.33}$$

Therefore, choosing the frequency-bias factors as $B_i = \beta_i$ forces each area to compensate entirely for its own load disturbances, avoiding steady-state power support from neighboring areas. In practice, however, the bias is only set close to β_i and coordinated by the system operator, allowing a controlled sharing of disturbances across areas while ensuring robust and stable transient performance despite changes in unit participation and load levels.

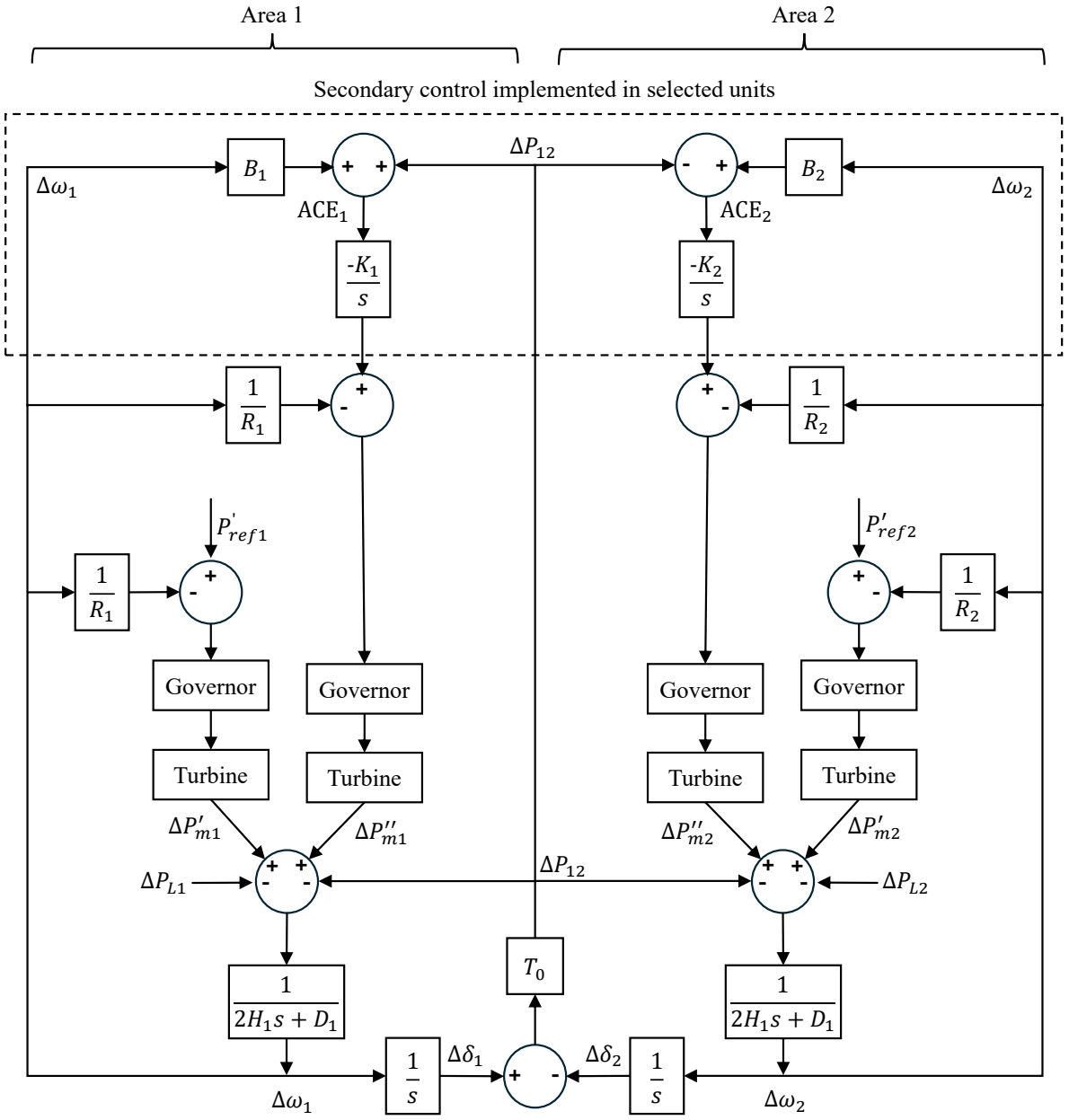

Figure 2.15. Control scheme for primary and secondary frequency control in a two-area interconnected system. Own work.

Figure 2.15 presents the complete control scheme for a two-area system, where both primary and secondary frequency control actions are explicitly represented. In each area, a portion of the generating

units contributes only through primary control, while others participate additionally in the AGC loop, receiving the respective ACE signal. This structure highlights the hierarchical nature of frequency regulation: the primary response provides an immediate stabilization of frequency deviations, whereas the secondary control gradually restores nominal frequency and scheduled tie-line power by coordinating unit set-points. In this way, the model integrates both local and centralized actions, ensuring a stable and balanced operation of interconnected systems.

2.5.3 Generalized AGC Scheme

Figure 2.16 presents a generalized block diagram of AGC, which integrates all the elements required for secondary frequency regulation in interconnected systems [6]. The scheme begins with the measurement stage, where system frequency ω and the active power flows on the tie-lines P_{tie} are continuously monitored by dedicated meters. The measured frequency is compared with the nominal reference ω_0, yielding the frequency deviation $\Delta\omega$, while the measured tie-line flows are compared with their scheduled tie-line power flow to obtain the interchange deviation ΔP_{tie}. These two deviations are then combined to quantify the ACE.

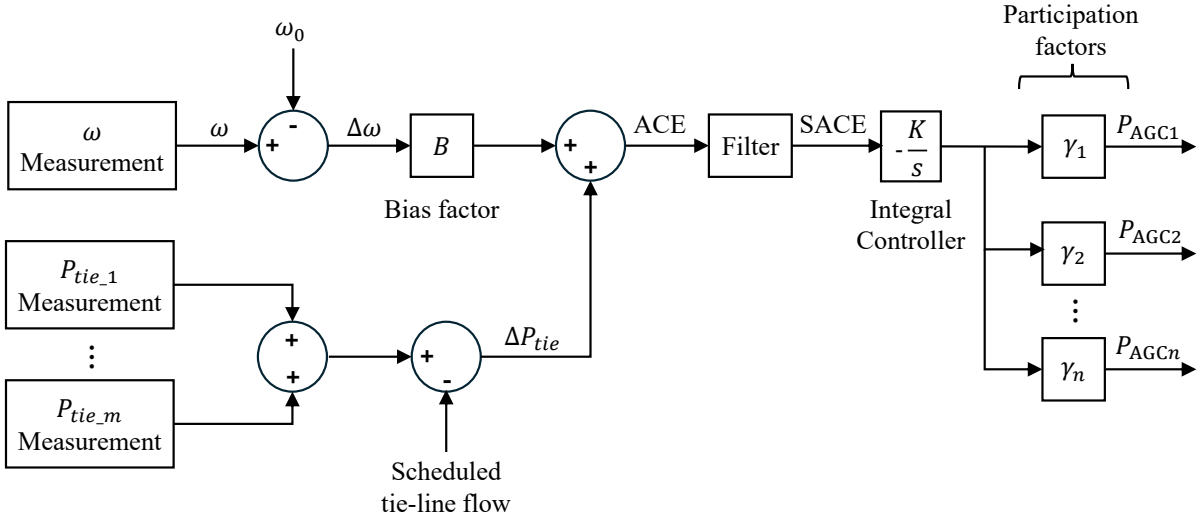

Figure 2.16. Block diagram of the AGC with participation factors. Own work.

Subsequently, the frequency deviation is weighted by the frequency-bias factor B, as defined in equation (2.31). The resulting ACE can thus be expressed as the algebraic sum of the weighted frequency deviation and the tie-line interchange deviation.

To prevent excessive or unnecessary actuation of the AGC, the ACE signal is passed through a low-pass filter. This stage smooths out high-frequency oscillations and small random variations in demand, producing the so-called smoothed area control error (SACE). The use of this filter avoids continuous small adjustments in the set-points of generating units, thereby reducing mechanical wear on turbine valves and extending the lifetime of control equipment.

The filtered signal is then processed by a secondary controller, which in its simplest form is an integral controller designed to drive the ACE to zero in steady state, thereby restoring both system frequency and scheduled power exchanges. In practice, this controller is often implemented as a PI or PID controller to accelerate error correction and improve damping and settling time, with the specific choice depending on the trade-off between simplicity, robustness, and performance.

The controller output represents the total secondary control effort in the area, which is distributed among the generating units participating in AGC through the participation factors γ_k. These constants define the share of the total AGC command allocated to each unit k, and satisfy the condition shown in equation (2.34), where n denotes the number of generating units assigned to AGC. This formulation ensures that the entire control effort is properly allocated among all participating AGC units.

$$\sum_{k=1}^{n} \gamma_k = 1 \tag{2.34}$$

The participation factors are typically set by the system operator based on economic dispatch criteria (fuel cost), unit availability, and ramping capabilities, so that the resulting allocation achieves both technical feasibility and economic efficiency. In practice, these factors determine how the secondary control effort is shared among the AGC-participating units, ensuring that no single generator is disproportionately loaded and that the response aligns with operational policies. The signals $P_{\mathrm{AGC}k}$ at the output of this stage represent the individual AGC commands for each generating unit k, which are then added to the reference set-points provided by the economic dispatch. In this way, the AGC output integrates seamlessly with the overall scheduling process, allowing the SFC to operate consistently with system-wide optimization objectives.

Chapter 3

Literature Review

This section reviews the technical literature relevant to this thesis. First, Section 3.1 surveys recent advances oriented to enhance AGC performance, highlighting key limitations in dynamic modeling fidelity and network representation. Next, Section 3.2 discusses works that apply the $N-1-1$ criterion to represent sequential contingencies in an operational context, emphasizing their implications for frequency recovery and system security. Then, Section 3.3 offers a brief overview of TS applications to support secure operation under contingencies. Finally, Section 3.4 synthesizes the key findings of the review and positions the main contributions of this study.

3.1 Advances and Challenges in AGC Operation

Power system frequency stability relies fundamentally on maintaining power balance between generation and load. Disturbances, such as generation outages, create imbalances that are initially corrected by the inertial response and by the primary frequency control through droop-governed responses [6]. After the primary frequency control action (15–30 seconds), a steady-state frequency deviation remains, which must be eliminated by the secondary frequency control, commonly implemented by the AGC [6, 11, 12].

Traditionally, AGC has been implemented as a simplified control strategy to maintain the system frequency within acceptable limits when optimal dispatch decisions are not directly available. Enhancing the ability of AGC to allocate regulation responsibilities efficiently under realistic operating conditions has become a growing concern for system operators and researchers [13].

Several works have suggested that the AGC could also contribute to optimizing power distribution among resources by aligning regulation signals with economic dispatch (ED) objectives. Notably, [14] establishes the necessary and sufficient conditions under which regulation participation factors can guarantee that the steady-state outputs of synchronous generators coincide with the global minimum of the ED problem. This duality between frequency regulation and cost efficiency highlights the potential of AGC as not only a stability mechanism but also an economically coordinated control layer.

Recent developments have integrated economic aspects and dc-based power flow constraints into AGC models to better capture system behavior [15–17]. However, these studies still neglect ac transmission characteristics, such as losses and load-voltage dependency, limiting their ability to represent real-world power systems.

Beyond these simplifications, another limitation lies in the transient modeling adopted in AGC studies. Although some references incorporate detailed generator models that include key components such as turbine–governor and excitation systems [3,16,17], many studies adopt simplified reduced-order models. In these cases, the models are implemented in environments such as MATLAB/Simulink [15, 18–23], which do not capture the full power system dynamics during disturbances.

In contrast, industry practices, particularly those followed by system operators and planners, rely on commercial-grade simulation tools like DIgSILENT PowerFactory (PF), PSCAD, or PSS®E. These

platforms offer robust capabilities to model the interaction between active and reactive power, including load-voltage dependency effects, represent steady-state losses, and perform transient simulations that more closely approximate real-system behavior.

Based on the reviewed literature, only three articles have adopted these high-fidelity tools to model AGC under realistic scenarios. For instance, [17] employs PSCAD, while [3] and [16] utilize DIgSILENT PF.

Among these references, the most comprehensive AGC representation is found in [3], which not only leverages a high-fidelity simulation environment but also addresses several modeling challenges identified in prior studies. The authors introduced a stochastic network-constrained AGC scheduling framework under $N-1$ generator contingencies. Key innovations included the incorporation of load-voltage dependency, transmission losses, and the ability to provide both regulation up and regulation down services, achieving a more efficient and economical assignment of AGC responsibilities. The resulting framework was validated through RMS-based simulations in DIgSILENT PF, confirming its effectiveness under transient conditions.

3.2 The N-1-1 Criterion

While the methodology described in [3] represents a significant improvement upon traditional AGC scheduling formulations, critical operational scenarios involving transmission line outages are neglected, whereas the use of corrective network reconfiguration strategies to reduce transmission congestion is also disregarded. These limitations become particularly relevant when moving toward more critical failure scenarios.

Power systems can experience severe disturbances, including sequential contingencies in which a second credible outage occurs before the system has fully recovered. These events are captured by the $N-1-1$ security criterion, which provides a more balanced compromise between robustness and conservatism compared to the traditional $N-1$ security standard.

According to [24] and [25], an $N-1-1$ event assumes that, with an initial condition in which a single generator, transmission circuit, single pole of a dc line, shunt device, or transformer is forced out of service, and following system adjustments, a 3-phase fault occurs on another single generator, transmission circuit, single pole of a different dc line, shunt device, or transformer. This succession of events may cause a dramatic redistribution of power flows and, consequently, severe stresses throughout the network, potentially leading to load shedding or a blackout [7], [26]. By modeling cascading failures, the $N-1-1$ analysis requires swift and adaptable corrective actions, such as generator redispatch and transmission reconfiguration strategies, to maintain power system stability.

Considering the $N-1-1$ security criterion in a steady-state operational condition, most studies focus on optimization-based approaches such as unit commitment (UC), optimal power flow (OPF), or power flow analysis. For example, [27] uses a sequential ac power flow method to simulate cascading outages and apply corrective actions, supporting reliability studies in the balancing area of the U.S. Midwest Independent System Operator (ISO). In [28], a contingency-constrained OPF is solved using a worst-case analysis with fixed UC decisions. In [29], the authors propose a contingency-constrained UC (CCUC) model using a branch-and-cut algorithm, accounting for the adjustment time between failures. More recently, [30] formulates a robust CCUC under renewable uncertainty and worst-case scenarios, solved via a nested column-and-constraint generation method. However, to the best of available knowledge, no prior work has addressed the $N-1-1$ security criterion in the context of frequency regulation using RMS-based transient simulations.

3.3 Transmission Switching Applied in Power System Operation

Given the need for fast and flexible corrective actions under N–1–1 scenarios, incorporating network reconfiguration strategies plays a crucial role in the AGC context. Among the corrective strategies available to handle such scenarios, TS stands out due to its proven benefits in flexibility and operational

efficiency [31]. TS is an ISO-managed operational tool that involves the intentional reconfiguration of the transmission network by opening or closing transmission lines. For instance, the Pennsylvania-New Jersey-Maryland (PJM) system operator has adopted technical operational procedures to identify TS actions that decrease congestion effects [32]. After a contingency, TS can be applied as a corrective measure to mitigate violations at significantly lower cost [33].

However, according to the extensive literature review described in [34], most TS applications are embedded in steady-state optimization frameworks. For example, [35] shows that TS can be integrated into the security-constrained OPF to meet the $N-1$ security criterion. Similarly, in [36], both preventive and corrective TS strategies are incorporated into the security-constrained UC (SCUC) problem, demonstrating their effectiveness in reducing power imbalances and system operating costs. The joint optimization of UC and TS under $N-1$ contingency scenarios is addressed in [37], where results highlight that TS can significantly alter generator schedules and reserve allocations to improve operational costs. Moreover, in [32], the corrective TS formulation is integrated into an SCUC problem to achieve $N-1-1$ compliance.

Unfortunately, to the best of current knowledge, the potential of TS to support AGC-based frequency regulation under transient conditions remains unexplored. This observation calls for a closer examination of how TS could enhance frequency stability in AGC scheduling under $N-1-1$ conditions.

3.4 Summary and Contributions

Table 3.1 extends the summary of recent developments in AGC operation methodologies presented in [3] by integrating the findings of the literature review conducted in this work. The table considers the following aspects: A) thermal limits; B) DC-based power flow formulation (CL for classical, and SF for shift factor); C) power losses included in the power flow problem; D) ramping constraints; E) cascading events; F) use of corrective TS; G) generation controllers such as automatic voltage regulator (AVR) and governor (GOV); H) the largest test system employed; and I) the software used to model and solve the optimization problem (MA for MATLAB, PC for PSCAD and CVX, SC for Simulink and CPLEX, MS for MATLAB and Simulink, MM for MATLAB and MOSEK, DI for DIgSILENT, MG for MATLAB and Gurobi, and PDG for Python, DIgSILENT, and Gurobi). References [17,23] do not report the software used for the dynamic simulation.

Table 3.1. State-of-the-art methodologies comparison

Ref.	A	B	C	D	E	F	G	H	I
[11]	✓	SF	✓	X	X	X	GOV	39-bus	MA
[15]	X	CL	✓	X	X	X	GOV	6-bus	MA
[16]	✓	CL	✓	X	X	X	AVR+GOV	40-bus	DI
[17]	X	CL	X	X	X	X	AVR+GOV	17-bus	PC
[3]	✓	SF	✓	✓	X	X	AVR+GOV	50-bus	PDG
[18]	X	X	X	X	X	X	GOV	118-bus	MG
[19]	✓	CL	X	X	X	X	GOV	24-bus	*
[20]	✓	SF	X	✓	X	X	GOV	118-bus	SC
[21]	X	X	X	X	X	X	GOV	39-bus	MS
[22]	✓	SF	X	✓	X	X	GOV	118-bus	MM
[23]	X	CL	✓	X	X	X	GOV	4-bus	*
This work	✓	SF	✓	✓	✓	✓	AVR+GOV	50-bus	PDG

From columns A-C, it is evident that only a limited number of studies model detailed transmission features (thermal limits, dc power-flow choice, and losses). Considering columns D and G, ramping constraints and generator dynamic controls (AVR, GOV) appear only occasionally. Similarly, columns

E and F show that none of the surveyed works implement corrective TS in coordination with AGC, nor consider cascading events. Column H shows the test power system used by the researchers. Also, notice that the problem size used in this thesis is comparable to those found in the literature using a complete dynamic model of generators (column G). Finally, column I reveals a predominant reliance on MATLAB-based environments, in contrast with commercial-grade tools commonly used by ISOs, such as DIgSILENT PF or PSCAD.

Motivated by the above limitations, this work presents a new approach for AGC scheduling that extends the framework described in [3] by (1) accounting for an $N-1-1$ security criterion involving generator and line outages, and (2) incorporating corrective TS. Thus, compared to [3], the consideration of $N-1-1$ contingency states requires an additional simulation stage to capture the second contingency, whereas the integration of TS involves nontrivial modifications to the optimization model.

In this context, an $N-1-1$ contingency state corresponds to a critical failure of a generating unit followed by a transmission line outage, assuming that the second event happens at the end of the primary frequency control. To represent the effect of the transmission network while considering line tripping and switching, a lossy shift factor-based formulation is adopted, improving the mathematical formulation introduced in [38]. The major modifications include its novel adaptation to the context of frequency regulation and its extension to capture the impact of transmission losses.

The proposed framework integrates a time-domain simulation platform and an optimization problem to determine, off-line, the optimal AGC decisions, i.e., the set of generating units to be scheduled for AGC and their participation factors, along with the optimal corrective TS decisions. The framework uses as inputs the pre-contingency generation schedule and dispatch, together with the set of candidate units for AGC. Moreover, uncertain $N-1-1$ contingency states under different operating conditions are considered as scenarios using two-stage stochastic programming.

Thus, the proposed framework fills the gap revealed by the literature review, namely the need to integrate TS into the AGC operation as a network flexibility mechanism to enable a more economical and resilient schedule of regulation responsibilities under $N-1-1$ events. Accordingly, the main contributions of this thesis are as follows:

1. A novel AGC scheduling framework is developed to include $N-1-1$ events, capturing the impact of a generator failure followed by the outage of a transmission line during the frequency recovery phase. This feature enhances the robustness of the AGC analysis under critical operational conditions.

2. TS is integrated as a corrective action within the AGC framework. By enabling network reconfiguration, TS enhances the economic efficiency and security of the AGC transient response, resulting in a more effective scheduling of regulation responsibilities among AGC candidate units.

Unlike many existing approaches based solely on static modeling or discretized AGC dynamics, the proposed framework is validated through RMS-based simulations in DIgSILENT PF. These simulations are conducted to verify steady-state restoration of nominal frequency and to confirm that TS actions do not cause significant adverse effects on frequency recovery or bus-voltage profiles. In addition, a complementary analysis examines how AGC schedules designed for single-generator outages ($N-1$ conditions) perform when subjected to more severe scenarios involving cascading system failures.

Chapter 4

Proposed Framework for AGC Scheduling Integrating Corrective TS

This chapter presents the proposed framework for AGC scheduling that integrates corrective TS actions. The chapter provides a complete description of the workflow, the information exchanged between modules, and the role of each component in producing an economical and secure schedule under sequential contingency events.

The proposed framework considers a time-domain simulation platform and an optimization problem to determine the optimal AGC decisions. The framework uses as inputs the pre-contingency generation schedule and dispatch, together with the set of candidate units for AGC. Furthermore, uncertain N–1–1 contingency states are solved by a two-stage stochastic programming methodology.

The simulation platform characterizes the system changes caused by an $N-1-1$ event at the end of the PFC, providing this information to the optimization problem. The proposed MILP problem determines the AGC schedule and TS actions. Participation factors are calculated using the results from both the simulation platform and the MILP problem. Finally, the simulation platform is used again to assess transient AGC behavior and the performance of TS actions.

The remainder of this chapter is organized as follows. Section 4.1 discusses the transient modeling considerations of frequency control under sequential contingencies. Section 4.2 presents the formulation of the proposed optimization problem. Section 4.3 details the proposed framework.

4.1 Frequency Regulation and Response under Sequential Contingencies

In this section, the frequency response modeling under $N{-}1{-}1$ events and the dynamic model used to represent AGC operation are technically described in detail.

4.1.1 Frequency Response under an $N-1-1$ Contingency Analysis

Under the adopted methodology, the $N-1-1$ analysis considers a cascading contingency event in which a generating unit outage is followed by a transmission line failure and tripping. Figure 4.1 illustrates the frequency system response for this $N{-}1{-}1$ event, including the application of TS actions in the SFC.

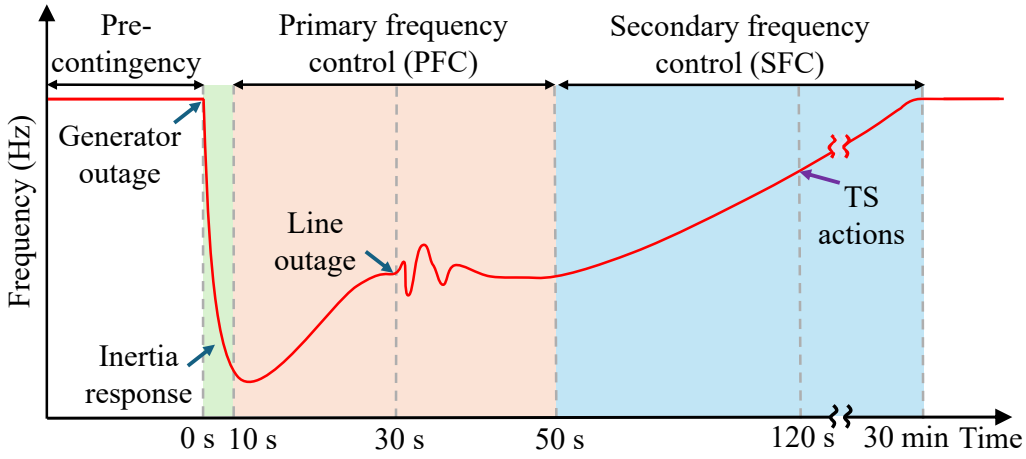

Figure 4.1. System frequency response under an $N-1-1$ event. Own work.

The response is divided into four phases:

(i) In the pre-contingency phase, the power system operates under normal conditions with all elements in service at nominal frequency.

(ii) A frequency oscillation occurs when a generation unit trips at $t = 0$ s, provoking an $N-1$ transient condition. During this phase, inertial and PFC responses begin to stabilize the frequency oscillation.

(iii) During the PFC, a short-circuit event occurs in the middle of a transmission line at $t = 30$ s, leading to an $N-1-1$ condition. We assume that the protection system detects the fault and clears it by opening the circuit breakers at both ends of the line within 110 ms. In the simulation platform, this is represented as a cascading event occurring at $t = 30.11$ s. During this phase, the PFC response achieves a steady-state frequency error that must be corrected in the SFC.

(iv) The subsequent transient phase corresponds to the coordinated post-contingency actions, starting with the activation of the AGC at $t = 50$ s for SFC and followed by TS actions executed by the ISO at $t = 120$ s. The assumed 70-second delay between AGC activation and TS execution accounts for detection, decision-making, and implementation times in real-time operation.

These modeling assumptions capture a realistic $N{-}1{-}1$ transient event, where frequency restoration and TS actions are coordinated to enhance system stability. In these $N-1-1$ simulations, the AGC operation is represented using the scheme described in the following subsection.

4.1.2 AGC Model

In this work, the AGC is designed to act only on the frequency error that remains after PFC has settled. Under the stressed $N-1-1$ conditions, the operating priority is to keep frequency close to nominal rather than to restore tie-line schedules. Compared with the generalized AGC scheme in Figure 2.16, tie-line power deviations are not considered, so that the frequency-bias factor is not necessary. Delays associated with frequency measurement are also neglected.

Figure 4.2 shows the composite DIgSILENT PF frame of the AGC scheme adopted in this work. The composite frame defines the external interface and signal routing for the AGC and contains two slots: (i) a frequency measurement slot with an *ElmPhi* element that computes the system frequency and feeds the signal *fmeas* to the AGC slot, and (ii) an AGC slot with an *ElmAgc* element, whose internal control logic is implemented in the DIgSILENT Simulation Language (DSL).

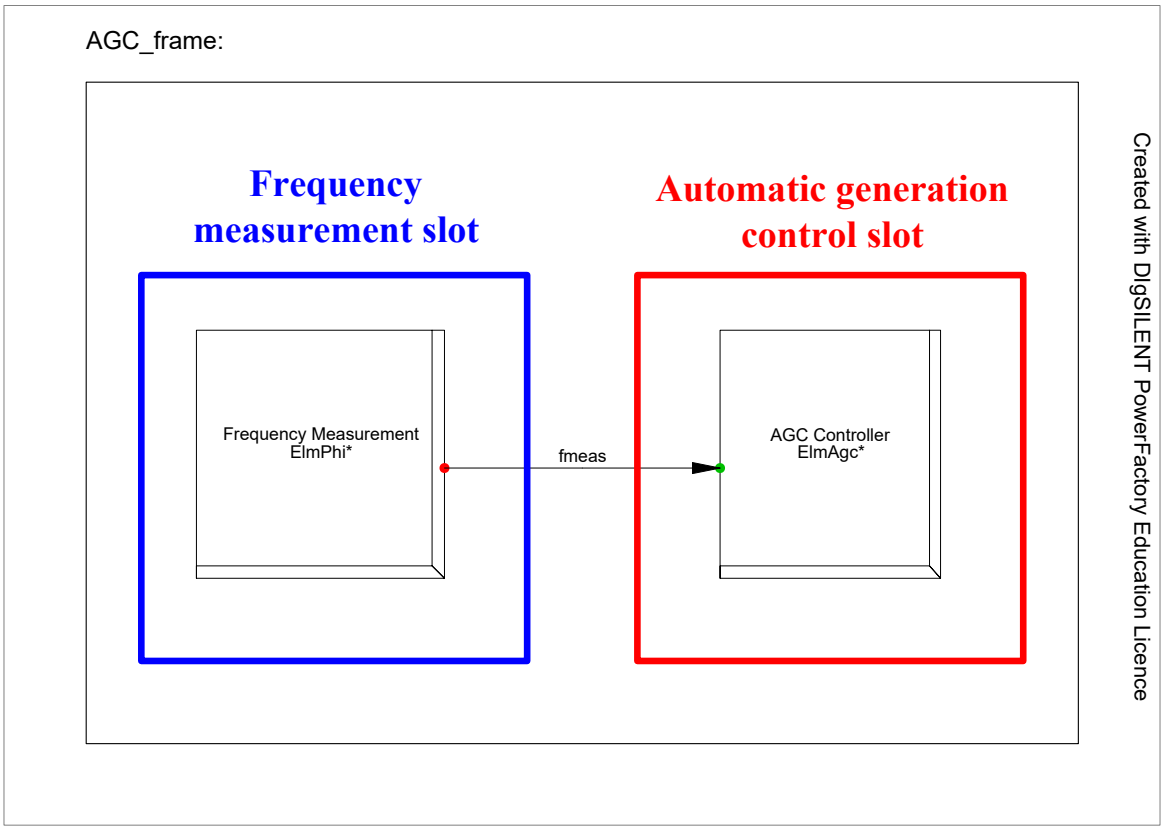

Figure 4.2. AGC composite frame implemented in DIgSILENT PF. Own work.

The internal structure of the AGC, developed in DSL, is shown in Figure 4.3. The frequency deviation is first computed by comparing the measured frequency with its nominal reference. An activation block is included to enable the AGC only after the PFC has settled, thereby avoiding overlap between primary and secondary actions. At the start ($t = 0$ s), the switch is OFF (0), and it is turned ON (1) at $t = 60$ s via a parameter event. In this way, AGC units participate only in SFC. Accordingly, the modeling of RoCoF and nadir characteristics associated with the primary response window is outside the scope of this study.

The ACE signal is then processed by a low-pass filter, implemented as a second-order Butterworth filter with a cutoff frequency of 0.11 Hz, to mitigate high-frequency noise and prevent unnecessary movements in governors and turbine valves. The filtered signal (SACE) is passed to a PI controller that sends different speed changer governor positions to the AGC units, provoking the total secondary control action required in the area. For each $N-1-1$ contingency state s and operating condition k, the PI controller distributes the generation deficit $\sum_{b\in\mathcal{B}} P^{\mathrm{Out}}_{b,s,k}$ among candidate units g according to their participation factors $\gamma_{g,s,k}$. The resulting signals P_{agc} correspond to the individual AGC commands added to the economic dispatch set-points of each unit.

The PI parameters were tuned according to the Ziegler–Nichols method [39], based on a contingency consisting of a 500 MW step load increase under the peak load condition, as in [3]. This method determines that $K_P = 24$ and $K_I = 10$.

To restore frequency to the nominal value in the steady state of each contingency s and operating condition k, the total contribution of AGC units, including regulation up $p^{\mathrm{Up}}_{g,s,k}$ and regulation down $p^{\mathrm{Dn}}_{g,s,k}$, must supply the generation deficit $\sum_{b\in\mathcal{B}} P^{\mathrm{Out}}_{b,s,k}$, as expressed in (4.1).

$$\sum_{g\in G^{\mathrm{AGC}}} \left(\Delta p^{\mathrm{Up}}_{g,s,k} - \Delta p^{\mathrm{Dn}}_{g,s,k}\right) = \sum_{b\in\mathcal{B}} P^{\mathrm{Out}}_{b,s,k};\ \forall s \in \mathcal{S}, \forall k \in \mathcal{K} \tag{4.1}$$

Last, for each contingency state s and operating condition k, participation factors $\gamma_{g,s,k}$ are calculated as the net regulation up and down contributions of generating unit g normalized by the generation deficit, as expressed in (4.2) [3]:

$$\gamma_{g,s,k} = \left(\Delta p^{\mathrm{Up}}_{g,s,k} - \Delta p^{\mathrm{Dn}}_{g,s,k}\right) \Big/ \sum_{b\in\mathcal{B}} P^{\mathrm{Out}}_{b,s,k};\ \forall g \in \mathcal{G}^{\mathrm{AGC}},\ \forall s \in \mathcal{S}, \forall k \in \mathcal{K} \tag{4.2}$$

Note that $\sum_{g\in\mathcal{G}^{\mathrm{AGC}}} \gamma_{g,s,k} = 1\ \forall s \in \mathcal{S}, \forall k \in \mathcal{K}$. Further details on AGC modeling and implementation can be found in [6] and [3].

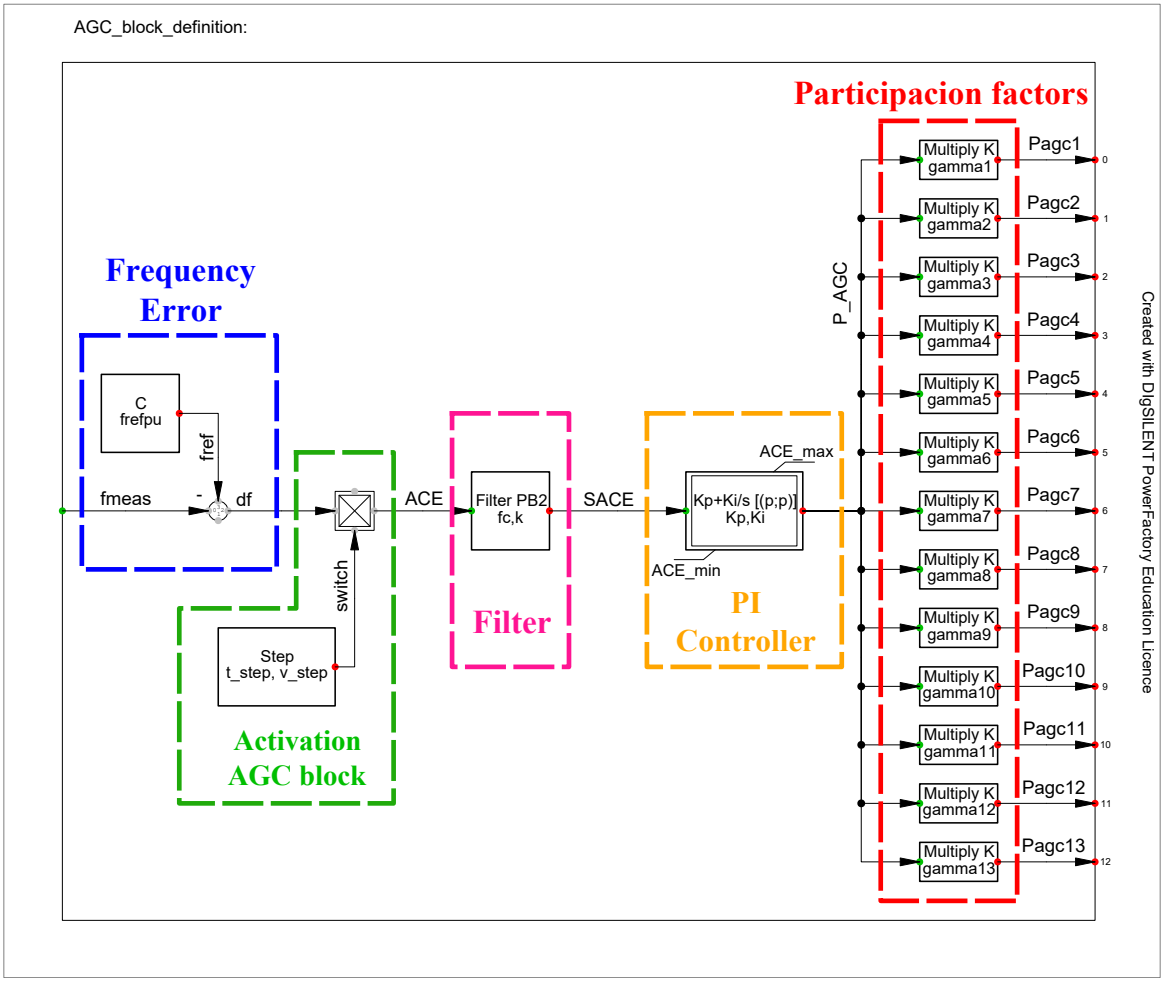

Figure 4.3. AGC scheme implemented in DIgSILENT PF. Own work.

4.2 Optimization Problem for AGC Scheduling with Corrective TS

This section describes the proposed two-stage stochastic optimization problem for day-ahead AGC scheduling, accounting for uncertain $N-1-1$ scenarios, extending the formulation introduced in [3] and summarized in Appendix B. Uncertainty is represented by a set $\mathcal{S}$ of contingency states (generator and line outages) and a set $\mathcal{K}$ of operating conditions. A scenario is the pair $(s,k) \in \mathcal{S} \times \mathcal{K}$ with joint probability $\pi_{s,k}$, i.e., the probability that contingency state s occurs under operating condition k.

The structure of the two-stage framework [40] is illustrated in Figure 4.4. First-stage decision variables correspond to the set of AGC units scheduled for regulation up (v_g^{Up}) and regulation down (v_g^{Dn}) across all operating conditions and contingency states. The second stage models system operation under a given contingency state s and operating condition k using a lossy dc power flow, where shift factors are employed to eliminate nodal voltage phase angles [41].

The variables related to the second stage involve the regulation up ($\Delta p_{g,s,k}^{\mathrm{Up}}$) and regulation down ($\Delta p_{g,s,k}^{\mathrm{Dn}}$) adjustments of AGC candidate units, the energy not supplied ($p_{b,s,k}^{\mathrm{Ue}}$), the branch power flows ($f_{l,s,k}$) together with their nonnegative components ($f_{l,s,k}^{\mathrm{Neg}}$) and ($f_{l,s,k}^{\mathrm{Pos}}$), the transmission power losses ($p_{b,s,k}^{\mathrm{Ue}}$), the switching status ($z_{l,s,k}$), and the virtual power flow ($\widetilde{f}_{l,s,k}$) employed to model the transmission switching action.

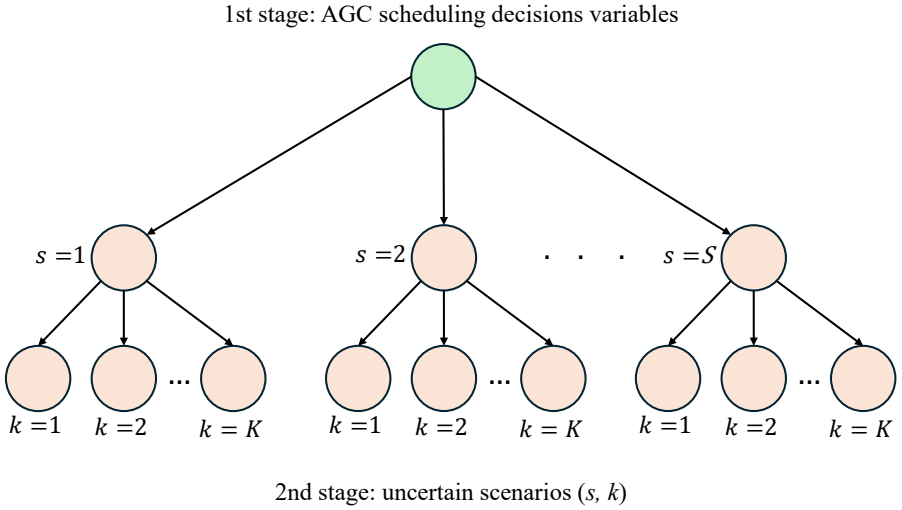

Figure 4.4. Two-stage stochastic framework for AGC scheduling under $N-1-1$ uncertainty. Own work.

4.2.1 Objective Function and Cost-Related Terms

The optimization minimizes the objective function (OF) in (4.3), which represents the total system cost. The OF comprises two components: (i) the scheduling cost associated with the AGC service and (ii) the expected operational cost.

The cost of AGC scheduling (Csfc) is captured in equation (4.3a). For each contingency state s and operating condition k, the expected operational cost comprises: (i) the fuel cost of AGC units ($\mathrm{Cop}_{s,k}$) given in equation (4.3b); (ii) the unserved energy cost ($\mathrm{Cue}_{s,k}$) defined in (4.3c); (iii) the power losses cost ($\mathrm{Cpl}_{s,k}$) specified in (4.3d); and (iv) the corrective TS cost ($\mathrm{Cts}_{s,k}$) formulated in (4.3e).

$$\mathrm{Min}\ \mathrm{Csfc} + \sum_{s\in\mathcal{S}}\sum_{k\in\mathcal{K}} \pi_{s,k}\left(\mathrm{Cop}_{s,k} + \mathrm{Cue}_{s,k} + \mathrm{Cpl}_{s,k} + \mathrm{Cts}_{s,k}\right) \tag{4.3}$$

$$\mathrm{Csfc} = \sum_{g\in\mathcal{G}^{\mathrm{AGC}}} C_g^{\mathrm{SFC}}\left(v_g^{\mathrm{Up}} + v_g^{\mathrm{Dn}}\right) \tag{4.3a}$$

$$\mathrm{Cop}_{s,k} = \sum_{g\in\mathcal{G}^{\mathrm{AGC}}} C_g^{\mathrm{Fuel}}\Big(\Delta p_{g,s,k}^{\mathrm{Up}} + \Delta p_{g,s,k}^{\mathrm{Dn}}\Big);\ \forall s\in\mathcal{S},\ \forall k\in\mathcal{K} \tag{4.3b}$$

$$\mathrm{Cue}_{s,k} = C^{\mathrm{Ue}} \sum_{b\in\mathcal{B}} p_{b,s,k}^{\mathrm{Ue}};\ \forall s\in\mathcal{S},\forall k\in\mathcal{K} \tag{4.3c}$$

$$\mathrm{Cpl}_{s,k} = C^{\mathrm{L}} \sum_{l\in\mathcal{L}} pl_{l,s,k};\ \forall s\in\mathcal{S},\forall k\in\mathcal{K} \tag{4.3d}$$

$$\mathrm{Cts}_{s,k} = C^{\mathrm{TS}} \sum_{l\in\mathcal{L}^{\mathrm{TS}}} \Big(1 - z_{l,s,k}\Big);\ \forall s\in\mathcal{S},\forall k\in\mathcal{K} \tag{4.3e}$$

In (4.3), power losses are penalized to avoid fictitious losses [3, 42]. This condition is produced in high-congestion transmission conditions. Using this approach, the operational model overcomes inconsistencies of linear lossy formulations, which may lead to impractical solutions. In this work, the value for C^{L} is determined by a sensitivity analysis.

4.2.2 Power Balance Supply

Since this work employs a shift factor formulation [43,44], only a single equality constraint is required to verify system-wide power balance. The DC-based power flow is then written using lossy shift factors and net nodal power injections [45, 46]. In the power flow formulation, voltage-dependent variations on steady-state power losses ($\Delta pl_{l,s,k}^{\mathrm{Volt}}$) and on customer loads ($\Delta D_{b,s,k}^{\mathrm{Volt}}$) are included. Equation (4.3) estimates the power balance constraint at the end of the SFC stage for each contingency state s and operating condition k. The *lhs* represents the total power supplied by units that remain in service, including the regulation up and down adjustments of AGC-participating units and any potential load shedding action, while the *rhs* represents the final demand and network losses, both accounting for voltage-dependent variations.

$$\Big(\sum_{g\in\mathcal{G}} P_{g,k}^{\mathrm{Pre}} - \sum_{b\in\mathcal{B}} P_{b,s,k}^{\mathrm{Out}}\Big) + \sum_{g\in\mathcal{G}^{\mathrm{AGC}}} \Big(\Delta p_{g,s,k}^{\mathrm{Up}} - \Delta p_{g,s,k}^{\mathrm{Dn}}\Big) + \sum_{b\in\mathcal{B}} p_{b,s,k}^{\mathrm{Ue}} = \sum_{b\in\mathcal{B}} \Big(D_{b,k}^{\mathrm{Pre}} - \Delta D_{b,s,k}^{\mathrm{Volt}}\Big) + \sum_{l\in\mathcal{L}} \Big(\mathrm{PL}_{l,k}^{\mathrm{Pre}} - \Delta pl_{l,s,k}^{\mathrm{Volt}}\Big);\ \forall s\in\mathcal{S},\forall k\in\mathcal{K} \tag{4.3}$$

According to [2], the variation in demand due to voltage-dependency at the end of the SFC can be approximated using the pre-contingency demand $D_{b,k}^{\mathrm{Pre}}$ and the demand at the end of the primary response $D_{b,s,k}^{\mathrm{PFC}}$. Hence, $\Delta D_{b,s,k}^{\mathrm{Volt}} \approx D_{b,s,k}^{\mathrm{Pre}} - D_{b,s,k}^{\mathrm{PFC}}$. Similarly, transmission power losses changes due to voltage-dependency are computed as $\Delta pl_{l,s,k}^{\mathrm{Volt}} = \mathrm{PL}_{l,k}^{\mathrm{Pre}} - pl_{l,s,k}$, where it is assumed that the post-contingency steady-state losses are obtained explicitly [2, 3, 45, 46].

Since the pre-contingency operating point satisfies $\sum_{g\in\mathcal{G}} P_{g,k}^{\mathrm{Pre}} = \sum_{b\in\mathcal{B}} D_{b,k}^{\mathrm{Pre}} + \sum_{l\in\mathcal{L}} \mathrm{PL}_{l,k}^{\mathrm{Pre}}$, the balance constraint (4.3) can be reformulated as (4.4) [2, 3]. Note that the net power adjustments provided by AGC units, along with potential load shedding actions, compensate for the power output of the failed generating unit and the variations in load and transmission losses caused by the disturbance.

$$\sum_{g\in\mathcal{G}^{\mathrm{AGC}}} \Big(\Delta p_{g,s,k}^{\mathrm{Up}} - \Delta p_{g,s,k}^{\mathrm{Dn}}\Big) + \sum_{b\in\mathcal{B}} p_{b,s,k}^{\mathrm{Ue}} = \sum_{b\in\mathcal{B}} P_{b,s,k}^{\mathrm{Out}} - \sum_{b\in\mathcal{B}} \Big(D_{b,k}^{\mathrm{Pre}} - D_{b,s,k}^{\mathrm{PFC}}\Big) - \sum_{l\in\mathcal{L}} \Big(\mathrm{PL}_{l,k}^{\mathrm{Pre}} - pl_{l,s,k}\Big);\ \forall s\in\mathcal{S},\forall k\in\mathcal{K} \tag{4.4}$$

4.2.3 Generation Operation and Load Shedding

The power adjustments for AGC units are restricted by expressions (4.5) and (4.6). Generator ramping capabilities are incorporated through (4.7) and (4.8), where the ramp-up and ramp-down limits are determined by the primary frequency response and the pre-contingency dispatch level. It

should be noted that they are influenced by the primary frequency response of each generation unit ($P^{\mathrm{PFC}}_{g,s,k}$) and the pre-contingency condition ($P^{\mathrm{Pre}}_{g,k}$). The binary AGC participation status is captured by (4.9). Last, the unserved energy is bounded by (4.10).

$$0 \leq \Delta p^{\mathrm{Up}}_{g,s,k} \leq \left(P^{\mathrm{Max}}_{g} - P^{\mathrm{Pre}}_{g,k}\right) v^{\mathrm{Up}}_{g};\ \forall g \in \mathcal{G}^{\mathrm{AGC}},\ \forall s \in \mathcal{S},\ \forall k \in \mathcal{K} \tag{4.5}$$

$$0 \leq \Delta p^{\mathrm{Dn}}_{g,s,k} \leq \left(P^{\mathrm{Pre}}_{g,k} - P^{\mathrm{Min}}_{g}\right) v^{\mathrm{Dn}}_{g};\ \forall g \in \mathcal{G}^{\mathrm{AGC}},\ \forall s \in \mathcal{S},\ \forall k \in \mathcal{K} \tag{4.6}$$

$$\Delta p^{\mathrm{Up}}_{g,s,k} \leq RU_g T^{\mathrm{SFC}} + \left(P^{\mathrm{PFC}}_{g,s,k} - P^{\mathrm{Pre}}_{g,k}\right);\ \forall g \in \mathcal{G}^{\mathrm{AGC}},\ \forall s \in \mathcal{S}, \forall k \in \mathcal{K} \tag{4.7}$$

$$\Delta p^{\mathrm{Dn}}_{g,s,k} \leq RD_g T^{\mathrm{SFC}} + \left(P^{\mathrm{Pre}}_{g,k} - P^{\mathrm{PFC}}_{g,s,k}\right);\ \forall g \in \mathcal{G}^{\mathrm{AGC}},\ \forall s \in \mathcal{S}, \forall k \in \mathcal{K} \tag{4.8}$$

$$v^{\mathrm{Up}}_{g}, v^{\mathrm{Dn}}_{g} \in \{0,1\};\ \forall g \in \mathcal{G}^{\mathrm{AGC}} \tag{4.9}$$

$$0 \leq p^{\mathrm{Ue}}_{b,s,k} \leq D^{\mathrm{PFC}}_{b,s,k};\ \forall b \in \mathcal{B},\ \forall s \in \mathcal{S},\ \forall k \in \mathcal{K} \tag{4.10}$$

In Figure 4.5, the graphical representation of the $\Delta p^{\mathrm{Up}}_{g,s,t}$ and $\Delta p^{\mathrm{Dn}}_{g,s,t}$ bounds are observed. To determine the power-down and power-up reserve capacity, a $T^{\mathrm{SFC}} = 15$ minutes is considered. Notice that the time T^{SFC} is used to obtain an adequate steady-state operational AGC condition.

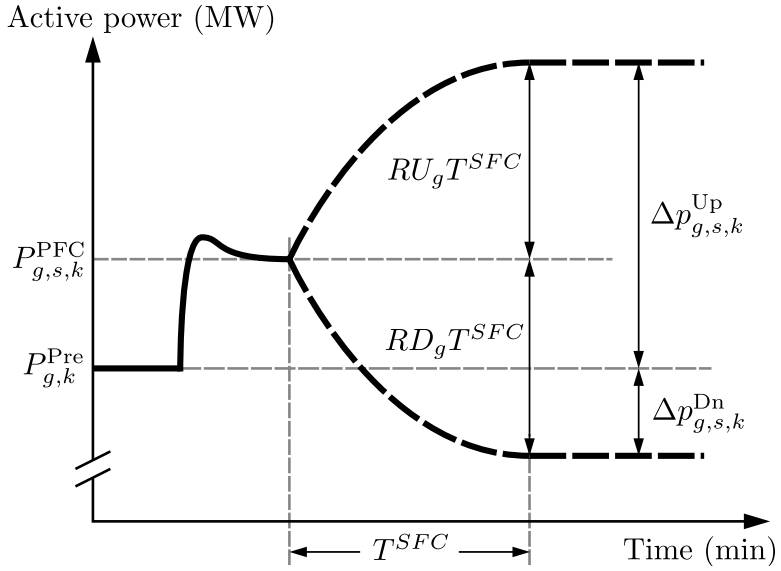

Figure 4.5. Generation limits considering ramp characteristics [3].

4.2.4 Transmission Network Operation

As is customary in operational power system problems, the transmission network is characterized using a lossy shift factor-based dc power flow. Notice that linear shift factors only depend on the topology of the grid [41]. In addition, the lossy power flow formulation distributes 50% of power losses as demand at each bus of the line [45, 46].

To capture the failure of a transmission element under the $N{-}1{-}1$ standard, this work incorporates the methodology proposed in [47] and [48]. Thus, post-contingency $N{-}1{-}1$ power flows are expressed in terms of post-contingency shift factors, which are computed from pre-contingency shift factors and line outage distribution factors (LODF). Using the LODF definition [41] and the notation in the cited references, the post-contingency power flow can be expressed as (4.11):

$$f^{N-1}_{l} = f^{N-0}_{l} + \mathrm{LODF}^{N-0}_{l,o_1}\, f^{N-0}_{o_1} \tag{4.11}$$

where f^{N-0}_{l} and $f^{N-0}_{o_1}$ are the pre-contingency power flows on the monitored line l and the outage line o_1, respectively; f^{N-1}_{l} is the post-contingency flow on line l with line o_1 out; and $\mathrm{LODF}^{N-0}_{l,o_1}$ is the line outage distribution factor for line l given the outage of line o_1.

Using the shift factor transformation, pre-contingency power line flows can be written in terms of net nodal injections. As a result, the post-contingency power flow on line l with line o_1 out is represented by equation (4.12).

$$f_l^{N-1} = \mathrm{SF}_l^{N-1}\mathbf{P_N} \tag{4.12}$$

where $\mathrm{SF}_l^{N-1} = \mathrm{SF}_l^{N-0} + \mathrm{LODF}_{l,o_1}^{N-0}\mathrm{SF}_{o_1}^{N-0}$ is the post-contingency shift-factor row for line l with line o_1 out, and $\mathbf{P_N}$ denotes the vector of net nodal injections.

Given the above, shift factors are indexed by s in this work to reflect their contingency-state dependency. In addition, a big-M-based disjunctive formulation relying on lossy shift factors and virtual power flows is employed to model TS actions. A similar methodology has been previously applied to transmission planning in [49] and to OPF in [38] without including transmission losses.

In comparison with the classical nodal formulation, this modeling strategy reduces the problem size because voltage angles are not included as decision variables, thereby improving the computational performance.

Accordingly, the power flow formulation, which is applied to non-switchable and switchable transmission lines, is modeled as follows:

1) Non-switchable Transmission Elements

Power flows are determined by (4.13) and bounded as specified in (4.14). Binary parameters $A_{l,s,k}$ are incorporated to enforce a zero-flow condition on branches that are out of service under a given $N-1-1$ contingency state.

Expression (4.13) has two components:

(i) The bracketed term, $\sum_{b\in\mathcal{B}} \mathrm{SF}_{l,b,s}[\,\cdot\,]$, gives the post-contingency power flow on branch l at the end of the SFC stage when no corrective TS actions are taken by the algorithm;

(ii) the sensitive term, $\sum_{l''\in\mathcal{L}^{\mathrm{TS}}}(\mathrm{SF}_{l,fr(l''),s} - \mathrm{SF}_{l,to(l''),s})\,\widetilde{f}_{l'',s,k}$, accounts for the incremental change in the power flow on branch l caused by the switching of a candidate branch l''. It uses the difference between the shift factors at the terminals of l'' multiplied by the virtual flow $\widetilde{f}_{l'',s,k}$. Here, $\widetilde{f}_{l'',s,k}$ is injected at $fr(l'')$ and withdrawn at $to(l'')$ in equal magnitude to nullify the branch flow l'', emulating its disconnection.

By superposition, adding both components yields $f_{l,s,k}$, i.e., the post-contingency power flow on branch l at the end of SFC under scenario (s,k) with the selected TS action. If no TS action is taken ($\widetilde{f}_{l'',s,k} = 0;\ \forall l'' \in \mathcal{L}^{\mathrm{TS}}$), the expression obtains the classical dc-based power flow on branch l [41].

$$\begin{aligned} f_{l,s,k} = \sum_{b\in\mathcal{B}} \mathrm{SF}_{l,b,s}\Bigg[\sum_{g\in\mathcal{G}_b} P_{g,k}^{\mathrm{Pre}} - P_{b,s,k}^{\mathrm{Out}} + p_{b,s,k}^{\mathrm{Ue}} + \sum_{g\in\mathcal{G}_b^{\mathrm{AGC}}} \left(\Delta p_{g,s,k}^{\mathrm{Up}} - \Delta p_{g,s,k}^{\mathrm{Dn}}\right) - D_{b,s,k}^{\mathrm{PFC}} - \\ 0.5 \sum_{l'\in\mathcal{L}|fr(l')=b} pl_{l',s,k} - 0.5 \sum_{l'\in\mathcal{L}|to(l')=b} pl_{l',s,k} \Bigg] + \sum_{l''\in\mathcal{L}^{\mathrm{TS}}} (\mathrm{SF}_{l,fr(l''),s} - \mathrm{SF}_{l,to(l''),s})\widetilde{f}_{l'',s,k}; \\ \forall l \notin \mathcal{L}^{\mathrm{TS}},\ \forall s \in \mathcal{S},\ \forall k \in \mathcal{K} \end{aligned} \tag{4.13}$$

$$|f_{l,s,k}| \le F_l^{\mathrm{Max}} A_{l,s,k};\ \forall l \notin \mathcal{L}^{\mathrm{TS}},\ \forall s \in \mathcal{S}, \forall k \in \mathcal{K} \tag{4.14}$$

2) Switchable Transmission Elements

Power flows are defined by (4.15) and limited in (4.16), whereas the associated virtual power flows must satisfy (4.17). In addition, the number of switching actions is bounded by (4.18).

In this case, expression (4.15) has three terms:

(i) The bracketed injection term $\sum_{b\in\mathcal{B}} \mathrm{SF}_{l,b,s}[\,\cdot\,]$;

(ii) The sensitivity term $\sum_{l''\in\mathcal{L}^{\mathrm{TS}}} \left(\mathrm{SF}_{l,fr(l''),s} - \mathrm{SF}_{l,to(l''),s}\right) \widetilde{f}_{l'',s,k}$, which captures the incremental power flow change on branch l caused by the switching of any candidate branch l'';

(iii) The term, $-\widetilde{f}_{l,s,k}$, corresponds to the virtual flow on candidate branch l.

$$f_{l,s,k} = \sum_{b\in\mathcal{B}} \mathrm{SF}_{l,b,s}\Bigg[\sum_{g\in\mathcal{G}_b} P^{\mathrm{Pre}}_{g,k} - P^{\mathrm{Out}}_{b,s,k} + p^{\mathrm{Ue}}_{b,s,k} + \sum_{g\in\mathcal{G}^{\mathrm{AGC}}_b}\left(\Delta p^{\mathrm{Up}}_{g,s,k} - \Delta p^{\mathrm{Dn}}_{g,s,k}\right) - D^{\mathrm{PFC}}_{b,s,k} -$$
$$0.5\sum_{l'\in\mathcal{L}|fr(l')=b} pl_{l',s,k} - 0.5\sum_{l'\in\mathcal{L}|to(l')=b} pl_{l',s,k}\Bigg] + \sum_{l''\in\mathcal{L}^{\mathrm{TS}}} (\mathrm{SF}_{l,fr(l''),s} - \mathrm{SF}_{l,to(l''),s})\widetilde{f}_{l'',s,k} - \widetilde{f}_{l,s,k};$$
$$\forall l\in\mathcal{L}^{\mathrm{TS}},\ \forall s\in\mathcal{S},\ \forall k\in\mathcal{K} \tag{4.15}$$
$$|f_{l,s,k}| \le z_{l,s,k} F^{\mathrm{Max}}_l A_{l,s,k};\ \forall l\in\mathcal{L}^{\mathrm{TS}},\ \forall s\in\mathcal{S},\ \forall k\in\mathcal{K} \tag{4.16}$$
$$|\widetilde{f}_{l,s,k}| \le (1 - z_{l,s,k}A_{l,s,k})M;\ \forall l\in\mathcal{L}^{\mathrm{TS}},\ \forall s\in\mathcal{S},\ \forall k\in\mathcal{K} \tag{4.17}$$
$$\sum_{l\in\mathcal{L}^{\mathrm{TS}}} z_{l,s,k} \ge |\mathcal{L}^{\mathrm{TS}}| - N^{Max};\ \forall s\in\mathcal{S},\forall k\in\mathcal{K} \tag{4.18}$$

The binary variable $z_{l,s,k}$ indicates the service state of a switchable branch. Consequently, two options can be analyzed as follows:

(i) If $z_{l,s,k} = 1$, constraint (4.17) forces $\widetilde{f}_{l,s,k} = 0$, so that $f_{l,s,k}$ equals the sum of the first two terms in (4.15). In other words, the power flow on branch l depends only on the switching contribution in the bracketed term and on the incremental power changes provoked by switching actions on the other candidate branches.

(ii) If $z_{l,s,k} = 0$, constraint (4.16) enforces the post-contingency power flow to zero $f_{l,s,k} = 0$. Substituting this condition into (4.15) and collecting terms yields the balance relation in (4.19). The achieved expression shows that, to emulate the disconnection of branch l by switching, the virtual flow $\widetilde{f}_{l,s,k}$, weighted by the $[1 - (\mathrm{SF}_{l,fr(l),s} - \mathrm{SF}_{l,to(l),s})]$ factor must exactly compensated by the pre-switching contribution captured by the bracketed term, as well as the incremental effects induced by the switching of the other candidate branches.

$$\widetilde{f}_{l,s,k}[1 - (\mathrm{SF}_{l,fr(l),s} - \mathrm{SF}_{l,to(l),s})] = \sum_{b\in\mathcal{B}} \mathrm{SF}_{l,b,s}\Bigg[\sum_{g\in\mathcal{G}_b} P^{\mathrm{Pre}}_{g,k} - P^{\mathrm{Out}}_{b,s,k} + p^{\mathrm{Ue}}_{b,s,k} + \sum_{g\in\mathcal{G}^{\mathrm{AGC}}_b}\left(\Delta p^{\mathrm{Up}}_{g,s,k} - \Delta p^{\mathrm{Dn}}_{g,s,k}\right)$$
$$- D^{\mathrm{PFC}}_{b,s,k} - \quad 0.5\sum_{l'\in\mathcal{L}|fr(l')=b} pl_{l',s,k} - 0.5\sum_{l'\in\mathcal{L}|to(l')=b} pl_{l',s,k}\Bigg] + \sum_{l''\in\mathcal{L}^{\mathrm{TS}}-l} (\mathrm{SF}_{l,fr(l''),s} - \mathrm{SF}_{l,to(l''),s})\widetilde{f}_{l'',s,k};$$
$$\forall l\in\mathcal{L}^{\mathrm{TS}},\ \forall s\in\mathcal{S},\ \forall k\in\mathcal{K} \tag{4.19}$$

3) Power Losses Modeling

For both non-switchable and switchable branches, resistive losses are considered in the mathematical formulation. To this end, the piecewise linear approximation proposed in [45, 46, 50, 51] is adopted. In this formulation, the difference between two non-negative variables, $f^{\mathrm{Pos}}_{l,s,k}$ and $f^{\mathrm{Neg}}_{l,s,k}$, is used to represent the power flow direction, as shown in equation (4.20). Flow limits are enforced by constraints (4.21) and (4.22). The linearized loss function is defined in equation (4.23), where the quadratic behavior of steady-state transmission losses is explicitly approximated using blocks and monotonically increasing slopes. Equation (4.24) ensures that the sum of these blocks is equal to the absolute value of the corresponding flow-related variable $f_{l,s,k}$. Block limits are imposed in (4.25). Expression (4.26) enforces

the non-negativity of variables $f^{\text{Pos}}_{l,s,k}$ and $f^{\text{Neg}}_{l,s,k}$. It is recommended to review [45] and [46] to obtain more details about the lossy power flow formulation.

$$f_{l,s,k} = f^{\text{Pos}}_{l,s,k} - f^{\text{Neg}}_{l,s,k};\ \forall l \in \mathcal{L},\ \forall s \in \mathcal{S},\ \forall k \in \mathcal{K} \tag{4.20}$$

$$f_{l,s,k} + 0.5\, pl_{l,s,k} \leq F^{\text{Max}}_{l};\ \forall l \in \mathcal{L},\ \forall s \in \mathcal{S}, \forall k \in \mathcal{K} \tag{4.21}$$

$$-f_{l,s,k} + 0.5\, pl_{l,s,k} \leq F^{\text{Max}}_{l};\ \forall l \in \mathcal{L},\ \forall s \in \mathcal{S},\ \forall k \in \mathcal{K} \tag{4.22}$$

$$pl_{l,s,k} = \left(G_l/B_l^2\right) \sum_{j \in \mathcal{J}} \left[(2j-1)\frac{F^{\text{Max}}_{l}}{|\mathcal{J}|}\right] \Delta f_{j,l,s,k};\ \forall l \in \mathcal{L},\ \forall s \in \mathcal{S}, \forall k \in \mathcal{K} \tag{4.23}$$

$$\sum_{j \in \mathcal{J}} \Delta f_{j,l,s,k} = f^{\text{Pos}}_{l,s,k} + f^{\text{Neg}}_{l,s,k};\ \forall l \in \mathcal{L},\ \forall s \in \mathcal{S},\ \forall k \in \mathcal{K} \tag{4.24}$$

$$0 \leq \Delta f_{j,l,s,k} \leq \frac{F^{\text{Max}}_{l}}{|\mathcal{J}|};\ \forall l \in \mathcal{L},\ \forall s \in \mathcal{S},\ \forall k \in \mathcal{K} \tag{4.25}$$

$$f^{\text{Pos}}_{l,s,k},\ f^{\text{Neg}}_{l,s,k} \geq 0;\ \forall l \in \mathcal{L},\ \forall s \in \mathcal{S},\ \forall k \in \mathcal{K} \tag{4.26}$$

In summary, the optimization problem minimizes the OF in (4.3) subject to constraints (4.4)–(4.10) and (4.13)–(4.26).

4.2.5 Computing the Regulation Participation Factors

The AGC must compensate not only for the lost generation $\sum_{b \in \mathcal{B}} P^{\text{Out}}_{b,s,k}$ but also for demand variations due to load-voltage dependency $\sum_{b \in \mathcal{B}} (D^{\text{Pre}}_{b,k} - D^{\text{PFC}}_{b,s,k})$ and changes in transmission power losses $\sum_{l \in \mathcal{L}} (\text{PL}^{\text{Pre}}_{l,k} - pl_{l,s,k})$. Thus, after solving the optimization problem, the participation factors $\gamma_{g,s,k}$ are calculated using (4.27), where $\hat{P}^{\text{Out}}_{s,k}$ represents the corrected generation deficit [3]:

$$\gamma_{g,s,k} = \left(\Delta p^{\text{Up}}_{g,s,k} - \Delta p^{\text{Dn}}_{g,s,k}\right) \Big/ \hat{P}^{\text{Out}}_{s,k};\ \forall g \in \mathcal{G}^{\text{AGC}},\ s \in \mathcal{S}, \forall k \in \mathcal{K} \tag{4.27}$$

$$\text{where } \hat{P}^{\text{Out}}_{s,k} = \sum_{b \in \mathcal{B}} P^{\text{Out}}_{b,s,k} - \sum_{b \in \mathcal{B}} \left(D^{\text{Pre}}_{b,k} - D^{\text{PFC}}_{b,s,k}\right) - \sum_{l \in \mathcal{L}} \left(\text{PL}^{\text{Pre}}_{l,k} - pl_{l,s,k}\right).$$

In contrast to (4.2), the corrected generation deficit $\hat{P}^{\text{Out}}_{s,k}$ corresponds to the *rhs* of (4.4), thus capturing the aggregated transient effects on demand and losses. Therefore, it serves as a bridge between power system dynamics and the economic allocation of the AGC regulation responsibilities, since $\gamma_{g,s,k}$ distributes $\hat{P}^{\text{Out}}_{s,k}$ among AGC power units according to the optimization outcome.

4.3 Implementation of the Proposed Framework

The framework takes as inputs the pre-contingency generation schedule and dispatch over a set of demand periods, together with the set of AGC candidate units. These inputs are specified in advance by the ISO. In this study, DIgSILENT PF is used as the time-domain simulation platform, while Gurobi is used to solve the optimization problem. Both components are integrated and exchange data within a Python environment.

The step-by-step implementation of the proposed framework is shown in Figure 4.6, whereas each step is explained in detail below:

(i) First, technical information about each operating condition is uploaded to DIgSILENT PF. Pre-contingency values are stored, including generation outputs ($P^{\text{Pre}}_{g,k}$), bus demands ($D^{\text{Pre}}_{b,k}$), and line losses ($\text{PL}^{\text{Pre}}_{l,k}$). Additionally, post-contingency shift factors are computed for all $N-1-1$ contingency states.

(ii) For each $N-1-1$ contingency state $s \in \mathcal{S}$ and operating condition $k \in \mathcal{K}$, RMS-based simulations are performed in DIgSILENT PF over a 50-second window, considering a generation outage followed by a short-circuit event on a transmission line, according to the sequence and timing described in Section 4.1.1. The resulting bus demands ($D^{\mathrm{PFC}}_{b,s,k}$), generator outputs ($P^{\mathrm{PFC}}_{g,s,k}$), and generation deficits ($P^{\mathrm{Out}}_{b,s,k}$) at the end of the PFC are extracted from DIgSILENT PF using the Python interface.

(iii) Once all combinations of N–1–1 contingency states and operating conditions have been simulated, the optimization problem is formulated using Python and solved by Gurobi. The optimization determines the statuses of AGC units for regulation up and regulation down tasks ($v^{\mathrm{Up}}_g, v^{\mathrm{Dn}}_g$), along with the corresponding power adjustments ($\Delta p^{\mathrm{Up}}_{g,s,k}, \Delta p^{\mathrm{Dn}}_{g,s,k}$). In addition, switching decisions $z_{l,s,k}$ and post-contingency transmission losses $pl_{l,s,k}$ are determined to give technical information to the ISO.

(iv) Participation factors $\gamma_{g,s,k}$ are computed according to (4.27) and loaded into DIgSILENT PF via a parameter event at $t = 0$ s. Additionally, the optimal switching decisions are configured as a switch event at $t = 120$ s. Subsequently, a 420-second transient simulation is executed to verify the system frequency response.

(v) Finally, frequency restoration and operational feasibility are verified for each combination of $N-1-1$ contingency states and operating conditions. The corresponding AGC solutions, namely v^{Up}_g, v^{Dn}_g, and $\gamma_{g,s,k}$, along with all switching decisions $z_{l,s,k}$, are stored in a contingency-specific AGC knowledge database for future reference and operational ISO support.

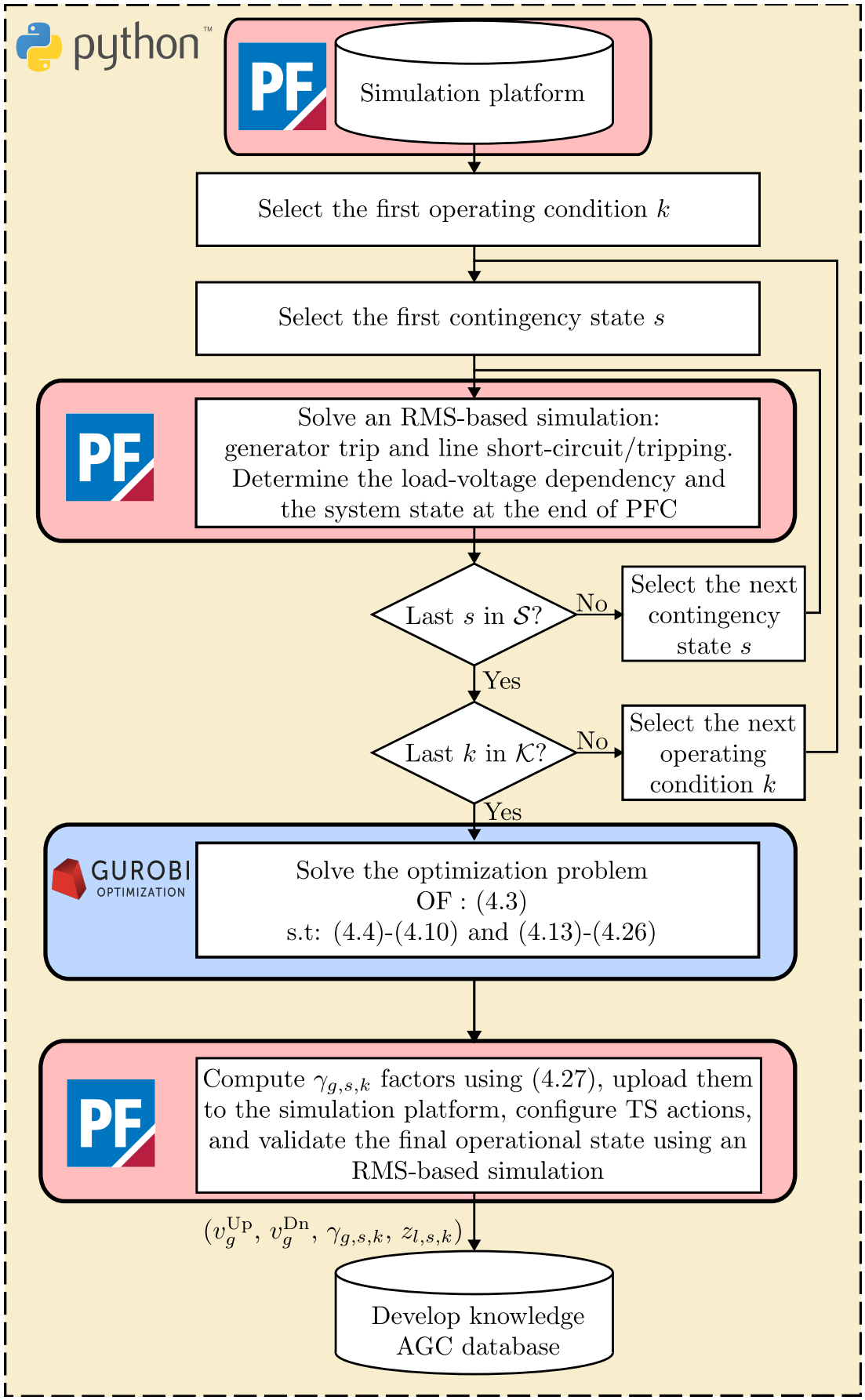

Figure 4.6. Flowchart for the proposed framework. Own work.

Chapter 5

Case Study and Numerical Results

This chapter presents the test system and experimental setup used to validate the proposed framework, establishes the operating conditions and contingency sets to be analyzed, and reports and discusses the resulting economic and technical performance as well as the dynamic behavior. Emphasis is placed on frequency restoration capability, congestion relief via TS, voltage-profile impacts under $N-1-1$ events and those associated with TS actions, and the accuracy of the proposed model relative to RMS validation.

The chapter is organized as follows. Section 5.1 presents the 50-bus case study on which the proposed framework is tested, including the network layout, AGC candidate units and TS candidates, operating conditions, and the $N-1-1$ contingency set. Section 5.2 evaluates an $N-1$ AGC scheduling formulation from the literature by testing its schedules under $N-1-1$ events and discussing the observed limitations.

Section 5.3 reports the results of the proposed framework under $N-1-1$ events, including: (i) an economic cost analysis; (ii) the impact of TS on AGC unit scheduling; (iii) analysis of TS actions across the $N-1-1$ contingency set; (iv) a severity assessment of $N-1-1$ events; (v) an accuracy assessment of the proposed framework against RMS-based simulations; and (vi) a transient-performance assessment covering frequency restoration and voltage response under $N-1-1$ events, including the effect of TS actions.

5.1 Case study

The proposed framework has been applied to a case study based on the 50-bus system previously described in [3]. The system is illustrated in Figure 5.1 and comprises four interconnected zones, 50 electrical buses, 26 synchronous machines, 41 transmission lines, 27 transformers, and 22 loads modeled as constant impedance.

In the power grid, blue circles denote generators that are candidates for AGC: 4 units in zone 1, 2 units in zone 2, 3 units in zone 3, and 4 units in zone 4. Among these candidates, $G4_1$, $G7_1$, $G4_2$, $G4_3$, $G6_3$, $G4_4$ and $G6_4$ are units with steam turbines, whereas $G2_1$, $G3_1$, $G3_2$, $G2_3$, $G2_4$, and $G3_4$ are units with gas turbines. Note that the notation Gx_y indicates the x-th generator located in the y-th zone. Automatic voltage regulator and governor models are included to capture the dynamic behavior of each gas and steam unit. The technical parameters of the system elements, along with the dynamic models of the generating units, are available in Appendix C.

As for the $N-1-1$ criterion, the following contingencies are modeled:

(i) For the first contingency, nine generator outages (marked with red circles) are considered, namely $G4_1$, $G5_1$, $G6_1$, $G2_2$, $G5_2$, $G5_3$, $G3_4$, $G5_4$, and $G7_4$.

(ii) For the second contingency, line failures are selected, ensuring they do not achieve an islanding condition. In cases where parallel lines exist, only a single line can trip. Moreover, the short-circuit event is provoked at the end of the PFC.

As a result, 252 contingency states per operating condition are considered in the two-stage methodology. Each scenario (s, k) is assumed to occur with equal probability, i.e., $\pi_{s,k} = 1/(|\mathcal{S}| \times |\mathcal{K}|)$. In this study, three representative operating conditions of the daily load cycle are considered:

(i) **Peak:** System demand is at its maximum. All loads are set to 100%.

(ii) **Shoulder:** System demand is moderate. All loads are set to 85% of peak with the same proportional factor for each bus.

(iii) **Off-peak:** System demand is at its minimum. All loads are set to 70% of peak and scaled proportionally for each bus.

For each operating condition, a lossy OPF is solved using the ISO-provided UC solution to obtain a feasible, economically efficient dispatch subject to generator and network constraints. Table 5.1 presents the technical details for each AGC candidate unit g, including fuel and SFC participation costs (C_g^{Fuel}, C_g^{SFC}), minimum and maximum power limits (P_g^{Min}, P_g^{Max}), and ramp limits (RU_g/RD_g). The table also reports the pre-contingency AGC dispatch for the three operating conditions: off-peak (P_{op}^{Pre}), shoulder (P_{sh}^{Pre}), and peak (P_{pk}^{Pre}).

Moreover, ten candidate lines are considered for the switching problem, namely $L1_1$, $L2_1$, $L4_1$, $L7_1$, $L2_2$, $L7_2$, $L2_4$, $L7_4$, $I1_3^{(1)}$, $I1_3^{(2)}$. In the Lx_y nomenclature, x and y index the line and the zone, respectively. In contrast, the Ix_y nomenclature refers to an inter-zone transmission line, where indices x and y correspond to the interconnected zones. The superscripts (1) and (2) distinguish two parallel circuits connecting the same pair of zones, where both options are treated as independent switching candidates.

To illustrate the benefit of the proposed framework, the analysis is divided into two sections with different objectives. First, the necessity of incorporating an $N-1-1$ criterion in AGC scheduling is empirically demonstrated by evaluating a literature-based model formulated under an $N-1$ criterion. The resulting schedules are then stress-tested against $N-1-1$ events to assess their effectiveness. Subsequently, the proposed framework is applied to assess the impact of TS on AGC performance under $N-1-1$ events. In addition, the accuracy of the proposed framework is evaluated using the steady-state response. In both cases, several instances (Ins) are examined.

Table 5.1. Technical characteristic for the AGC candidate units

Gen	C_g^{Fuel} ($/MWh)	C_g^{SFC} ($)	P_g^{Min} (MW)	P_g^{Max} (MW)	RU_g/RD_g (MW/min)	P_{op}^{Pre} (MW)	P_{sh}^{Pre} (MW)	P_{pk}^{Pre} (MW)
$G2_1$	200	3000	50	520	8	50	400	400
$G3_1$	160	2500	50	520	6	155	420	420
$G4_1$	50	1800	50	500	6	350	350	350
$G7_1$	60	2100	50	500	5	298	299	299
$G3_2$	90	500	50	520	7	400	400	400
$G4_2$	60	2800	50	500	6	400	400	400
$G2_3$	210	1500	50	520	8	50	270	400
$G4_3$	50	3500	50	500	5	400	400	400
$G6_3$	80	4600	50	500	7	400	400	400
$G2_4$	300	12000	50	520	8	50	50	420
$G3_4$	100	1200	50	520	8	400	400	400
$G4_4$	50	5000	50	500	5	400	400	400
$G6_4$	160	3200	50	520	6.5	400	400	400

For the mathematical formulation, a C^{Ue} of \$30,000/MWh is adopted, obtained by multiplying the highest generation cost in the system by a factor of 100, ensuring that its effect remains significant despite being distributed across a large set of scenarios [52–54]. Transmission losses are approximated using six blocks with a value of C^{L} equal to \$500/MWh. Additionally, C^{TS} is set to \$50 for each TS action to reflect breaker operation and maintenance overhead and to improve computational robustness by discouraging spurious, low-benefit switching [38].

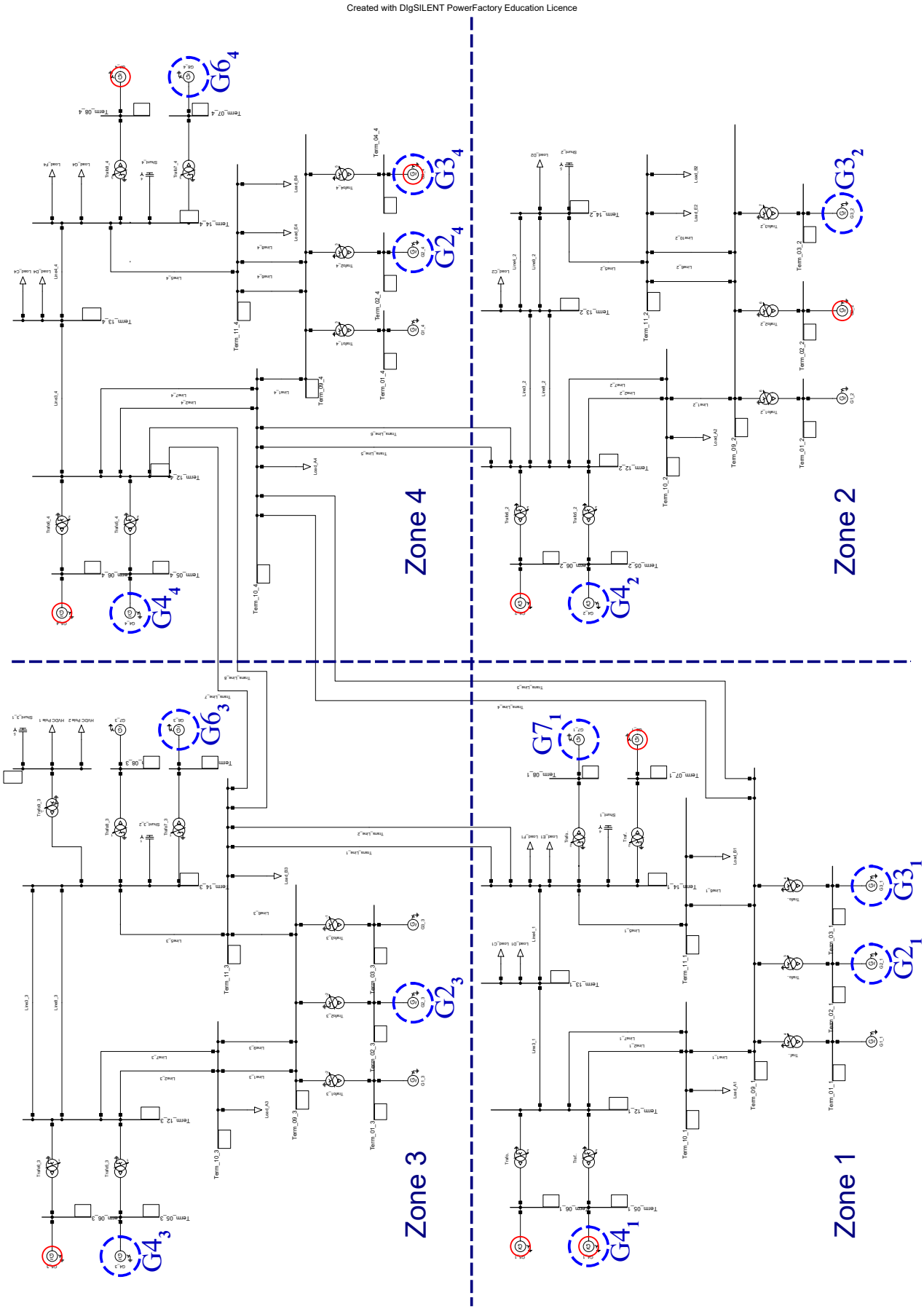

Figure 5.1. Electrical power system test composed of four interconnected zones. Own work.

5.2 Evaluation of $N-1$ AGC Scheduling under $N-1-1$ Events

In this case, the AGC scheduling framework introduced in [3] is solved under an $N-1$ criterion, with the TS problem excluded because the original formulation does not consider it. This $N-1$ analysis examines solely the outage of the aforementioned nine generating units for the three representative load conditions: off-peak, shoulder, and peak. Two instances are solved, referred to as M1 and M2. M1 considers only regulation up (Δp^{Up}), while M2 extends M1 by adding regulation down (Δp^{Dn}).

Simulation results are assessed in terms of economic and computational performance, and the effectiveness of the resulting AGC schedule under $N-1$ events.

5.2.1 Economic Analysis

Table 5.2 summarizes the cost results for each instance obtained by Gurobi. In particular, M2 achieves the minimum total cost, reflecting a reduction of 2.73% compared to M1. This improvement is driven by a 12.78% reduction in SFC costs and a 3.39% decrease in transmission losses. Despite a modest 1.05% increase in operating cost, the overall costs are improved by M2.

Consistent with [3], M2 outperforms M1 because it enables both regulation up and down characteristics, allowing the AGC schedule to shift responsibilities toward cheaper units and relieve flows that contribute to power losses. Under the $N-1$ scenarios considered, both instances exhibit zero unserved energy, confirming the operational feasibility of the AGC schedules.

Table 5.2. Costs under $N-1$ Events

Ins	SFC ($)	Expected Costs			Total ($)
		Operating ($)	Unserved Energy ($)	Losses ($)	
M1	18,000	61,014.90	0.00	75,621.54	154,636.44
M2	15,700	61,654.22	0.00	73,055.42	150,409.64

5.2.2 Computational Performance Analysis

Table 5.6 reports the computational complexity indicators for the two instances, including the number of decision variables (n), constraints (Θ), and non-zero elements. Additionally, it includes the formulation time (t_{for}), the solver time (t_{sol}), and the achieved optimality gap.

Table 5.3. Simulation Performance for $N-1$ Events

Ins	n	Θ	Non-zero	t_{for} (s)	t_{sol} (s)	GAP (%)
M1	20,074	29,619	191,484	0.96	0.82	0.00
M2	20,438	30,321	208,413	0.98	0.93	0.00

As expected, M2 contains more decision variables and constraints than M1 because it includes regulation up and down variables. Accordingly, the number of non-zero elements is also higher. Despite the larger model size, both instances achieve formulation and solution times below 1 s and terminate with a zero optimality gap. These results indicate that the $N-1$ analysis could support real-time power system applications.

5.2.3 Transient response against $N-1-1$ events

Table 5.4 presents the resulting AGC schedules. As can be seen, both instances schedule five regulation up units, with M2 additionally scheduling one regulation down unit. Note, however, that the selected regulation up units differ across the two instances.

Table 5.4. AGC Unit Schedule under $N-1$ Events

Ins	Regulation Up	Regulation Down
M1	$G4_2$, $G4_3$, $G4_4$, $G6_3$, $G7_1$	–
M2	$G3_2$, $G4_2$, $G4_3$, $G4_4$, $G7_1$	$G4_1$

To assess the performance of these schedules under cascading failures, the occurrence of two additional events for the peak condition are simulated: (i) an $N-1$ event only involving the outage of generator $G6_1$ at $t = 10$ s, and (ii) an $N-1-1$ event comprising the outage of generator $G6_1$ at $t = 10$ s and the transient failure of line $L6_1$ after the PFC response (at $t = 40$ s). Notice that the short-circuit is cleared by the protection system at $t = 40.11$ s (110 ms). For visualization purposes, all events are initialized 10 s later than the time specified in Subsection 4.1.1.

The solutions of M1 and M2 allow the system to restore the frequency to its nominal value at the end of the SFC after both $N-1$ and $N-1-1$ contingency states. The key difference lies in the impact on the network loading. Figure 5.2 illustrates the loading of line $L3_1$ for each instance under both disturbances. As can be seen, the $N-1$ event causes a temporary overload of 103.00% on line $L3_1$ at the end of the PFC, which is quickly mitigated by the AGC in M1 and M2, decreasing the transmission loading to 97.60% and 96.34%, respectively. By contrast, the cascading outage of generator $G6_1$ and line $L6_1$ results in a sustained overload of 126.90% along the PFC, which is reduced in the SFC to a transmission loading of 119.40% and 119.20% for M1 and M2, respectively.

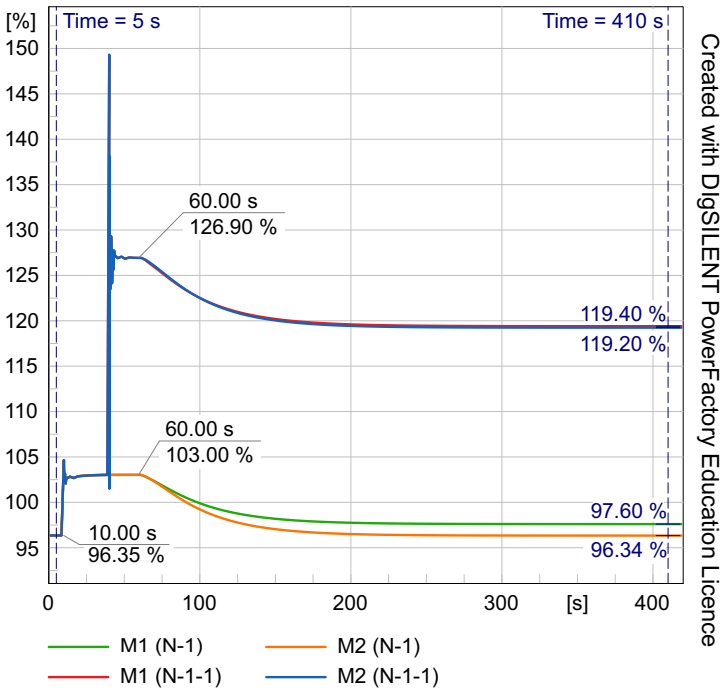

Figure 5.2. Loading evolution of line $L3_1$ under $N-1$ ($G6_1$ outage) and $N-1-1$ ($G6_1$ + $L6_1$ outage) contingency states at peak load condition. Own work.

These results show that, although the M1 and M2 AGC schedules effectively restore frequency and handle single-generator contingencies, they cannot ensure secure transmission operation under $N-1-1$

events. At the observed overloading level, line $L3_1$ could remain in service for 10–15 minutes before the ISO intervenes to mitigate transmission overloading. The ISO considers load shedding and corrective redispatch as corrective options.

If the transmission overloading continues, the system protection on line $L3_1$ will operate, removing the line and further stressing the network. The resulting conditions could trigger cascading trips and jeopardize system stability, potentially leading to a partial or a power system blackout.

5.3 Proposed Framework under $N-1-1$ Events

For this second analysis, the effectiveness of the proposed framework is evaluated for the above-described 252 $N-1-1$ contingency states and the three load conditions. Four instances of the proposed optimization model are considered, referred to as M3, M4, M5, and M6.

(i) M3 includes regulation up and neglects TS.

(ii) M4 aggregates regulation down and neglects TS.

(iii) M5 allows one TS action per $N-1-1$ contingency state combined with regulation up.

(iv) M6 extends M5 by also considering regulation down.

Simulation results are evaluated, focusing on economic evaluation, scheduling of AGC units, analysis of TS actions across scenarios, the severity of $N-1-1$ scenarios, the accuracy of the proposed model, and the transient influence of the proposed framework.

5.3.1 Economic Analysis

Table 5.5 summarizes the costs obtained by Gurobi for each instance. As can be seen, M5 and M6 achieve the lowest total costs, representing cost reductions of 50.76% and 50.82% compared to M3, and 17.92% and 18.02% relative to M4, respectively. Moreover, M5 and M6 fully eliminate the need for unserved energy, unlike M3 and M4. This is achieved by employing corrective TS actions, which reconfigure the transmission network to mitigate overloads and increase transfer capability to load buses.

Table 5.5. Costs under $N-1-1$ Events

Ins	SFC ($)	Expected Costs				Total ($)
		Operating ($)	Unserved Energy ($)	Losses ($)	TS ($)	
M3	23,200	62,127.98	134,817.69	86,857.07	–	307,002.74
M4	31,700	62,613.29	10,964.30	78,891.14	–	184,168.73
M5	10,700	60,136.54	0.00	80,270.51	60.12	151,167.17
M6	11,200	60,316.01	0.00	79,404.21	60.32	150,980.54

In terms of operating costs, models M5 and M6 report expected values of \$60,136.54 and \$60,316.01, corresponding to reductions of 3.2% and 2.9% compared to M3, and 4.0% and 3.7% compared to M4. The SFC cost decreases significantly to \$10,700 and \$11,200 for M5 and M6, representing reductions of 53.9% and 51.7% compared to M3, and 66.3% and 64.7% relative to M4. The TS drives this improvement in the AGC allocation of regulation responsibilities. By relieving the overload and redirecting flows, TS concentrates the required response on a smaller and cheaper set of units.

Regarding losses costs, M5 incurs a value of \$80,270.51, representing a 7.6% reduction compared to M3, but a slight increase of 1.7% relative to M4. Similarly, M6 reports a cost of \$79,404.21, which is

8.6% lower than M3 but 0.7% higher than M4. This modest increase in expected transmission losses compared to M4 is attributed to the elimination of unserved energy in M5 and M6. Because demand is fully supplied, power transfers are higher than in M4, which raises line loading and, consequently, resistive losses.

The introduction of the corrective TS in M5 and M6 adds a marginal cost of about \$60, which corresponds to the implementation of around 300 switching actions across all scenarios. Despite its low cost, this additional action plays a decisive role by enhancing the quality of the solution and enabling significant overall cost reductions.

In summary, TS not only eliminates unserved energy but also improves system economic performance by reducing expected operational and SFC costs, thereby validating its effectiveness under critical conditions. A detailed analysis of the TS actions is presented later.

5.3.2 Computational Performance Analysis

Table 5.6 reports the computational complexity indicators for all instances. As expected, M5 and M6 exhibit a moderate increase in model size and computational burden compared to M3 and M4. This growth is attributed to the incorporation of binary variables as well as the formulation of virtual power flows required to model the TS. Specifically, compared to M3, the number of decision variables and constraints in M5 increases by approximately 2.7% and 2.2%, respectively. Similarly, M6 exhibits a 2.6% increase in decision variables and a 2.2% increase in constraints relative to M4.

Table 5.6. Simulation Performance for $N-1-1$ Events

Ins	n	Θ	Non-zero	t_{for} (s)	t_{sol} (min)	GAP (%)
M3	561,721	827,874	5,145,984	18.48	1.18	0.0000
M4	571,562	847,530	5,523,093	19.46	1.44	0.0000
M5	576,841	846,450	5,332,824	32.42	78.42	0.0152
M6	586,682	866,106	5,709,933	24.75	111.67	0.0734

While the t_{for} remains comparable across all instances, the t_{sol} for M5 and M6 increases significantly, reaching 78.42 and 111.67 minutes, respectively. This increase is given by the higher complexity, remaining acceptable considering the off-line nature of the proposed framework. Nevertheless, M5 and M6 provide feasible and high-quality solutions, with optimality gaps remaining below 0.1%.

5.3.3 Analysis of AGC Unit Scheduling

Table 5.7 presents the scheduling of AGC responsibilities for the four instances. Note that M3 and M4 schedule eight and nine regulation up units, respectively, with M4 additionally scheduling three regulation down units. In contrast, both M5 and M6 schedule five regulation up units, with M6 additionally scheduling one regulation down unit. Despite the greater number of scheduled units in M3 and M4, neither instance avoids unserved energy, whereas M5 and M6 achieve a more secure power system operation.

The superior performance featured by M5 and M6 is enabled by the flexibility provided by TS, which reduces network congestion and allows more economical generating units to be scheduled. As a result, this decongestion effect translates into lower operational costs, as evidenced by the reductions in operating costs reported in Table 5.5. Moreover, SFC cost is also reduced due to more effective AGC deployment, further contributing to the overall cost savings achieved by M5 and M6 compared to M3 and M4.

Table 5.7. AGC Unit Schedule under $N-1-1$ Events

Ins	Regulation Up	Regulation Down
M3	$G2_3$, $G3_2$, $G4_2$, $G4_3$, $G4_4$ $G6_3$, $G6_4$, $G7_1$	–
M4	$G2_3$, $G3_2$, $G3_4$, $G4_2$, $G4_3$ $G4_4$, $G6_3$, $G6_4$, $G7_1$	$G2_1$, $G3_1$, $G4_1$
M5	$G3_2$, $G4_1$, $G4_2$, $G4_3$, $G7_1$	–
M6	$G3_2$, $G4_1$, $G4_2$, $G4_3$, $G7_1$	$G3_2$

5.3.4 Analysis of Transmission Switching Actions

Table 5.8 reports how often each candidate line was switched under the $N-1-1$ scenarios for the M5 and M6 instances. As shown, switching decisions are concentrated under shoulder and peak load conditions, with negligible usage under off-peak conditions. In M5, under peak conditions, there are 168 of 303 actions (55.45%) and under shoulder conditions 133 (43.90%), with only 2 under off-peak conditions. M6 exhibits a similar distribution: 169 of 304 under peak conditions (55.60%), 132 under shoulder conditions (43.42%), and 3 under off-peak conditions (1.0%). These results indicate that TS actions are primarily required by higher loading system conditions.

Table 5.8. Number of TS Actions across $N-1-1$ Events

	M5			M6		
Line	Off-peak	Shoulder	Peak	Off-peak	Shoulder	Peak
$L1_1$	1	127	2	1	122	–
$L2_1$	–	–	–	–	–	–
$L4_1$	–	4	166	1	4	168
$L7_1$	–	–	–	–	–	–
$L2_2$	–	–	–	–	–	–
$L7_2$	–	–	–	–	–	–
$L2_4$	1	1	–	1	3	–
$L7_4$	–	–	–	–	–	–
$I1_3^{(1)}$	–	1	–	–	3	1
$I1_3^{(2)}$	–	–	–	–	–	–
Total	2	133	168	3	132	169

Simulation results also show that the switching selection is highly concentrated on a small subset of transmission elements. Line $L4_1$ dominates under peak load conditions for both instances and appears consistently under shoulder conditions, identifying $L4_1$ as the principal reconfiguration lever under stressed conditions. Line $L1_1$ exhibits substantial activity under shoulder conditions and little to no activity under peak load conditions, suggesting a complementary role that is most effective outside the most heavily loaded conditions. Other candidates play marginal roles: $L2_4$ is barely used under off-peak and shoulder conditions, and the interface element $I1_3^{(1)}$ appears occasionally. Several candidates are never selected across all scenarios ($L2_1$, $L7_1$, $L2_2$, $L7_2$, $L7_4$, $I1_3^{(2)}$), indicating low marginal benefit under the tested conditions.

Comparing M5 and M6, the total number of switching actions is essentially unchanged (303 vs. 304). Hence, enabling down-regulation does not reduce reliance on TS but slightly alters the selection of lines during peak and shoulder periods. In particular, $L1_1$ is not selected in M6.

5.3.5 Influence of Transmission Switching Cost

To quantify the impact of switching costs, instance M6 is solved for different values of $C^{\mathrm{TS}} \in \{0, 50, 100, 500, 1000\}$. Simulation results are evaluated considering the 252 $N-1-1$ contingency states for the three load conditions.

The results are shown in Table 5.9. As can be seen, total cost increases monotonically with C^{TS}, reflecting both the explicit TS charge and the indirect effect of reduced topological flexibility. While the SFC cost remains unchanged ($11,200) and the AGC schedule is invariant across runs, the number of TS actions drops markedly as the penalty rises (from 520 to 194). With fewer switching options, operating costs increase modestly because redispatch must rely more on costlier configurations, whereas expected losses decline slightly. Note that all solutions yield zero unserved energy.

In practical terms, higher values of C^{TS} limit topology reconfiguration, increasing system congestion, and then operating costs. Conversely, low switching penalties enable more frequent TS actions, improving congestion and operating costs at the expense of a small increase in power losses.

Regarding computational performance, solution times are similar to the baseline with $C^{\mathrm{TS}} = 50$. Across the tested values, they differ by less than about 40 minutes. The differences are mostly explained by the final optimality gap. Cases with a large final gap are solved faster (e.g., $C^{\mathrm{TS}} = 1000$). However, all cases remain tractable.

Table 5.9. Impact of TS Penalty on Costs, Switching Actions, and Computational Metrics under the $N-1-1$ Events for M6

C^{TS}	SFC	Expected Costs				Total	TS	t_{sol}	GAP
		Operating	Unserved	Losses	TS				
	($)	($)	Energy ($)	($)	($)	($)	(#)	(min)	(%)
0	11,200	60,275.38	0.00	79,395.40	0.00	150,870.78	520	107.06	0.0679
50	11,200	60,316.01	0.00	79,404.21	60.32	150,980.54	304	116.67	0.0734
100	11,200	60,327.76	0.00	79,396.85	113.89	151,038.50	287	95.90	0.0694
500	11,200	60,533.73	0.00	79,251.20	434.52	151,419.45	219	120.84	0.0413
1000	11,200	60,718.46	0.00	79,172.19	769.84	151,860.49	194	78.02	0.2432

5.3.6 Severity Assessment of $N-1-1$ Scenarios

This subsection examines the network effects observed in all simulations to identify the most severe $N-1-1$ contingency states for the three operating conditions. Peak results are presented in Table 5.10, shoulder results in Table 5.11, and off-peak results in Table 5.12. In each table, the ten highest loadings for the corresponding operating condition are reported, including the pre-contingency value, the loading after the generator outage, and the loading after the subsequent line outage.

Under the peak condition (Table 5.10), the most severe case occurs on line $L3_1$ under the sequential outages $G6_1/L6_1$. Loading increases from 96.35% in pre-contingency to 103.00% after the generator outage and reaches 126.90% after the line outage. The transmission contingency provoked the higher overloading condition. Another severe case occurs at interface $I2_4^{(1)}$ under the $G5_2/I2_4^{(2)}$ sequential event, where loading exceeds the thermal limit and reaches 102.47%. Several additional cases achieve a loading between 90 to 98 percent after line outages, reducing operating margin even when the thermal limit is not exceeded.

For the shoulder condition (Table 5.11), the most stressed case occurs on line $L3_1$ under $G6_1/L6_1$. Loading increases from 90.15% in pre-contingency to 97.53% after the generator outage and reaches 115.77% after the line outage. The interface $I2_4^{(1)}$ under $G5_2/I2_4^{(2)}$ ends at 99.51%, which indicates that the principal risk materializes only after the second event. The remaining cases stay below 85% after the occurrence of a $N-1-1$ event.

Table 5.10. Top-10 Line Loading Severities across $N-1-1$ Contingency States — Peak Condition

Line	Contingency state	Pre-contingency (%)	Generator Outage (%)	Line Outage (%)
$L3_1$	$G6_1/L6_1$	96.35	103.00	126.90
$I2_4^{(1)}$	$G5_2/I2_4^{(2)}$	31.10	51.71	102.474
$L3_3$	$G5_2/L8_3$	53.65	54.40	98.307
$L1_3$	$G5_3/L9_3$	44.44	55.89	97.196
$L3_4$	$G7_4/L5_4$	52.42	71.51	95.950
$L4_4$	$G5_3/L3_4$	31.99	36.64	93.402
$L5_4$	$G7_4/L3_4$	14.49	24.77	92.701
$L10_2$	$G5_2/L6_2$	48.68	49.34	91.563
$L4_1$	$G5_1/L3_1$	19.04	37.72	91.244
$L9_3$	$G5_3/L5_3$	44.44	55.89	90.684

In the off-peak condition (Table 5.12), the maximum severity occurs at interface $I2_4^{(1)}$ under $G5_2/I2_4^{(2)}$. Loading increases from 31.43% in pre-contingency to 52.54% after the generator outage, achieving an overloading of 104.72% after the line outage. Line $L3_1$ remains highly loaded but subcritical under $G5_3/L7_1$, finishing at 89.54% after the line outage.

Comparing results across operating conditions, two contingency sequences are persistent in the three top ten lists. The pair $G5_2/I2_4^{(2)}$ repeatedly stresses interface $I2_4^{(1)}$, finishing above the thermal limit in peak and off-peak and at 99.51% in shoulder. The pair $G5_2/L8_3$ consistently raises the loading of line $L3_3$, with a final loading condition of 98.30% in peak, 76.79% in shoulder, and 58.97% in off-peak. Line $L3_1$ also appears in the three lists under different contingency pairs, which indicates a possible vulnerability of this element.

In summary, the second line outage contingency is the principal driver of line loading severity, compromising power system security. In critical cases, it accounts for approximately 70 to 77% of the total increase from pre-contingency to the final $N-1-1$ state.

Table 5.11. Top-10 Line Loading Severities across $N-1-1$ Contingency States — Shoulder Condition

Line	Contingency state	Pre-contingency (%)	Generator Outage (%)	Line Outage (%)
$L3_1$	$G6_1/L6_1$	90.15	97.53	115.77
$I2_4^{(1)}$	$G5_2/I2_4^{(2)}$	29.73	50.04	99.510
$L3_2$	$G2_2/L8_2$	38.20	43.13	83.14
$L4_2$	$G2_2/L9_2$	41.73	49.00	82.91
$L1_4$	$G3_4/L3_4$	13.11	18.07	79.58
$L4_4$	$G5_3/L6_1$	28.88	29.08	79.54
$L4_1$	$G5_1/L3_1$	19.38	29.67	77.60
$L6_1$	$G5_3/L3_1$	28.79	34.34	77.55
$L1_1$	$G5_2/L3_1$	14.57	11.66	76.83
$L3_3$	$G5_2/L8_3$	42.01	42.62	76.79

Table 5.12. Top-10 Line Loading Severities across $N-1-1$ Contingency States — Off-peak Condition

Line	Contingency state	Pre-contingency (%)	Generator Outage (%)	Line Outage (%)
$I2_4^{(1)}$	$G5_2/I2_4^{(2)}$	31.435	52.548	104.728
$L3_1$	$G5_3/L7_1$	75.55	83.00	89.54
$L1_1$	$G5_2/L3_1$	11.76	15.70	81.06
$L3_2$	$G2_2/L8_2$	35.24	35.12	67.71
$L4_2$	$G2_2/L9_2$	40.33	39.85	67.50
$L4_4$	$G5_4/L3_4$	26.77	31.30	65.57
$L4_1$	$G5_1/L3_1$	16.71	27.87	63.94
$L3_4$	$G7_4/L5_1$	37.90	57.06	60.40
$L3_3$	$G5_2/L8_3$	32.13	32.79	58.97
$L5_4$	$G7_4/L3_4$	11.57	2.01	55.35

5.3.7 Accuracy of the Proposed Framework

This subsection assesses the consistency between the AGC power requirement ($\mathrm{P}^{\mathrm{AGC}}$), the output of selected AGC units, and the associated operating costs (Cop), as obtained from the M6 instance and from the transient RMS-based validation in DIgSILENT PF. The comparison covers the ten highest-loading contingency states for each operating condition reported in the previous subsection. For most comparisons, the relative error (RE) and the mean absolute percentage error (MAPE) are used. The MAPE) is computed by (5.1).

$$\mathrm{MAPE}(X) = \frac{100}{N} \sum_{i=1}^{N} \left| \frac{x_i^{\mathrm{PF}} - x_i^{\mathrm{M6}}}{x_i^{\mathrm{PF}}} \right| \tag{5.1}$$

where X denotes the quantity under comparison; x_i^{PF} is the value of X obtained from DIgSILENT PF for contingency state i; x_i^{M6} is the corresponding value from the M6 optimization; and N is the number of contingency states. If $x_i^{\mathrm{PF}} = 0$, that case is excluded from the average.

Table 5.13 reports the peak condition results. The average relative error in P^{AGC} between the M6 solution (G) and the transient RMS-based validation (D) across the ten scenarios is 3.29%, and the maximum error is 4.91%. Positive errors indicate that the optimization overestimates the AGC requirement, and as a result, the Gurobi solution yields slightly higher operating costs than the DIgSILENT PF. Last, the cost gap is small and consistent with the observed P^{AGC} deviations.

In addition, generator adjustments track the optimization closely, with a MAPE) of 3.41% ($G4_1$), 3.98% ($G7_1$), 1.40% ($G3_2$), 3.42% ($G4_2$), and 3.30% ($G4_3$). Notably, scenarios that include the TS action on $L4_1$ exhibit an average P^{AGC} error of 3.96%, whereas scenarios without TS show 1.27%. Nevertheless, all errors remain below 5%, indicating accurate representation of the peak-condition.

Table 5.14 presents the shoulder-condition results. The relative error in P^{AGC} averages 2.41% and reaches a maximum of 4.85%. Most scenarios remain below 3%, which indicates a tight match in the AGC requirement under this operating point. Generator adjustments remain close to the optimization targets. The MAPE) by unit is 2.63% for $G4_1$, 4.90% for $G7_1$, 3.62% for $G3_2$, 3.26% for $G4_2$, and 2.54% for $G4_3$, with all values below 5%.

TS is used less frequently than in the peak study because only four scenarios include TS actions, three on $L1_1$ and one on $L4_1$. Contingency states with TS show slightly higher P^{AGC} errors than those without TS, yet all remain under 5%. The cost differences are small and consistent with the observed P^{AGC} deviations, and they are narrower than in the peak condition due to the lower error levels and fewer TS interventions.

Table 5.13. M6 Solution: AGC Adjustments per Selected Unit, TS Action, and Operating Cost under Peak Condition

Contingency state	Sof	$G4_1$ (MW)	$G7_1$ (MW)	$G3_2$ (MW)	$G4_2$ (MW)	$G4_3$ (MW)	P^{AGC} (MW)	RE (%)	Cop ($)	TS
$G6_1/L6_1$	D	7.1	83.9	0.0	97.4	84.4	272.9	2.76	15,457.6	$L4_1$
	G	7.3	86.7	0.0	100.0	86.7	280.6		15,898.5	
$G5_2/I2_4^{(2)}$	D	102.8	87.9	5.4	96.1	88.3	380.5	3.92	21,080.9	$L4_1$
	G	106.9	92.0	5.3	100.0	91.9	396.0		21,933.1	
$G5_2/L8_3$	D	103.1	88.1	64.2	96.1	36.6	388.2	3.21	23,821.6	$L4_1$
	G	107.3	92.2	63.5	100.0	38.1	401.1		24,516.1	
$G5_3/L9_3$	D	102.3	87.8	0.0	96.3	88.4	374.8	3.80	20,582.4	$L4_1$
	G	106.2	91.7	0.0	100.0	91.8	389.6		21,397.2	
$G7_4/L5_4$	D	100.7	58.7	0.0	95.8	86.3	341.5	4.27	18,621.2	$L4_1$
	G	105.1	61.6	0.0	100.0	90.1	356.8		19,453.8	
$G5_3/L3_4$	D	101.0	81.0	0.0	95.2	86.9	364.1	4.91	19,965.4	$L4_1$
	G	106.1	85.5	0.0	100.0	91.2	382.9		20,999.0	
$G7_4/L3_4$	D	102.1	20.1	0.0	99.0	87.4	308.5	1.08	16,615.6	–
	G	103.1	20.4	0.0	100.0	88.3	311.9		16,797.5	
$G5_2/L6_2$	D	101.6	76.4	0.0	95.7	87.2	360.9	4.41	19,766.8	$L4_1$
	G	106.1	80.3	0.0	100.0	91.2	377.6		20,682.0	
$G5_1/L3_1$	D	98.4	89.3	0.0	98.7	89.9	376.4	1.42	20,701.1	–
	G	99.7	91.0	0.0	100.0	91.1	381.8		21,001.9	
$G5_3/L5_3$	D	104.1	89.1	14.9	96.8	89.6	394.4	3.14	22,174.4	$L4_1$
	G	107.5	92.5	14.6	100.0	92.5	407.2		22,869.5	

Table 5.15 presents the off-peak results. Two scenarios, $G2_2/L8_2$ and $G2_2/L9_2$, display negative P^{AGC} because an over-frequency event requires regulation down. In these cases, the required AGC is small in magnitude, and the absolute mismatches are low, 3.1 MW for $G2_2/L8_2$ and 2.6 MW for $G2_2/L9_2$, even though the reported relative errors are 19.32% and 14.80%. Excluding those two contingency states, the average relative error in P^{AGC} falls from 4.58% to 1.45%.

Consistent with the previous conditions, the generator adjustments remain close to the optimization results. The MAPE) by unit is 1.48% for $G4_1$, 7.67% for $G7_1$, 5.53% for $G3_2$, 0.96% for $G4_2$, and 1.37% for $G4_3$. The larger values correspond to units whose outputs differ more between the optimization solution and the dynamic simulation. Moreover, TS appears in only one scenario, involving the switching of $L2_4$ and yielding a P^{AGC} error of 1.84%.

In summary, the proposed framework captures AGC behavior with high fidelity under $N-1-1$ events. Furthermore, TS does not hinder model accuracy, remaining below 5%.

Table 5.14. M6 Solution: AGC Adjustments per Selected Unit, TS Action, and Operating Cost under Shoulder Condition

Contingency state	Sof	$G4_1$ (MW)	$G7_1$ (MW)	$G3_2$ (MW)	$G4_2$ (MW)	$G4_3$ (MW)	P^{AGC} (MW)	RE (%)	Cop ($)	TS
$G6_1/L6_1$	D	96.2	79.1	0.0	6.4	82.2	263.8	4.85	14,046.6	$L1_1$
	G	102.9	82.3	0.0	6.9	85.2	277.3		14,756.2	
$G5_2/I2_4^{(2)}$	D	106.3	0.0	101.3	97.7	91.6	396.9	1.04	24,874.2	$L1_1$
	G	108.8	0.0	98.5	100.0	93.7	401.0		24,993.4	
$G2_2/L8_3$	D	95.7	62.0	0.0	98.7	90.0	346.4	2.08	18,924.9	–
	G	96.9	65.6	0.0	100.0	91.2	353.7		19,341.2	
$G2_2/L9_2$	D	95.4	60.7	0.0	98.7	89.9	344.7	2.11	18,826.5	–
	G	96.7	64.3	0.0	100.0	91.1	352.1		19,248.0	
$G3_4/L3_4$	D	88.8	73.8	14.8	81.7	76.6	335.8	4.35	18,934.3	$L4_1$
	G	91.2	74.9	14.2	88.7	82.1	351.0		19,754.3	
$G5_3/L6_1$	D	103.6	86.2	0.0	94.6	89.2	373.7	4.79	20,490.8	$L1_1$
	G	108.0	92.9	0.0	98.6	93.0	392.4		21,537.0	
$G5_1/L3_1$	D	105.9	88.1	0.0	96.7	91.2	382.0	2.21	20,946.5	–
	G	105.0	92.8	0.0	100.0	92.8	390.6		21,457.5	
$G5_3/L3_1$	D	0.0	88.7	101.8	98.8	91.8	381.1	0.63	25,000.1	–
	G	0.0	92.8	97.8	100.0	92.9	383.5		25,015.3	
$G5_2/L3_1$	D	0.0	89.6	116.3	99.0	92.7	397.6	0.28	26,421.9	–
	G	0.0	93.6	111.6	100.0	93.6	398.8		26,339.4	
$G5_2/L8_3$	D	107.6	89.9	18.5	98.7	92.9	407.5	1.82	22,998.6	–
	G	109.0	94.1	17.8	100.0	94.1	415.0		23,403.1	

Table 5.15. M6 Solution: AGC Adjustments per Selected Unit, TS Action, and Operating Cost under Off-peak Condition

Contingency state	Sof	$G4_1$ (MW)	$G7_1$ (MW)	$G3_2$ (MW)	$G4_2$ (MW)	$G4_3$ (MW)	P^{AGC} (MW)	RE (%)	Cop ($)	TS
$G5_2/I2_4^{(2)}$	D	114.1	0.0	120.0	100.0	73.2	407.3	-1.44	26,167.2	–
	G	110.6	0.0	120.0	100.0	70.9	401.6		25,878.0	
$G5_3/L7_1$	D	105.8	91.1	2.3	98.8	94.0	392.0	1.84	21,592.9	$L2_4$
	G	107.1	95.0	2.3	100.0	95.1	399.3		22,006.7	
$G5_2/L3_1$	D	0.0	92.4	120.0	99.5	95.3	407.2	0.04	27,078.6	–
	G	0.0	95.7	115.9	100.0	95.7	407.3		26,957.8	
$G2_2/L8_2$	D	0.0	0.0	-19.0	0.0	0.0	-19.0	-19.32	1,710.0	–
	G	0.0	0.0	-15.9	0.0	0.0	-15.9		1,433.1	
$G2_2/L9_2$	D	0.0	0.0	-20.3	0.0	0.0	-20.3	-14.80	1,824.3	–
	G	0.0	0.0	-17.7	0.0	0.0	-17.7		1,589.1	
$G5_4/L3_4$	D	108.8	91.2	5.1	98.7	94.0	397.8	1.92	21,996.1	–
	G	110.2	95.2	4.9	100.0	95.3	405.6		22,430.0	
$G5_1/L3_1$	D	104.7	90.7	0.0	98.8	93.6	387.8	1.90	21,286.2	–
	G	105.9	94.7	0.0	100.0	94.7	395.3		21712.7	
$G7_4/L5_1$	D	107.8	72.7	0.0	98.9	92.9	372.4	1.78	20,336.1	–
	G	109.0	76.2	0.0	100.0	94.0	379.1		20,719.9	
$G5_2/L8_3$	D	109.9	92.2	17.0	99.0	95.1	413.3	1.49	23,255.3	–
	G	111.1	96.0	16.3	100.0	96.1	419.5		23,588.5	
$G7_4/L3_4$	D	106.8	8.9	54.1	98.6	92.1	360.6	1.26	21,271.0	–
	G	108.3	11.4	52.1	100.0	93.4	365.2		21,460.6	

5.3.8 Transient Performance Assessment

This subsection assesses the transient performance of the proposed framework in three aspects: (i) the capability to restore system frequency to nominal following the considered $N-1-1$ events; (ii) the effects of corrective TS in post-contingency overloads; and (iii) whether executing TS adversely affects the subsequent frequency and voltage responses. In addition, the severity of the $N-1-1$ sequence is examined in terms of bus voltage response.

1) Frequency Restoration Assessment and Overloading Mitigation

To highlight the advantages of the TS-based instances, the transient performance under the worst-case scenario is evaluated using RMS-based simulations in DIgSILENT PF for the peak load condition. The worst-case scenario corresponds to the outage of generator $G6_1$ at $t = 10$ s, followed by the failure of line $L6_1$ at $t = 40$ s, and the short-circuit clearance at $t = 40.11$ s. As in the previous section and for visualization purposes, all events are initialized 10 s later than the timings specified in Subsection 4.1.1.

Table 5.16 presents the resulting participation factors for all instances. Positive values indicate regulation up assignments, whereas negative values correspond to regulation down tasks. As shown, instances M5 and M6 yield identical values of $\gamma_{g,s,k}$, both involving the switching of line $L4_1$. In contrast, the participation factors in M3 and M4 do not sum to one due to the presence of unserved energy.

This situation can be explained by analyzing the balance equation (4.4), where the *rhs* (the corrected deficit) is supplied on the *lhs* by the sum of AGC adjustments and unserved energy. Since each $\gamma_{g,s,k}$ in (4.27) is defined as a unit's AGC adjustment normalized by the corrected deficit, the sum $\sum_{g\in\mathcal{G}^{\text{AGC}}}\gamma_{g,s,k}$ represents the AGC share of that deficit. If part of the deficit is supplied by the unserved energy variables, the total AGC response is smaller than the corrected deficit. Consequently, the participation factors sum to less than one. In contrast, when unserved energy is zero, these factors sum to one.

Table 5.16. AGC Unit Participation Factors for the Worst-Case Scenario

Ins	$G2_1$	$G3_1$	$G4_1$	$G7_1$	$G3_2$	$G4_2$	$G2_3$	$G4_3$	$G6_3$	$G2_4$	$G3_4$	$G4_4$
M3	–	–	–	0.13	–	–	–	0.13	0.08	–	–	–
M4	-0.23	-0.17	-0.17	0.18	–	–	0.25	0.18	0.21	–	0.25	0.18
M5	–	–	0.03	0.30	–	0.36	–	0.31	–	–	–	–
M6	–	–	0.03	0.30	–	0.36	–	0.31	–	–	–	–

Without TS, neither M3 nor M4 prevents severe overloads on transmission line $L3_1$, resulting in load shedding at bus 13 in zone 1. Specifically, M3 requires the curtailment of 440.45 MW, while M4 reduces this amount to 30.24 MW through improved AGC scheduling and generation redispatch. In contrast, the use of TS in M5 and M6 allows the system to relieve the overload on line $L3_1$, fully avoiding the need for load shedding.

Figure 5.3 shows the transient evolution of the loading on line $L3_1$ under the M4 and M6 schedules without load shedding actions. To better illustrate the impact of considering the $N-1-1$ criterion on AGC scheduling, the line loading evolution for the M2 instance, i.e., under an $N-1$ criterion, is also included. As can be seen, while the M4 schedule reduces the overloading compared with the M2 schedule, it is still insufficient to bring the line loading within secure limits. In contrast, the AGC scheduling strategies in M6, enhanced by corrective TS actions, effectively reduce the loading on line $L3_1$ below its thermal capacity, ensuring a secure post-contingency operational condition.

Finally, Figure 5.4 depicts the system's frequency response under the worst-case scenario for the M6 solution. The frequency drops to a nadir of 49.87 Hz and returns to its nominal value at the end of the SFC. A transient deviation is observed around the $L6_1$ fault clearance and the $L4_1$ switching event. During the short circuit on $L6_1$, the frequency briefly peaks at 50.36 Hz ($t = 40.05$ s). After the line trips, the frequency achieved 49.80 Hz ($t = 42.60$ s) and settles near 49.96 Hz by the end of

PFC. These deviations are brief and remain within acceptable limits, so stability is not compromised. The switching of $L4_1$ provokes only small perturbations and does not degrade the SFC recovery. These results confirm that the TS-based instances not only eliminate post-contingency overloads but also maintain frequency stability.

It is worth noting that, once the M5 and M6 solutions were validated through RMS-based simulations, the frequency returned to its nominal value for all $N-1-1$ contingency states and operating conditions considered in this study.

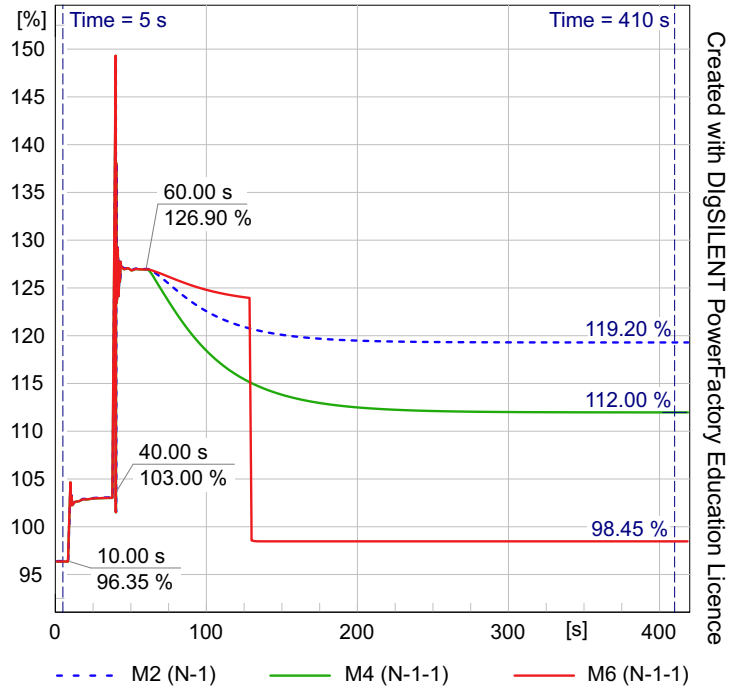

Figure 5.3. Loading evolution of $L3_1$ for the worst-case scenario. Own work.

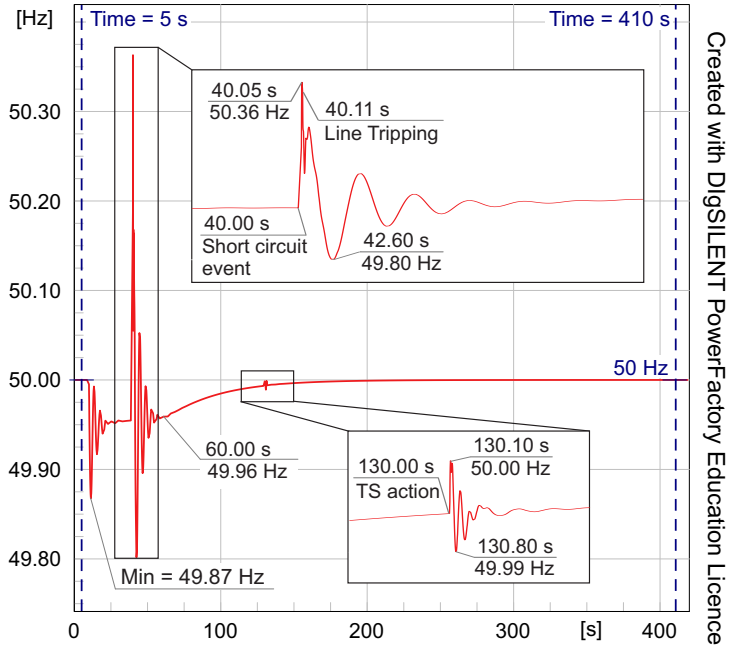

Figure 5.4. Frequency response under the worst-case scenario for the M6 solution. Own work.

2) Voltage Response under $N-1-1$ Events and TS

In this subsection, the degradation of the voltage profile due to $N-1-1$ and TS actions is analyzed. The M6 solution was implemented in DIgSILENT PF and evaluated through RMS-based simulations for the worst contingency states under peak and shoulder conditions, as well as the second-worst contingency state under the off-peak condition.

Table 5.17 summarizes the main results, reporting for each event (generator outage, line outage, and TS action) the pre-contingency voltage (V_{pre}) and the maximum deviation observed (ΔV) at the buses in the four zones. The notation Tx_y indicates the x-th bus located in the y-th zone. In addition, the pre-contingency value is taken at the instant immediately before the event. By convention, $\Delta V > 0$ denotes a voltage decrease relative to V_{pre}, whereas $\Delta V < 0$ denotes a voltage increase relative to V_{pre}.

Notice that scenario A comprises the $G6_1$ generator outage, the $L6_1$ line outage, and switching of $L4_1$ at the peak condition; scenario B comprises the same outage set and switching at the shoulder condition; and scenario C comprises the $G5_3$ generator outage, the $L7_1$ line outage, and switching of $L2_4$ at the off-peak condition. Appendix D provides transient simulation results for all cases.

Table 5.17. Voltage comparison across selected scenarios.

scenario	Generator outage			Line outage			TS		
	Bus	V_{pre} (p.u.)	ΔV (p.u.)	Bus	V_{pre} (p.u.)	ΔV (p.u.)	Bus	V_{pre} (p.u.)	ΔV (p.u.)
A	$T13_1$	1.013	0.007	$T11_1$	1.019	0.886	$T13_1$	1.007	0.018
	$T14_2$	1.005	0.005	$T13_2$	1.007	0.376	$T13_2$	1.013	0.001
	$T15_3$	1.011	0.006	$T11_3$	1.015	0.469	$T11_3$	1.012	-0.006
	$T13_4$	1.016	0.005	$T10_4$	1.022	0.504	$T12_4$	1.017	-0.004
B	$T13_1$	1.014	0.006	$T11_1$	1.020	0.886	$T10_1$	1.026	0.038
	$T11_2$	1.016	0.007	$T13_2$	1.008	0.368	$T11_2$	1.016	-0.003
	$T9_3$	1.010	0.005	$T11_3$	1.016	0.469	$T11_3$	1.013	0.006
	$T13_4$	1.018	0.005	$T10_4$	1.022	0.509	$T10_4$	1.024	-0.004
C	$T13_1$	1.015	0.008	$T10_1$	1.024	0.519	$T11_1$	1.022	0.001
	$T13_2$	1.009	0.008	$T13_2$	1.009	0.175	$T10_2$	1.029	0.001
	$T10_3$	1.016	0.016	$T11_3$	1.017	0.249	$T14_3$	1.020	0.001
	$T13_4$	1.019	0.008	$T10_4$	1.023	0.237	$T14_4$	1.030	0.001

Across all zones and scenarios, line outages are the principal driver of voltage degradation, with the largest ΔV occurring at buses close to the faulted element. Scenario A shows the most severe impact, with a maximum deviation of 0.886 p.u. at $T11_1$ and the highest average line–outage effect across zones (about 0.559 p.u.). This average impact is essentially tied with Scenario B and is higher than scenario C (approximately 0.295 p.u.).

By contrast, the TS action produces only small localized deviations, keeping voltages close to pre-contingency levels. The largest TS deviation in the table is 0.038 p.u. at $T10_1$ (scenario B), while most TS entries lie within ± 0.02 p.u., and these deviations are comparable in magnitude to those from the generator outages (0.005–0.016 p.u.). Note that some TS deviations are negative (e.g., $T11_3$ and $T12_4$ in scenario A), indicating a slight voltage increase relative to V_{pre}.

In summary, the results indicate that TS is a flexible recourse action that supports AGC scheduling and enhances system security under severe contingencies, provoking only minor deviations in the voltage profile and without compromising voltage and frequency stability.

Chapter 6

Conclusions and Further Research

Modern grids are operating with higher loading conditions, increasing their vulnerability to disturbances, degrading system security due to factors like reduced inertia from renewable integration, increased complexity, and potential for cascading failures. To partially address these vulnerabilities, this work has presented a novel framework for AGC scheduling that integrates corrective TS to enhance frequency stability, economic operation, and system flexibility during the SFC stage under $N-1-1$ events. The framework is designed to be solved off-line, quantifying the set of generating units to be scheduled for the AGC requirements, along with the optimal corrective TS decisions.

In this study, the achieved methodology combines a time-domain simulation platform with a two-stage stochastic MILP optimization model that considers transmission losses, load-voltage dependency, and uncertain $N-1-1$ contingency states. The framework uses as inputs the pre-contingency schedule and dispatch together with the set of AGC candidate units, all defined by the ISO in advance. The $N-1-1$ event considered corresponds to the outage of a generating unit followed by a transmission line short-circuit and tripping at the end of the PFC, under a given operating condition.

The robustness assessment of the recent approach shows it is insufficient to maintain secure operation under $N-1-1$ events. Although frequency is restored, persistent line overloads remain, increasing the risk of load shedding or subsequent line trips. These findings indicate that an N–1-based framework cannot ensure reliable operation under more severe, sequential contingencies.

By contrast, the proposed framework directly addresses these limitations by introducing corrective TS and explicitly modeling $N-1-1$ events, yielding more resilient operating schedules that withstand severe contingencies. Results show that TS relieves transmission overloads, eliminates unserved energy, and lowers operating costs, ensuring secure performance under $N-1-1$ events. In addition, TS enables a more efficient AGC schedule by allowing the selection of fewer units, thereby reducing SFC costs. In addition, the proposed framework reproduces AGC behavior with high fidelity under $N-1-1$ events, as shown by the close match to the outputs of the scheduled units measured after SFC in DIgSILENT PF. Moreover, the inclusion of TS does not degrade the accuracy of the model.

Finally, the simulations confirmed that frequency was restored by the resulting AGC schedule in conjunction with the TS actions. Moreover, the inclusion of TS did not adversely affect the frequency response or the voltage profile, confirming its value as a support mechanism for enabling secure operation.

6.1 Further Research

Future research will scale the proposed framework to real-sized power systems and explore its potential to support near-real-time decision making. To keep solving times practical, decomposition-based techniques and parallelization could be investigated.

Another line of work will integrate variable renewable resources, such as wind and photovoltaic power units, and enable their participation in SFC. This requires explicitly modeling variability and forecast uncertainty to assess performance under complex operating conditions.

Additional flexibility mechanisms beyond TS will also be considered. In particular, battery energy storage systems (BESS) will be incorporated with dual roles (energy arbitrage and SFC participation). These models have to account for state of charge dynamics, cycling limits, and degradation costs, together with appropriate remuneration schemes.

To obtain a more realistic network representation, the framework will extend the network constraints to an ac power flow model. Second-order cone (SOC) relaxations should be investigated as a tractable alternative, evaluating their accuracy and computational performance.

Finally, methods will be developed to identify and screen critical $N-1-1$ contingencies, enabling scenario reduction. Sensitivity metrics, risk ranking, and clustering will be employed to detect cascade precursors, and the reduced set should be validated through transient power system simulations to preserve security while reducing computational burden.

Bibliography

[1] N. Hatziargyriou, J. Milanovic, C. Rahmann, V. Ajjarapu, C. Canizares, I. Erlich, D. Hill, I. Hiskens, I. Kamwa, B. Pal, P. Pourbeik, J. Sanchez-Gasca, A. Stankovic, T. Van Cutsem, V. Vittal, and C. Vournas, "Definition and classification of power system stability – revisited extended," *IEEE Transactions on Power Systems*, vol. 36, no. 4, pp. 3271–3281, Jul. 2021.

[2] D. Bolbarań, "Implementación del control automático de generación en sistemas de potencia considerando asignación óptima de generación y restricciones de transmisión," *Undergraduate thesis (in Spanish)*, Departamento of Electrical Engineering, Universidad Técnica Federico Santa María, Chile, 2022.

[3] V. H. Hinojosa, D. Bolbarán, E. Gil, and G. Gutierrez-Alcaraz, "Enhancing automatic generation control performance under uncertainty and congestion through detailed transmission modeling and strategic selection of units," *IEEE Transactions on Power Systems*, vol. 40, no. 3, pp. 2389–2400, May. 2025.

[4] NEPLAN. Turbine-governor models: Standard dynamic turbine governor systems in neplan power system analysis tool. Accessed: Sep. 15, 2025. [Online]. Available: https://n9.cl/zrvwf6

[5] M. M. Rahman, S. H. Dadon, M. He, M. Giesselmann, and M. M. Hasan, "An overview of power system flexibility: High renewable energy penetration scenarios," *Energies*, vol. 17, no. 24, p. 6393, Dec. 2024.

[6] P. Kundur, *Power System Stability and Control*, 2nd ed. New York, NY, USA: McGraw-Hill, 2022.

[7] H. Zhang, C. Zhai, G. Xiao, and T.-C. Pan, "Identifying critical risks of cascading failures in power systems," *IET Generation, Transmission & Distribution*, vol. 13, no. 12, pp. 2438–2445, May. 2019.

[8] DIgSILENT, "Powerfactory," Jul 2025. [Online]. Available: https://www.digsilent.de/en/powerfactory.html

[9] Python, "Python," May 2025. [Online]. Available: http://www.python.org

[10] Gurobi, "Software Gurobi," May 2025. [Online]. Available: http://www.gurobi.com

[11] S. Baros, Y. C. Chen, and S. V. Dhople, "Examining the economic optimality of automatic generation control," *IEEE Transactions on Power Systems*, vol. 36, no. 5, pp. 4611–4620, Sep. 2021.

[12] F. Gonzalez-Longatt, A. Steliuk, and V. H. Hinojosa, "Flexible automatic generation control system for embedded HVDC links," in *Proc. 2015 IEEE Eindhoven PowerTech*, Eindhoven, The Netherlands, Jul. 2015, pp. 1–6.

[13] R. Verma, S. K. Gawre, N. Patidar, and S. Nandanwar, "A state of art review on the opportunities in automatic generation control of hybrid power system," *Electric Power Systems Research.*, vol. 226, Jan. 2024, Art. no. 1109945.

[14] S. Baros, Y. C. Chen, and S. V. Dhople, "Examining the economic optimality of automatic generation control," *IEEE Transactions on Power Systems*, vol. 36, no. 5, pp. 4611–4620, Sep. 2021.

[15] R. Patel, C. Li, X. Yu, and B. McGrath, "Optimal automatic generation control of an interconnected power system under network constraints," *IEEE Transactions on Industrial Electronics*, vol. 65, no. 9, pp. 7220–7228, Sep. 2018.

[16] R. Patel, C. Li, L. Meegahapola, B. McGrath, and X. Yu, "Enhancing optimal automatic generation control in a multi-area power system with diverse energy resources," *IEEE Transactions on Power Systems*, vol. 34, no. 5, pp. 3465–3475, Sep. 2019.

[17] Z. Wang, F. Liu, S. H. Low, C. Zhao, and S. Mei, "Distributed frequency control with operational constraints, Part I: Per-node power balance," *IEEE Transactions Smart Grid*, vol. 10, no. 1, pp. 40–52, Jan. 2019.

[18] Y. Shen, W. Wu, and S. Sun, "Stochastic model predictive control based fast-slow coordination automatic generation control," *IEEE Transactions on Power Systems*, vol. 39, no. 3, pp. 5259–5271, May. 2024.

[19] D. Cai, E. Mallada, and A. Wierman, "Distributed optimization decomposition for joint economic dispatch and frequency regulation," *IEEE Transactions on Power Systems*, vol. 32, no. 6, pp. 4370–4385, Nov. 2017.

[20] G. Zhang, J. McCalley, and Q. Wang, "An AGC dynamics-constrained economic dispatch model," *IEEE Transactions on Power Systems*, vol. 34, no. 5, pp. 3931–3940, Sep. 2019.

[21] X. Zhang, Z. Xu, T. Yu, B. Yang, and H. Wang, "Optimal mileage based AGC dispatch of a GenCo," *IEEE Transactions on Power Systems*, vol. 35, no. 4, pp. 2516–2526, Jul. 2020.

[22] L. Liu, Z. Hu, X. Duan, and N. Pathak, "Data-driven distributionally robust optimization for real-time economic dispatch considering secondary frequency regulation cost," *IEEE Transactions on Power Systems*, vol. 36, no. 5, pp. 4172–4184, Sep. 2021.

[23] N. Li, C. Zhao, and L. Chen, "Connecting automatic generation control and economic dispatch from an optimization view," *IEEE Transactions on Control of Network Systems*, vol. 3, no. 3, pp. 254–264, Jul. 2016.

[24] NERC. Transmission planning standards. Accessed: May. 23, 2025. [Online]. Available: https://www.nerc.com/pa/Stand/Pages/ReliabilityStandards.aspx

[25] X. Xu, M. Elkhatib, R. Yousefian, J. Tang, B. Choi, L. Huang, Y. Mao, and A. Berner, "Automatic n-1-1 system stability study of the pjm system," in *2020 IEEE Power Energy Society General Meeting (PESGM)*, Aug. 2020, pp. 1–5.

[26] *System Performance Under Normal (No Contingency) Conditions (Category A)*, North American Electric Reliability Corporation (NERC) Std. TPL-001-0.1, Feb. 2014, NERC Standard.

[27] D. Chatterjee, J. Webb, Q. Gao, M. Y. Vaiman, M. M. Vaiman, and M. Povolotskiy, "N-1-1 AC contingency analysis as a part of NERC compliance studies at Midwest ISO," in *Proc. IEEE PES T&D 2010*, New Orleans, LA, USA, Apr. 2010, pp. 1–7.

[28] N. Fan, R. Chen, and J.-P. Watson, "N-1-1 contingency-constrained optimal power flow by interdiction methods," in *Proc. 2012 IEEE Power and Energy Society General Meeting*, San Diego, CA, USA, Jul. 2012, pp. 1–6.

[29] Z. Guo, R. L.-Y. Chen, N. Fan, and J.-P. Watson, "Contingency-constrained unit commitment with intervening time for system adjustments," *IEEE Transactions on Power Systems*, vol. 32, no. 4, pp. 3049–3059, Jul. 2017.

[30] D. Zuniga, J. Ruiz, F. Neng, and Q. Feng, "N-1-1 contingency-constrained unit commitment with renewable integration and corrective actions," *Annals of Operations Research*, vol. 316, pp. 1–19, Sep. 2022.

[31] K. W. Hedman, S. S. Oren, and R. P. O'Neill, "Optimal transmission switching: Economic efficiency and market implications," *Journal of Regulatory Economics*, vol. 40, pp. 111–140, Jun. 2011.

[32] M. Abdi-Khorsand, M. Sahraei-Ardakani, and Y. M. Al-Abdullah, "Corrective transmission switching for N-1-1 contingency analysis," *IEEE Transactions on Power Systems*, vol. 32, no. 2, pp. 1606–1615, Mar. 2017.

[33] S. Yang, W. Chen, X. Zhang, and Y. Jiang, "Blocking cascading failures with optimal corrective transmission switching considering available correction time," *International Journal of Electrical Power & Energy Systems*, vol. 141, p. 108248, Oct. 2022.

[34] M. Numan, M. F. Abbas, M. Yousif, S. S. M. Ghoneim, A. Mohammad, and A. Noorwali, "The role of optimal transmission switching in enhancing grid flexibility: A review," *IEEE Access*, vol. 11, pp. 32 437–32 463, Mar. 2023.

[35] K. W. Hedman, R. P. O'Neill, E. B. Fisher, and S. S. Oren, "Optimal transmission switching with contingency analysis," *IEEE Transactions on Power Systems*, vol. 24, no. 3, pp. 1577–1586, Aug. 2009.

[36] R. Saavedra, A. Street, and J. M. Arroyo, "Day-ahead contingency-constrained unit commitment with co-optimized post-contingency transmission switching," *IEEE Transactions on Power Systems*, vol. 35, no. 6, pp. 4408–4420, May. 2020.

[37] K. W. Hedman, M. C. Ferris, R. P. O'Neill, E. B. Fisher, and S. S. Oren, "Co-optimization of generation unit commitment and transmission switching with N-1 reliability," *IEEE Transactions on Power Systems*, vol. 25, no. 2, pp. 1052–1063, Jan. 2010.

[38] P. A. Ruiz, E. Goldis, A. M. Rudkevich, M. C. Caramanis, C. R. Philbrick, and J. M. Foster, "Security-constrained transmission topology control MILP formulation using sensitivity factors," *IEEE Transactions on Power Systems*, vol. 32, no. 2, pp. 1597–1605, Mar. 2017.

[39] J. Graf, *PID Control: Ziegler-Nichols Tuning.* Scotts Valley, CA, USA: CreateSpace Independent Publishing Platform, 2013.

[40] A. Conejo, M. Carrion, and J. Morales, *Decision Making Under Uncertainty in Electrical Markets*, 1st ed. New York, NY, USA: Springer, 2010.

[41] A. J. Wood, B. F. Wollenberg, and G. B. Sheblé, *Power Generation, Operation and Control*, 3rd ed. Hoboken, NJ, USA: Wiley, 2014.

[42] O. W. Akinbode and K. W. Hedman, "Fictitious losses in the DCOPF with a piecewise linear approximation of losses," in *Proc. 2013 IEEE Power and Energy Society General Meeting*, Vancouver, BC, Canada, Jul. 2013, pp. 1–5.

[43] F. Gonzalez-Longatt and J. Rueda, *Power Factory Applications for Power System Analysis.* Springer, 2014.

[44] A. J. Ardakani and F. Bouffard, "Identification of umbrella constraints in dc-based security-constrained optimal power flow," *IEEE Transactions on Power Systems*, vol. 28, no. 4, pp. 3924–3934, Jul. 2013.

[45] G. Gutiérrez-Alcaraz, B. Díaz-López, J. M. Arroyo, and V. H. Hinojosa, "Large-scale preventive security-constrained unit commitment considering $n - k$ line outages and transmission losses," *IEEE Transactions on Power Systems*, vol. 37, no. 3, pp. 2032–2041, Sep. 2022.

[46] S. Ramírez-López, G. Gutierrez-Alcaraz, J. M. Arroyo, and V. H. Hinojosa, "Corrective n-k security-constrained unit commitment using lossy shift factors and fictitious injections," *Journal of Modern Power Systems and Clean Energy*, to be published.

[47] V. H. Hinojosa and J. Velásquez, "Improving the mathematical formulation of security-constrained generation capacity expansion planning using power transmission distribution factors and line outage distribution factors," *Electric Power Systems Research*, vol. 140, pp. 391–400, Jul. 2016.

[48] V. Hinojosa and F. Gonzalez-Longatt, "Stochastic security-constrained generation expansion planning methodology based on a generalized line outage distribution factors," in *Proc. 2017 IEEE Manchester PowerTech*, Manchester, UK, Jun. 2017, pp. 1–6.

[49] V. H. Hinojosa and J. Sepúlveda, "Solving the stochastic transmission capacity expansion planning problem based on generalized partial transmission distribution factors," in *Proc. 2019 IEEE Milan PowerTech*, Milan, Italy, Jun. 2019, pp. 1–6.

[50] H. Zhang, V. Vittal, G. T. Heydt, and J. Quintero, "A mixed-integer linear programming approach for multi-stage security-constrained transmission expansion planning," *IEEE Transactions on Power Systems*, vol. 27, no. 2, pp. 1125–1133, May. 2012.

[51] H. Zhang, G. T. Heydt, V. Vittal, and J. Quintero, "An improved network model for transmission expansion planning considering reactive power and network losses," *IEEE Transactions on Power Systems*, vol. 28, no. 3, pp. 3471–3479, Aug. 2013.

[52] E. Heylen, G. Deconinck, and D. Van Hertem, "Impact of value of lost load on performance of reliability criteria and reliability management," in *Proc. 2015 IEEE Eindhoven PowerTech*, Eindhoven, The Netherlands, Jul. 2015, pp. 1–6.

[53] M. Ovaere, E. Heylen, S. Proost, G. Deconinck, and D. Van Hertem, "How detailed value of lost load data impact power system reliability decisions," *Energy Policy*, vol. 132, pp. 1064–1075, Sep. 2019.

[54] ENTSO-E. Methodology for the calculation of the value of lost load (VoLL), the cost of new entry (CONE) and the reliability standard. Accessed: Jun. 15, 2025. [Online]. Available: https://n9.cl/mn6jn1

Appendices

Appendix A

Turbine and Governor Models

This appendix presents block diagrams of representative governor/turbine models and their parameter definitions for steam, gas, hydro, and combined-cycle units. Widely adopted structures are included, such as TGOV1 (steam), GAST (gas), and HYGOV4 (hydro), together with an aggregate model for combined-cycle plants (GGOV1). For detailed formulations and additional variants, review in detail [4].

A.1 TGOV1 model

The TGOV1 model is a generic turbine/governor representation used to simulate steam units It includes the speed-droop governor, servo/actuator, and turbine dynamics that shape the fast active power response. Figure A.1 illustrates the model structure, and Table A.1 summarizes its parameters.

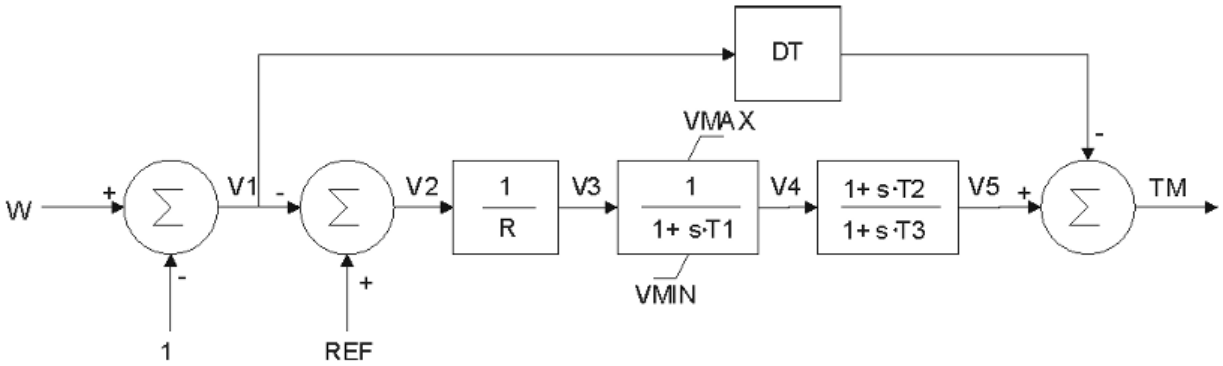

Figure A.1. Block diagram of the TGOV1 steam turbine and governor [4].

Table A.1. TGOV1 Parameters

Parameter	Type	Description
R	PU	Permanent droop
T1	Seconds	Steam bowl time constant
VMAX	PU	Maximum valve position
VMIN	PU	Minimum valve position
T2	Seconds	Time constant
T3	Seconds	Time constant
DT	PU	Turbine damping coefficient
MWBASE	Active Power	Base for power values

A.2 GAST model

The GAST model represents the governor and fuel-control system of a simple-cycle gas turbine and is used to simulate primary frequency response. Figure A.2 illustrates the model, and Table A.2 summarizes the description of its parameters.

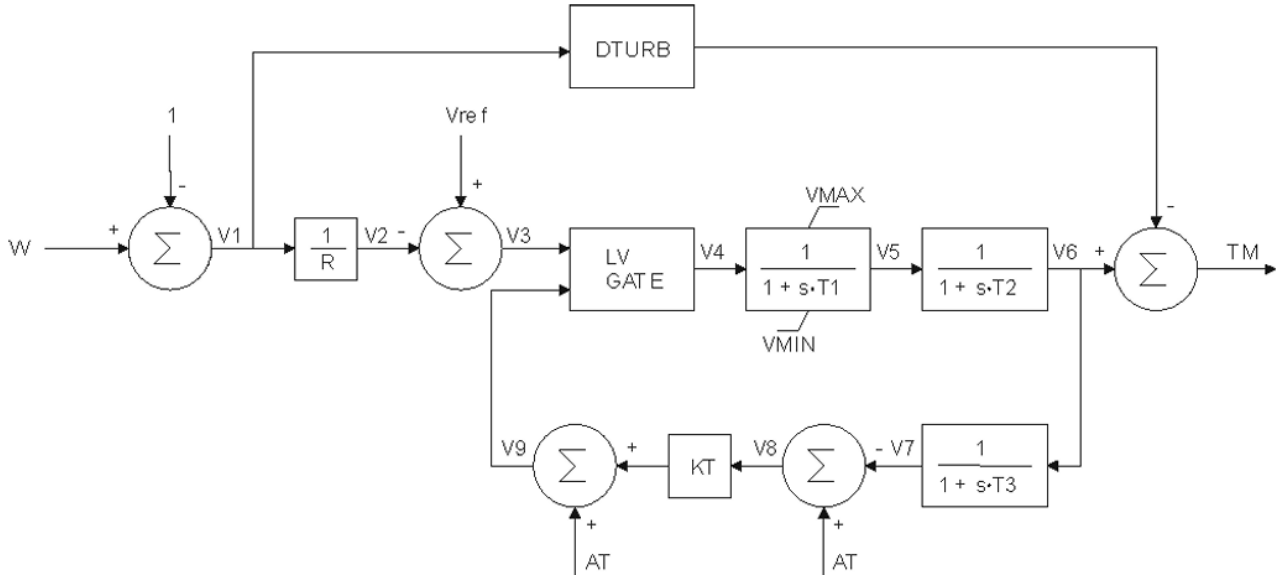

Figure A.2. Block diagram of the GAST gas turbine and governor [4].

Table A.2. GAST Parameters

Parameter	Type	Description
R	PU	Permanent droop
T1	Seconds	Governor mechanism time constant
T2	Seconds	Turbine power time constant
T3	Seconds	Turbine exhaust temperature time constant
AT	PU	Ambient temperature load limit
KT	PU	Temperature limiter gain
VMAX	PU	Maximum turbine power
VMIN	PU	Minimum turbine power
DTRUB	PU	Turbine damping factor

A.3 HYGOV4 model

The HYGOV4 model represents the hydraulic governor and turbine of a hydro unit. It is most suitable for reaction turbines with wicket-gate control (e.g., Francis and Kaplan) and can be adapted to impulse units (e.g., Pelton). Figure A.3 illustrates the model structure, and Table A.3 lists its parameters.

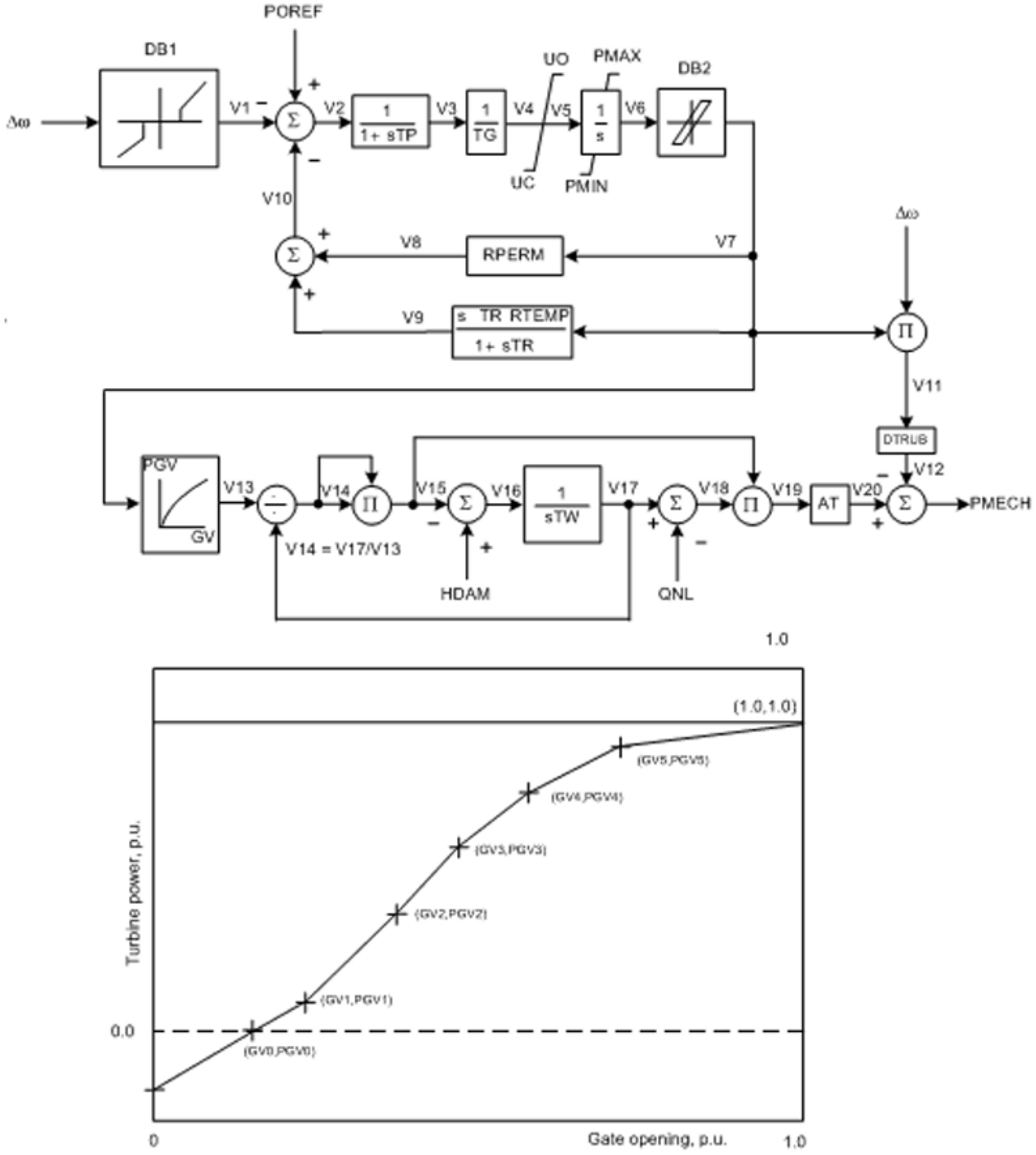

Figure A.3. Block diagram of the HYGOV4 hydro turbine and governor [4].

Table A.3. HYGOV4 Parameters

Parameter	Type	Description
DB1	PU	Intentional deadband width
TP	Seconds	Pilot servo time constant
TG	Seconds	Gate servo time constant
UO	PU	Max gate opening velocity
UC	PU	Max gate closing velocity
PMAX	PU	Maximum gate opening
PMIN	PU	Minimum gate opening
DB2	PU	Unintentional dead-band
EPS	PU	Intentional db hysteresis
RPERM	PU	Permanent droop
RTEMP	PU	Temporary droop
TR	Seconds	Dashpot time constant
DTURB	PU	Turbine damping factor
HDAM	PU	Head available at dam
TW	Seconds	Water inertia time constant
QNL	PU	No-load flow at nominal head
AT	PU	Turbine gain
GV0	PU	Nonlinear gain point 0
PGV0	PU	Nonlinear gain point 0
GV1	PU	Nonlinear gain point 1
PGV1	PU	Nonlinear gain point 1
GV2	PU	Nonlinear gain point 2
PGV2	PU	Nonlinear gain point 2
GV3	PU	Nonlinear gain point 3
PGV3	PU	Nonlinear gain point 3
GV4	PU	Nonlinear gain point 4
PGV4	PU	Nonlinear gain point 4
GV5	PU	Nonlinear gain point 5
PGV5	PU	Nonlinear gain point 5

A.4 GGOV1 Model

The GGOV1 model represents the governor and fuel/limit control of an industrial gas turbine. It is commonly applied to combined-cycle units. The structure includes a speed-droop governor, fuel-valve/actuator dynamics, and key limiters. Figure A.4 illustrates the model, and Table A.4 lists its parameters.

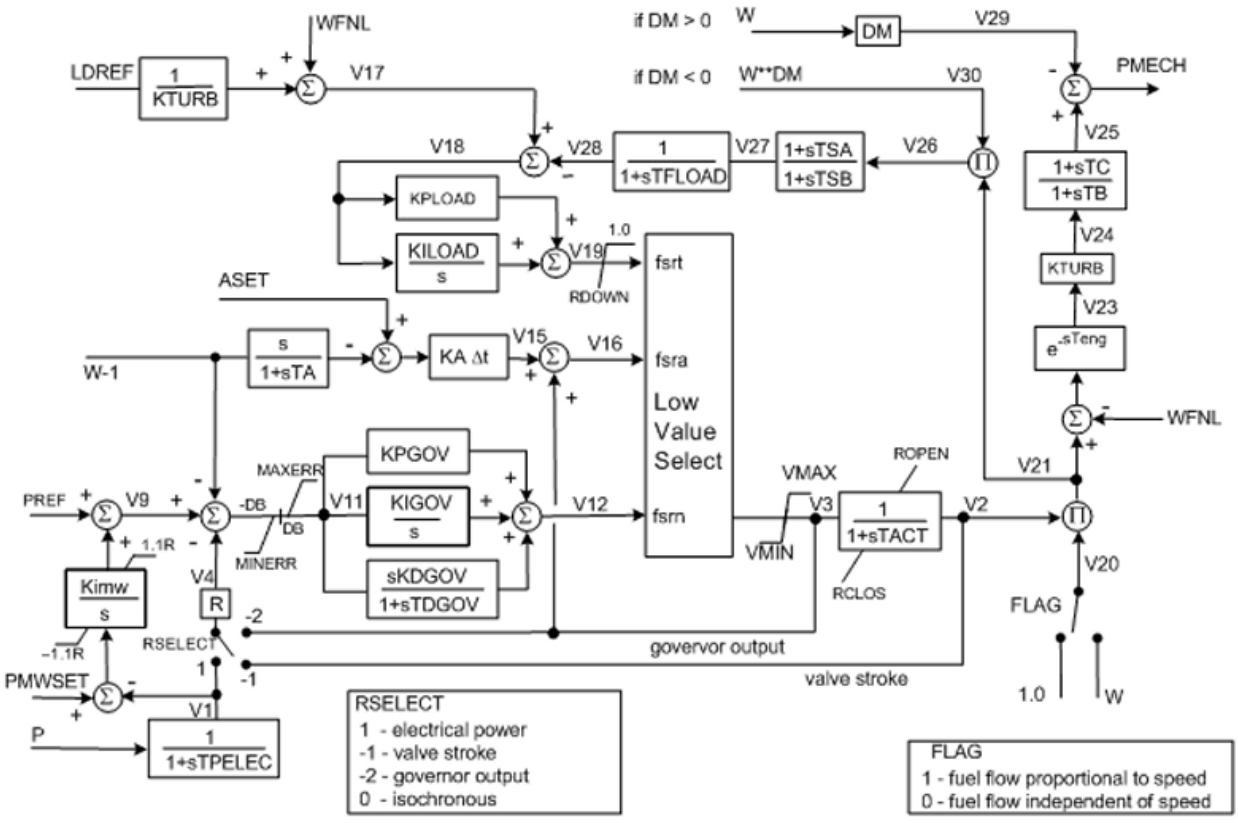

Figure A.4. Block diagram of the GG0V1 for combined cycle units and governor [4].

Table A.4. GGOV1 Parameters

Parameter	Type	Description
R	PU	Permanent droop
TPELEC	Seconds	Electrical power transducer time constant
MAXERR	PU	Maximum value for speed error signal
MINERR	PU	Minimum value for speed error signal
KPGOV	PU	Governor proportional gain
KIGOV	PU	Governor integral gain
KDGOV	PU	Governor derivative gain
TDGOV	Seconds	Governor derivative controller time constant
VMAX	PU	Maximum valve position limit
VMIN	PU	Minimum valve position limit
TACT	Seconds	Actuator time constant
KTURB	PU	Turbine gain
WFNL	PU	No-load fuel flow
TB	Seconds	Turbine lag time constant
TC	Seconds	Turbine lead time constant
TENG	Seconds	Transport time delay for diesel engine
TFLOAD	Seconds	Load limiter time constant
KPLOAD	PU	Load limiter proportional gain for PI controller
KILOAD	PU	Load limiter integral gain for PI controller
LDREF	PU	Load limiter reference value
DM	PU	Speed sensitivity coefficient
ROPEN	PU	Maximum valve opening rate
RCLOSE	PU	Minimum valve opening rate
KIMW	PU	Power controller (reset) gain
PMWSET	ActivePower	Power controller setpoint
ASET	PU	Acceleration limiter setpoint
KA	PU	Acceleration limiter gain
TA	Seconds	Acceleration limiter time constant
TRATE	ActivePower	Base for power values
DB	PU	Speed governor dead band
TSA	Seconds	Temperature detection lead time constant
TSB	Seconds	Temperature detection lag time constant
RUP	PU	Maximum rate of load limit increase
RDOWN	PU	Maximum rate of load limit decrease
RSELECT	Enum	Feedback signal for droop (Rselect).
F_FLAG	Boolean	Switch for fuel source characteristic.

Appendix B

AGC Scheduling Formulation under $N-1$ Generator Outages

The stochastic two-stage decision-making problem introduced in [3] for AGC scheduling under $N-1$ generator contingencies is described as follows:

Objective function: The stochastic objective function (24) minimizes the scheduling cost of AGC services (Csfc) and the expected operational cost under N-1 contingencies. In the first stage, the model selects the AGC units enabled to increase (v_g^{Inc}) or decrease (v_g^{Dec}) their output across all periods and scenarios. The second stage evaluates the recourse cost after each contingency, weighted by its probability (π_s), and considers the fuel cost of AGC units ($\text{Cop}_{s,t}$), the load shedding ($\text{Cue}_{s,t}$), and the power losses ($\text{Cpl}_{s,t}$). Power losses are penalized using the VOLL value to avoid fictitious losses.

$$\text{Min: Csfc} + \sum_{s\in\mathcal{S}} \pi_s \Big[\sum_{t\in\mathcal{T}} \big(\text{Cop}_{s,t} + \text{Cue}_{s,t} + \text{Cpl}_{s,t}\big) \Big] \tag{24}$$

$$\text{Csfc} = \sum_{g\in\mathcal{G}^{\text{AGC}}} C_g^{\text{AGC}} \Big(v_g^{\text{Inc}} + v_g^{\text{Dec}} \Big) \tag{24a}$$

$$\text{Cop}_{s,t} = \sum_{g\in\mathcal{G}^{\text{AGC}}} C_g^{\text{Fuel}} \Big(\Delta p_{g,s,t}^{\text{Inc}} + \Delta p_{g,s,t}^{\text{Dec}} \Big) \tag{24b}$$

$$\text{Cue}_{s,t} = \text{VOLL} \sum_{b\in\mathcal{B}} p_{b,s,t}^{\text{Ue}} \tag{24c}$$

$$\text{Cpl}_{s,t} = \text{VOLL} \sum_{l\in\mathcal{L}} pl_{l,s,t} \tag{24d}$$

The operational problem is modeled using an $N-1$ DC-based lossy OPF formulation as follows:

Power balance supply: The power balance ensures that post-contingency imbalances are compensated at the end of the CSF by the AGC units for each $N-1$ contingency scenario s and operational period t (25).

$$\sum_{g\in\mathcal{G}^{\text{AGC}}} \Big(\Delta p_{g,s,t}^{\text{Inc}} - \Delta p_{g,s,t}^{\text{Dec}} \Big) + \sum_{b\in\mathcal{B}} p_{b,s,t}^{\text{Ue}} = P_{s,t}^{\text{Out}} - \sum_{b\in\mathcal{B}} \Big(D_{b,s,t}^{\text{Pre}} - D_{b,s,t}^{\text{PFC}} \Big) - \sum_{l\in\mathcal{L}} \Big(\text{PL}_{l,t}^{\text{Pre}} - pl_{l,s,t} \Big); \quad \forall s \in \mathcal{S}, \forall t \in \mathcal{T} \tag{25}$$

Transmission network lossy shift-factor modeling: The power flow problem is modeled using the linear lossy shift-factor formulation, as expressed in (26). Considering that only $N-1$ generation contingencies are included, the shift factors remain constant since there are no topological changes in the power grid. In the lossy formulation, 50% of the power losses are distributed as additional demand at each end bus of the affected line [45, 46]. Using positive and negative components (f_l^{Pos}, f_l^{Neg}) in the power flow definition (27), transmission power flow limits are imposed in (28) - (29).

$$f_{l,s,t} = \sum_{b\in\mathcal{B}} \mathrm{SF}^{\mathrm{Loss}}_{l,b}\Big[\sum_{g\in\mathcal{G}_b}\Big(P^{\mathrm{Pre}}_{g,s,t} - P^{\mathrm{Out}}_{g,s,t}\Big) + p^{\mathrm{Ue}}_{b,s,t} + \sum_{g\in\mathcal{G}^{agc}_b}\Big(\Delta p^{\mathrm{Inc}}_{g,s,t} - \Delta p^{\mathrm{Dec}}_{g,s,t}\Big) - D^{\mathrm{PFC}}_{b,s,t} -$$
$$0.5\sum_{l'\in\mathcal{L}|fr(l')=b} pl_{l',s,t} - 0.5\sum_{l'\in\mathcal{L}|to(l')=b} pl_{l',s,t}\Big];\ \forall l\in\mathcal{L},\forall s\in\mathcal{S},\forall t\in\mathcal{T} \tag{26}$$

$$f_{l,s,t} = f^{\mathrm{Pos}}_{l,s,t} - f^{\mathrm{Neg}}_{l,s,t};\ \forall l\in\mathcal{L},\forall s\in\mathcal{S},\forall t\in\mathcal{T} \tag{27}$$

$$f_{l,s,t} + 0.5\,pl_{l,s,t} \le F^{\mathrm{Max}}_{l};\ \forall l\in\mathcal{L},\forall s\in\mathcal{S},\forall t\in\mathcal{T} \tag{28}$$

$$-f_{l,s,t} + 0.5\,pl_{l,s,t} \le F^{\mathrm{Max}}_{l};\ \forall l\in\mathcal{L},\forall s\in\mathcal{S},\forall t\in\mathcal{T} \tag{29}$$

Steady-state power losses are explicitly modeled in the optimization problem by approximating their quadratic behavior using segments of monotonically increasing slopes. This linearization is presented from (30) to (33).

$$pl_{l,s,t} = \big(G_l/B_l^2\big)\sum_{j\in\mathcal{J}}\Big[(2j-1)\frac{F^{\mathrm{Max}}_l}{|\mathcal{J}|}\Big]\Delta f_{k,l,s,t};\ \forall l\in\mathcal{L},\forall s\in\mathcal{S},\forall t\in\mathcal{T} \tag{30}$$

$$\sum_{j\in\mathcal{J}}\Delta f_{j,l,s,t} = f^{\mathrm{Pos}}_{l,s,t} + f^{\mathrm{Neg}}_{l,s,t};\ \forall l\in\mathcal{L},\forall s\in\mathcal{S},\forall t\in\mathcal{T} \tag{31}$$

$$0 \le \Delta f_{1,l,s,t} \le \frac{F^{\mathrm{Max}}_l}{|\mathcal{J}|};\ \forall l\in\mathcal{L},\forall s\in\mathcal{S},\forall t\in\mathcal{T} \tag{32}$$

$$f^{\mathrm{Pos}}_{l,s,t},\ f^{\mathrm{Neg}}_{l,s,t} \ge 0;\ \forall l\in\mathcal{L},\forall s\in\mathcal{S},\forall t\in\mathcal{T} \tag{33}$$

Generation and unserved energy modeling: Constraints (34) and (35) limit power increases and decreases in AGC units, respectively. Unserved energy is modeled by constraint (36). Ramp limits are imposed in constraints (37)–(38), considering both the primary frequency response $P^{\mathrm{PFC}}_{g,s,t}$ and the pre-contingency dispatch $P^{\mathrm{Pre}}_{g,t}$. Finally, binary AGC activation decisions are defined in constraint (39).

$$0 \le \Delta p^{\mathrm{Inc}}_{g,s,t} \le \big(P^{\mathrm{Max}}_g - P^{\mathrm{Pre}}_{g,t}\big)v^{\mathrm{Inc}}_g;\ \forall g\in\mathcal{G}^{\mathrm{AGC}},\forall s\in\mathcal{S},\forall t\in\mathcal{T} \tag{34}$$

$$0 \le \Delta p^{\mathrm{Dec}}_{g,s,t} \le \big(P^{\mathrm{Pre}}_{g,t} - P^{\mathrm{Min}}_g\big)v^{\mathrm{Dec}}_g;\ \forall g\in\mathcal{G}^{\mathrm{AGC}},\forall s\in\mathcal{S},\forall t\in\mathcal{T} \tag{35}$$

$$0 \le p^{\mathrm{Ue}}_{b,s,t} \le D^{\mathrm{PFC}}_{b,s,t};\ \forall b\in\mathcal{B},\forall s\in\mathcal{S},\forall t\in\mathcal{T} \tag{36}$$

$$\Delta p^{\mathrm{Inc}}_{g,s,t} \le RU_g T^{\mathrm{SFC}} + \big(P^{\mathrm{PFC}}_{g,s,t} - P^{\mathrm{Pre}}_{g,t}\big);\ \forall g\in\mathcal{G}^{\mathrm{AGC}},\forall s\in\mathcal{S},\forall t\in\mathcal{T} \tag{37}$$

$$\Delta p^{\mathrm{Dec}}_{g,s,t} \le RD_g T^{\mathrm{SFC}} + \big(P^{\mathrm{Pre}}_{g,t} - P^{\mathrm{PFC}}_{g,s,t}\big);\ \forall g\in\mathcal{G}^{\mathrm{AGC}},\forall s\in\mathcal{S},\forall t\in\mathcal{T} \tag{38}$$

$$v^{\mathrm{Inc}}_g, v^{\mathrm{Dec}}_g \in \{0,1\};\ \forall g\in\mathcal{G}^{\mathrm{AGC}} \tag{39}$$

Computing the regulation participation factors: Participation factors γ_g are recalculated using (40) to account for generation outages, load changes from voltage dependency, and transmission losses.

$$\gamma_g = \Big(\Delta p^{\mathrm{Inc}}_g - \Delta p^{\mathrm{Dec}}_g\Big)\Big/\hat{P}^{\mathrm{Out}}_s; \tag{40}$$

$$\hat{P}^{\mathrm{Out}}_s = P^{\mathrm{Out}}_{s,t} - \sum_{b\in\mathcal{B}}\Big(D^{\mathrm{Pre}}_{b,s,t} - D^{\mathrm{PFC}}_{b,s,t}\Big) - \sum_{l\in\mathcal{L}}\Big(\mathrm{PL}^{\mathrm{Pre}}_{l,t} - pl_{l,s,t}\Big)$$

Appendix C

System Data

C.1 Generator Technical Data

Table C.1 reports the technical specifications of the generating units used in the study, including bus assignment, turbine type, minimum and maximum limits, ramp-down and ramp-up rates, linear fuel-cost coefficient, and the fixed cost associated with participation in the SFC.

Table C.1. Generator Technical Data

Unit	Bus/Code	Turbine Type	P_g^{Min} [MW]	P_g^{Max} [MW]	RU_g/RD_g [MW/min]	C_g^{Fuel} [$/MWh]	C_g^{AGC} [$]
$G1_1$	Term_01_1 / $T1_1$	gas	50	520	8	140	4000
$G2_1$	Term_02_1 / $T2_1$	gas	50	520	8	200	3000
$G3_1$	Term_03_1 / $T3_1$	gas	50	520	6	160	2500
$G4_1$	Term_05_1 / $T5_1$	steam	50	500	6	50	1800
$G5_1$	Term_06_1 / $T6_1$	steam	50	500	4	60	4500
$G6_1$	Term_07_1 / $T7_1$	steam	50	500	4	60	2700
$G7_1$	Term_08_1 / $T8_1$	steam	50	500	5	60	2100
$G1_2$	Term_01_2 / $T1_2$	gas	50	520	8	140	800
$G2_2$	Term_02_2 / $T2_2$	gas	50	520	6	120	600
$G3_2$	Term_03_2 / $T3_2$	gas	50	520	7	90	500
$G4_2$	Term_05_2 / $T5_2$	steam	50	500	6	60	2800
$G5_2$	Term_06_2 / $T6_2$	steam	50	500	4	60	6000
$G1_3$	Term_01_3 / $T1_3$	gas	50	520	8	140	1000
$G2_3$	Term_02_3 / $T2_3$	gas	50	520	8	210	1500
$G3_3$	Term_03_3 / $T3_3$	gas	50	520	6	100	900
$G4_3$	Term_05_3 / $T5_3$	steam	50	500	5	50	3500
$G5_3$	Term_06_3 / $T6_3$	steam	50	500	4	60	850
$G6_3$	Term_07_3 / $T7_3$	steam	50	500	7	80	4600
$G7_3$	Term_08_3 / $T8_3$	steam	50	500	4	60	7000
$G1_4$	Term_01_4 / $T1_4$	gas	50	520	8	140	2000
$G2_4$	Term_02_4 / $T2_4$	gas	50	520	8	300	12000
$G3_4$	Term_04_4 / $T4_4$	gas	50	520	8	100	1200
$G4_4$	Term_05_4 / $T5_4$	steam	50	500	5	50	5000
$G5_4$	Term_06_4 / $T6_4$	steam	50	500	4	60	3900
$G6_4$	Term_07_4 / $T7_4$	steam	50	520	6.5	160	3200
$G7_4$	Term_08_4 / $T8_4$	steam	50	500	3	60	1400

C.2 Unit Dispatch Schedules

Table C.2 presents the scheduled dispatch of the generating units across the three operating load conditions considered: off-peak, shoulder, and peak.

Table C.2. Unit Dispatch Schedules by Operating Condition

Unit	Off-peak [MW]	Shoulder [MW]	Peak [MW]
$G1_1$	–	–	83.11
$G2_1$	50.00	400.00	400.00
$G3_1$	154.83	420.00	420.00
$G4_1$	350.00	350.00	350.00
$G5_1$	400.00	400.00	400.00
$G6_1$	298.03	298.54	299.18
$G7_1$	298.03	298.54	299.18
$G1_2$	50.00	400.00	–
$G2_2$	50.00	400.00	400.00
$G3_2$	400.00	400.00	400.00
$G4_2$	400.00	400.00	400.00
$G5_2$	400.00	400.00	400.00
$G1_3$	–	–	400.00
$G2_3$	50.00	269.57	400.00
$G3_3$	238.19	400.00	400.00
$G4_3$	400.00	400.00	400.00
$G5_3$	400.00	400.00	400.00
$G6_3$	400.00	400.00	400.00
$G7_3$	400.00	400.00	400.00
$G1_4$	50.00	–	170.40
$G2_4$	50.00	50.00	420.00
$G3_4$	400.00	400.00	400.00
$G4_4$	400.00	400.00	400.00
$G5_4$	400.00	400.00	400.00
$G6_4$	400.00	400.00	400.00
$G7_4$	400.00	400.00	400.00

C.3 Dynamic models

This section summarizes the dynamic models used for the generating units. Figure C.1 shows the IEEEG1 turbine-governor used for each steam power unit. Figure C.2 shows the GAST turbine-governor used for each gas power unit. Figure C.3 shows the ZHITEX automatic voltage regulator applied to all power units. All models are taken from the DIgSILENT PowerFactory standard library, and they are implemented using DSL.

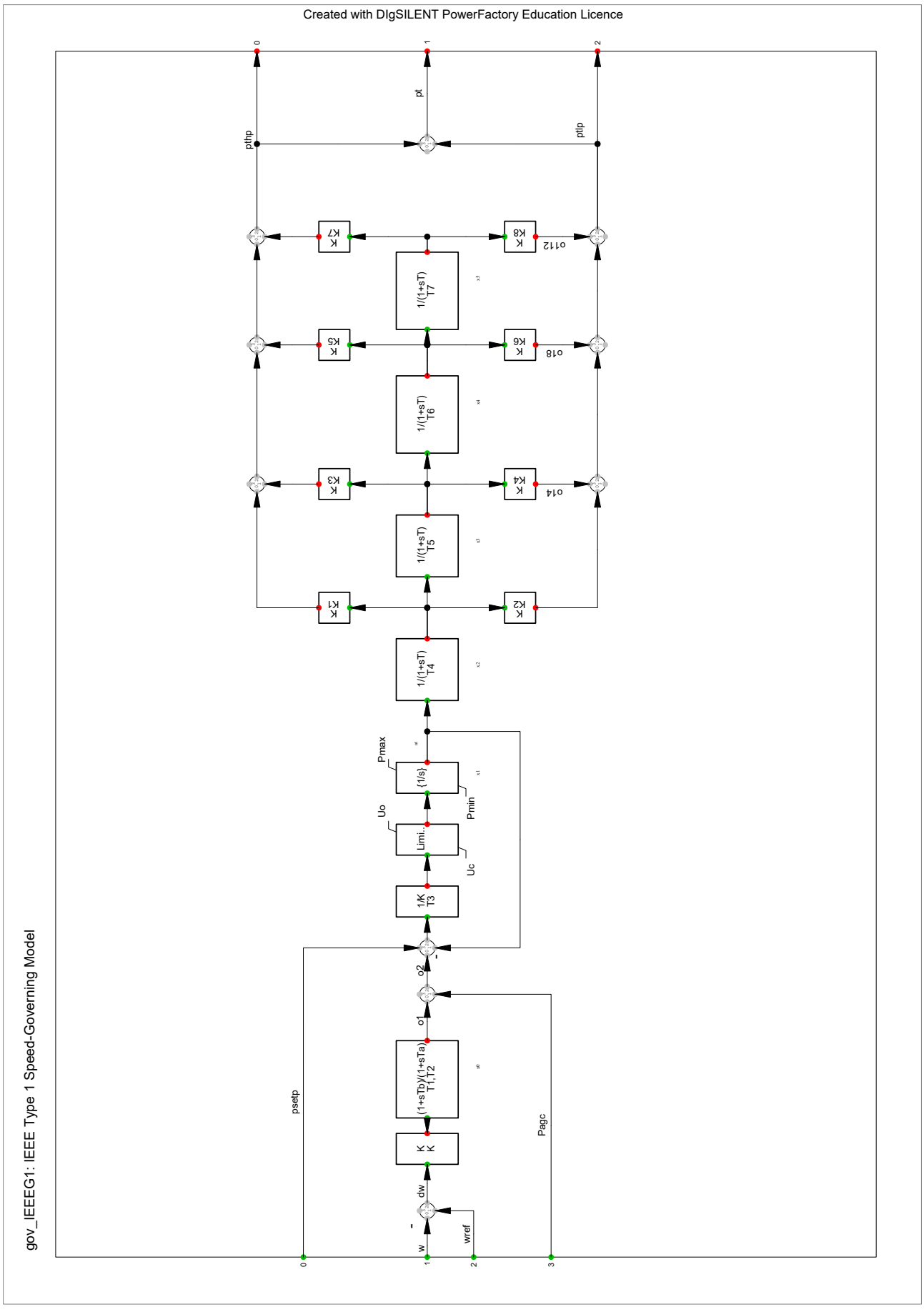

Figure C.1. IEEEG1 turbine-governor model for steam units

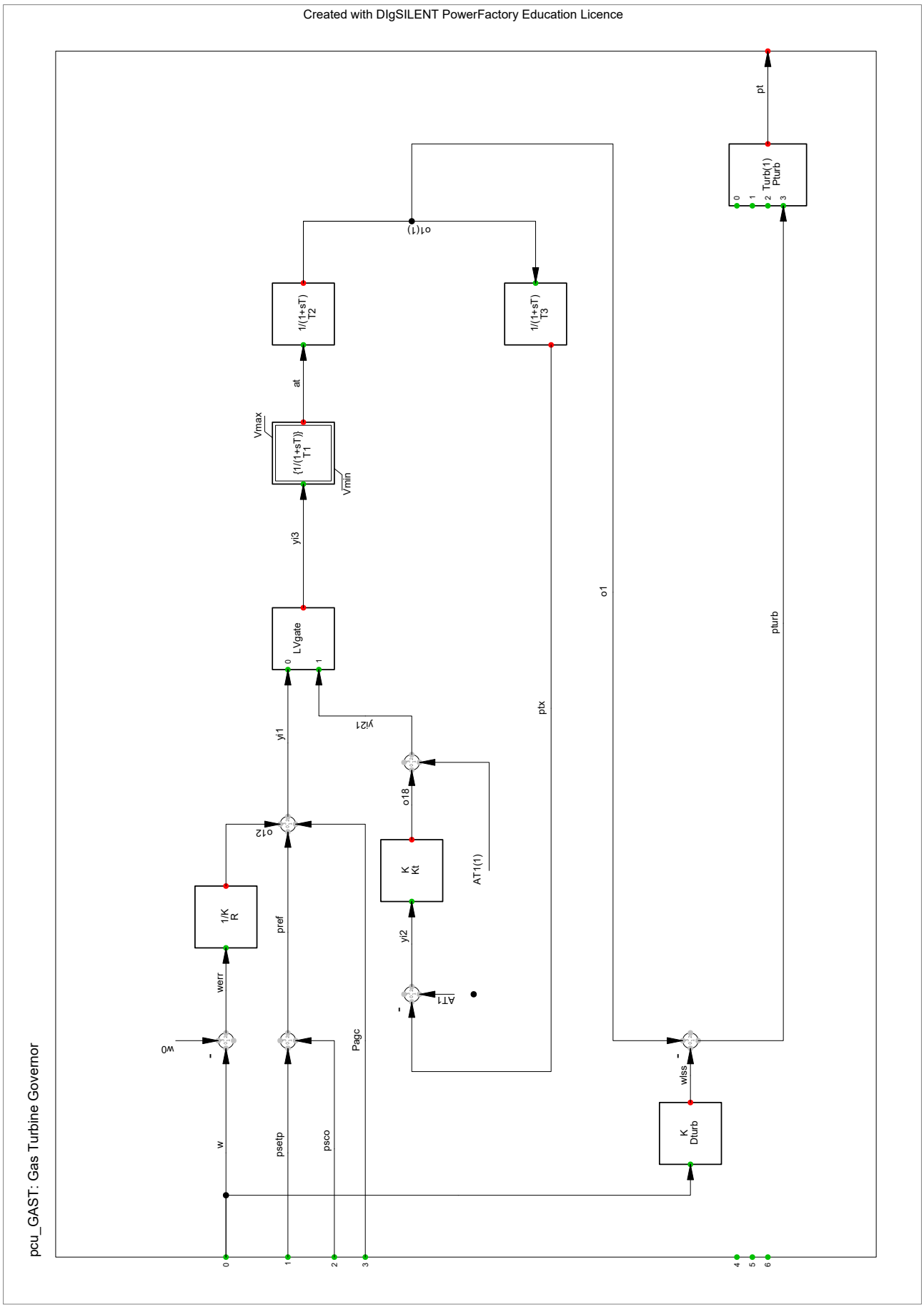

Figure C.2. gasT turbine-governor model for gas units

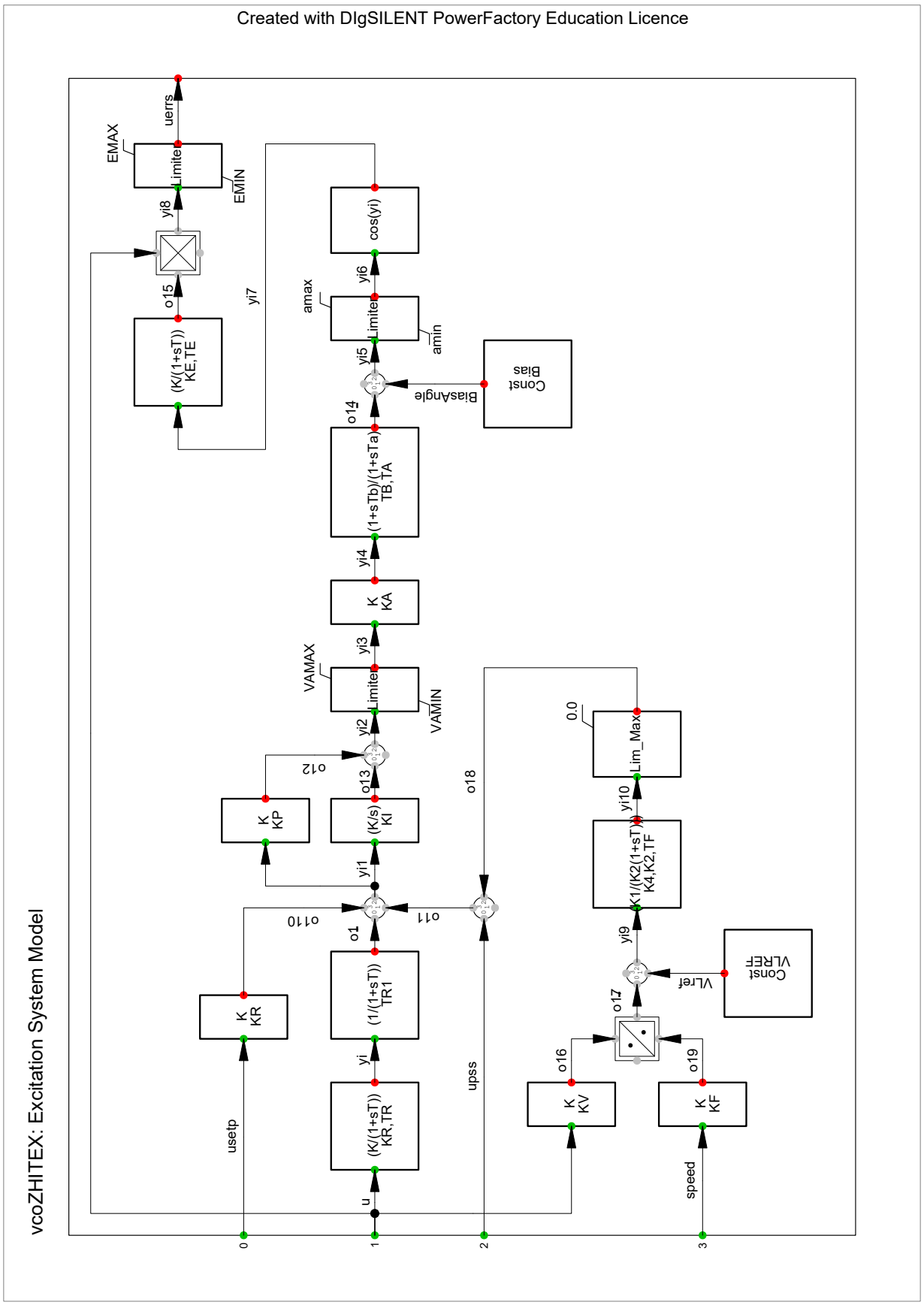

Figure C.3. ZHITEX automatic voltage regulator for all generators

C.4 Transmission Line Data

Table C.3 presents the transmission line data used in this study. For each line, the table reports the sending and receiving buses, the series resistance and reactance, the total shunt susceptance, and the thermal rating.

Table C.3. Transmission Line Data

Name/ Code	From/ Code	To/ Code	R [ohm]	X [ohm]	B [uS]	S_{max} [MVA]
Line1_1 / $L1_1$	Term_10_1 / $T10_1$	Term_09_1 / $T9_1$	0.46	4	112.8	796.74
Line2_1 / $L2_1$	Term_12_1 / $T12_1$	Term_10_1 / $T10_1$	2.30	20	141.0	796.74
Line3_1 / $L3_1$	Term_12_1 / $T12_1$	Term_13_1 / $T13_1$	0.23	2	14.1	736.99
Line4_1 / $L4_1$	Term_13_1 / $T13_1$	Term_14_1 / $T14_1$	0.2875	2.5	70.5	796.74
Line5_1 / $L5_1$	Term_14_1 / $T14_1$	Term_11_1 / $T11_1$	0.575	5	141.0	796.74
Line6_1 / $L6_1$	Term_11_1 / $T11_1$	Term_09_1 / $T9_1$	0.46	4	112.8	956.09
Line7_1 / $L7_1$	Term_12_1 / $T12_1$	Term_10_1 / $T10_1$	2.30	20	141.0	796.74
Line1_2 / $L1_2$	Term_10_2 / $T10_2$	Term_09_2 / $T9_2$	0.0058	0.05	1.41	796.74
Line2_2 / $L2_2$	Term_12_2 / $T12_2$	Term_10_2 / $T10_2$	2.30	20	141.0	826.62
Line3_2 / $L3_2$	Term_12_2 / $T12_2$	Term_13_2 / $T13_2$	0.23	2	14.1	1195.12
Line4_2 / $L4_2$	Term_13_2 / $T13_2$	Term_14_2 / $T14_2$	1.15	10	70.5	796.74
Line5_2 / $L5_2$	Term_14_2 / $T14_2$	Term_11_2 / $T11_2$	1.15	10	282.0	1593.49
Line6_2 / $L6_2$	Term_11_2 / $T11_2$	Term_09_2 / $T9_2$	0.46	4	28.2	1046.92
Line7_2 / $L7_2$	Term_12_2 / $T12_2$	Term_10_2 / $T10_2$	2.30	20	141.0	826.62
Line8_2 / $L8_2$	Term_12_2 / $T12_2$	Term_13_2 / $T13_2$	0.23	2	14.1	1195.12
Line9_2 / $L9_2$	Term_13_2 / $T13_2$	Term_14_2 / $T14_2$	1.15	10	70.5	796.74
Line10_2 / $L10_2$	Term_11_2 / $T11_2$	Term_09_2 / $T9_2$	0.46	4	28.2	1046.92
Line1_3 / $L1_3$	Term_10_3 / $T10_3$	Term_09_3 / $T9_3$	1.84	16	112.8	796.74
Line2_3 / $L2_3$	Term_12_3 / $T12_3$	Term_10_3 / $T10_3$	0.575	5	141.0	796.74
Line3_3 / $L3_3$	Term_12_3 / $T12_3$	Term_14_3 / $T14_3$	1.38	12	84.6	1234.95
Line5_3 / $L5_3$	Term_14_3 / $T14_3$	Term_11_3 / $T11_3$	0.575	20	141.0	796.74
Line6_3 / $L6_3$	Term_11_3 / $T11_3$	Term_09_3 / $T9_3$	0.46	16	112.8	796.74
Line7_3 / $L7_3$	Term_12_3 / $T12_3$	Term_10_3 / $T10_3$	0.575	5	141.0	796.74
Line8_3 / $L8_3$	Term_12_3 / $T12_3$	Term_14_3 / $T14_3$	1.38	12	84.6	1234.95
Line9_3 / $L9_3$	Term_10_3 / $T10_3$	Term_09_3 / $T09_3$	1.84	16	112.8	796.74
Line1_4 / $L1_4$	Term_10_4 / $T10_4$	Term_09_4 / $T9_4$	0.46	4	112.8	1035.77
Line2_4 / $L2_4$	Term_12_4 / $T12_4$	Term_10_4 / $T10_4$	2.30	20	141.0	796.74
Line3_4 / $L3_4$	Term_12_4 / $T12_4$	Term_13_4 / $T13_4$	0.23	2	14.1	1195.12
Line4_4 / $L4_4$	Term_13_4 / $T13_4$	Term_14_4 / $T14_4$	0.2875	2.5	70.5	876.42
Line5_4 / $L5_4$	Term_14_4 / $T14_4$	Term_11_4 / $T11_4$	0.575	5	141.0	1195.12
Line6_4 / $L6_4$	Term_11_4 / $T11_4$	Term_09_4 / $T9_4$	0.46	4	112.8	995.93
Line7_4 / $L7_4$	Term_12_4 / $T12_4$	Term_10_4 / $T10_4$	2.30	20	141.0	796.74
Line8_4 / $L8_4$	Term_11_4 / $T11_4$	Term_09_4 / $T9_4$	0.46	4	112.8	995.93
Trans_Line_1/$I1_3^{(1)}$	Term_11_3 / $T11_3$	Term_14_1 / $T14_1$	0.345	3	84.6	796.74
Trans_Line_2/$I1_3^{(2)}$	Term_11_3 / $T11_3$	Term_14_1 / $T14_1$	0.345	3	84.6	796.74
Trans_Line_3/$I1_4^{(1)}$	Term_10_4 / $T10_4$	Term_09_1 / $T9_1$	0.8625	7.5	211.5	796.74
Trans_Line_4/$I1_4^{(2)}$	Term_10_4 / $T10_4$	Term_09_1 / $T9_1$	0.8625	7.5	211.5	796.74
Trans_Line_5/$I2_4^{(1)}$	Term_10_4 / $T10_4$	Term_12_2 / $T12_2$	1.15	10	282.0	796.74
Trans_Line_6/$I2_4^{(2)}$	Term_10_4 / $T10_4$	Term_12_2 / $T12_2$	1.15	10	282.0	796.74
Trans_Line_7/$I3_4^{(1)}$	Term_12_4 / $T12_4$	Term_11_3 / $T11_3$	0.575	5	141.0	796.74
Trans_Line_8/$I3_4^{(2)}$	Term_12_4 / $T12_4$	Term_11_3 / $T11_3$	0.575	5	141.0	796.74

C.5 Transformer Data

Table C.4 summarizes the main parameters of each transformer, including the high- and low-voltage buses, rated apparent power, nominal voltages, and short-circuit voltage. All transformers are configured with vector group YNd1 and equipped with an on-load tap changer (OLTC) that provides ±8 steps with an increment of 1.25% per step.

Table C.4. Two-winding transformer data

Name	HV Bus/Code	LV Bus/Code	$S_{\max}$ [MVA]	HV [kV]	LV [kV]	Short-circuit voltage [%]
Trafo1_1	Term_09_1 / $T9_1$	Term_01_1 / $T1_1$	700	230	16.50	14.4
Trafo1_2	Term_09_2 / $T9_2$	Term_01_2 / $T1_2$	700	230	16.50	14.4
Trafo1_3	Term_09_3 / $T9_3$	Term_01_3 / $T1_3$	700	230	16.50	14.4
Trafo1_4	Term_09_4 / $T9_4$	Term_01_4 / $T1_4$	700	230	16.50	14.4
Trafo2_1	Term_09_1 / $T9_1$	Term_02_1 / $T2_1$	700	230	16.50	14.4
Trafo2_2	Term_09_2 / $T9_2$	Term_02_2 / $T2_2$	700	230	16.50	14.4
Trafo2_3	Term_09_3 / $T9_3$	Term_02_3 / $T2_3$	700	230	16.50	14.4
Trafo2_4	Term_09_4 / $T9_4$	Terma_02_4 / $T2_4$	700	230	16.50	14.4
Trafo3_1	Term_09_1 / $T9_1$	Term_03_1 / $T3_1$	700	230	16.50	14.4
Trafo3_2	Term_09_2 / $T9_2$	Term_03_2 / $T3_2$	700	230	16.50	14.4
Trafo3_3	Term_09_3 / $T9_3$	Term_03_3 / $T3_3$	700	230	16.50	14.4
Trafo4_4	Term_09_4 / $T9_4$	Term_04_4 / $T4_4$	700	230	16.50	14.4
Trafo5_1	Term_12_1 / $T12_1$	Term_05_1 / $T5_1$	500	230	18.00	12.5
Trafo5_2	Term_12_2 / $T12_2$	Term_05_2 / $T5_2$	500	230	18.00	12.5
Trafo5_3	Term_12_3 / $T12_3$	Term_05_3 / $T5_3$	500	230	18.00	12.5
Trafo5_4	Term_12_4 / $T12_4$	Term_05_4 / $T5_4$	500	230	18.00	12.5
Trafo6_1	Term_12_1 / $T12_1$	Term_06_1 / $T6_1$	500	230	18.00	12.5
Trafo6_2	Term_12_2 / $T12_2$	Term_06_2 / $T6_2$	500	230	18.00	12.5
Trafo6_3	Term_12_3 / $T12_3$	Term_06_3 / $T6_3$	500	230	18.00	12.5
Trafo6_4	Term_12_4 / $T12_4$	Term_06_4 / $T6_4$	500	230	18.00	12.5
Trafo7_1	Term_14_1 / $T14_1$	Term_07_1 / $T7_1$	900	230	13.80	8.79
Trafo7_3	Term_14_3 / $T14_3$	Term_07_3 / $T7_3$	900	230	13.80	8.79
Trafo7_4	Term_14_4 / $T14_4$	Term_07_4 / $T7_4$	900	230	13.80	8.79
Trafo8_1	Term_14_1 / $T14_1$	Term_08_1 / $T8_1$	900	230	13.80	8.79
Trafo8_3	Term_14_3 / $T14_3$	Term_08_3 / $T8_3$	900	230	13.80	8.79
Trafo8_4	Term_14_4 / $T14_4$	Term_08_4 / $T8_4$	900	230	13.80	8.79
Trafo9_3	Term_15_3 / $T15_3$	Term_14_3 / $T14_3$	3000	345	230	7.00

C.6 Load Data

Table C.5 shows the active power demand for each load, assigned to its bus, under peak, shoulder, and off-peak operating conditions, together with the corresponding power factor (PF).

Table C.5. Load data

Load	Area	Bus/ Code	Peak [MW]	Shoulder [MW]	Off-peak [MW]	PF [-]
Load_A1	Area1	Term_10_1/$T10_1$	200.00	170.00	140.00	0.95
Load_B1	Area1	Term_11_1/$T11_1$	300.00	255.00	210.00	0.95
Load_C1	Area1	Term_13_1/$T13_1$	400.00	340.00	280.00	0.94
Load_D1	Area1	Term_13_1/$T13_1$	300.00	255.00	210.00	0.94
Load_E1	Area1	Term_14_1/$T14_1$	350.00	297.50	245.00	0.94
Load_F1	Area1	Term_14_1/$T14_1$	350.00	297.50	245.00	0.94
Load_A2	Area2	Term_10_2/$T10_2$	500.00	425.00	350.00	0.95
Load_B2	Area2	Term_11_2/$T11_2$	280.00	238.00	196.00	0.95
Load_C2	Area2	Term_13_2/$T13_2$	300.00	255.00	210.00	0.95
Load_D2	Area2	Term_14_2/$T14_2$	700.00	595.00	490.00	0.95
Load_E2	Area2	Term_11_2/$T11_2$	700.00	595.00	490.00	0.95
HVDC Pole_1	Area3	Term_15_3/$T15_3$	1250.00	1062.50	875.00	0.89
HVDC Pole_2	Area3	Term_15_3/$T15_3$	1250.00	1062.50	875.00	0.89
Load_A3	Area3	Term_10_3/$T10_3$	150.00	127.50	105.00	0.95
Load_B3	Area3	Term_11_3/$T11_3$	250.00	212.50	175.00	0.95
Load_A4	Area4	Term_10_4/$T10_4$	200.00	170.00	140.00	0.95
Load_B4	Area4	Term_11_4/$T11_4$	300.00	255.00	210.00	0.95
Load_C4	Area4	Term_13_4/$T13_4$	600.00	510.00	420.00	0.95
Load_D4	Area4	Term_13_4/$T13_4$	200.00	170.00	140.00	0.95
Load_E4	Area4	Term_11_4/$T11_4$	200.00	170.00	140.00	0.95
Load_F4	Area4	Term_14_4/$T14_4$	400.00	340.00	280.00	0.95
Load_G4	Area4	Term_14_4/$T14_4$	400.00	340.00	280.00	0.95

Appendix D

Bus Voltage Profiles under $N-1-1$ Events and Transmission Switching

After solving the M6 instance and implementing the solution in DIgSILENT PF, this appendix reports the voltage profile results for two cases: (i) the worst contingency states under peak and shoulder operating conditions, and (ii) the second-worst contingency state under the off-peak condition. Figures D.1–D.4 summarize the results across the four zones for the peak condition. For each zone, an overall voltage profile is provided, along with zoomed views isolating generator outage, line outage, and TS events.

Similarly, Figures D.5–D.8 and D.9–D.12 present the corresponding results for the shoulder and off-peak conditions, respectively. These figures confirm that, by the end of the SFC stage, voltages remain within acceptable limits. Additionally, TS actions do not provoke significant voltage degradation compared with the other outage events.

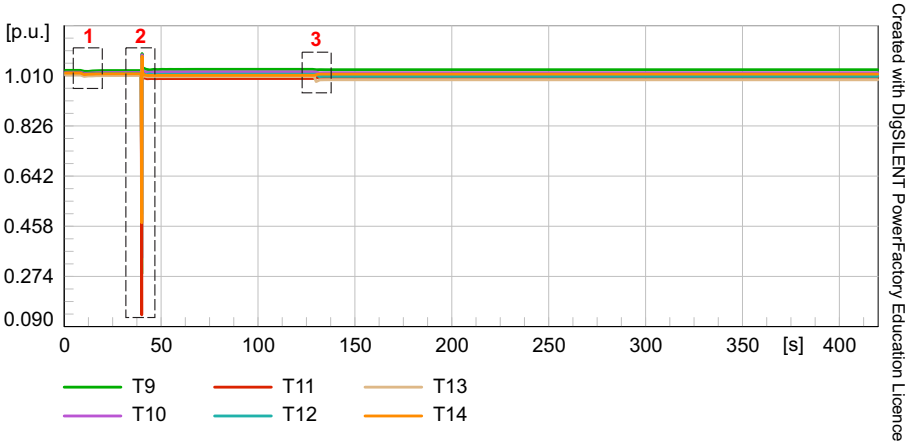

(a) Overall voltage profile in zone 1. Highlighted windows 1–3 correspond to the events below.

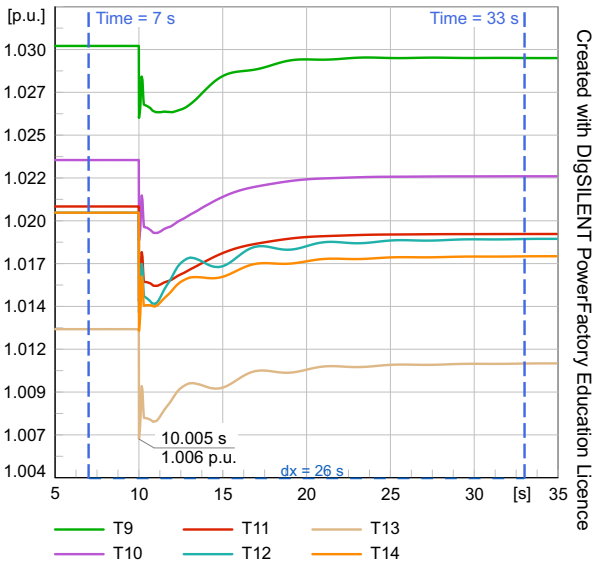

(b) Event 1: $G6_1$ outage

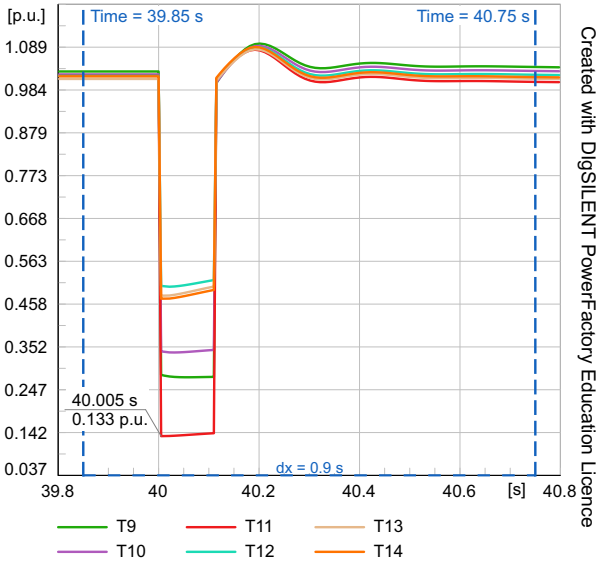

(c) Event 2: $L6_1$ short-circuit and clearance

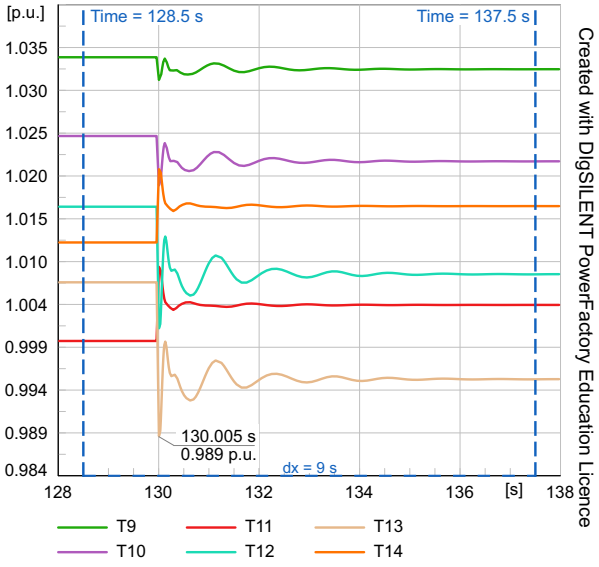

(d) Event 3: $L4_1$ switching

Figure D.1. Voltage response in zone 1 under the worst contingency state at peak condition for the M6 solution. Own work.

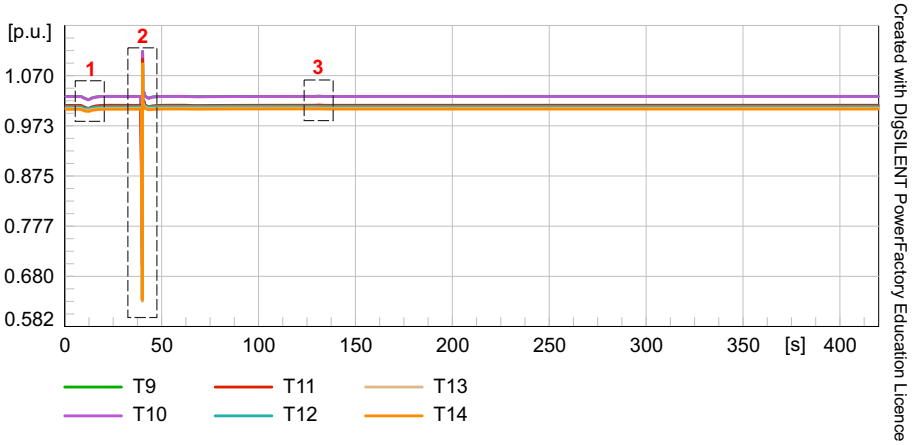

(a) Overall voltage profile in zone 2. Highlighted windows 1–3 correspond to the events below.

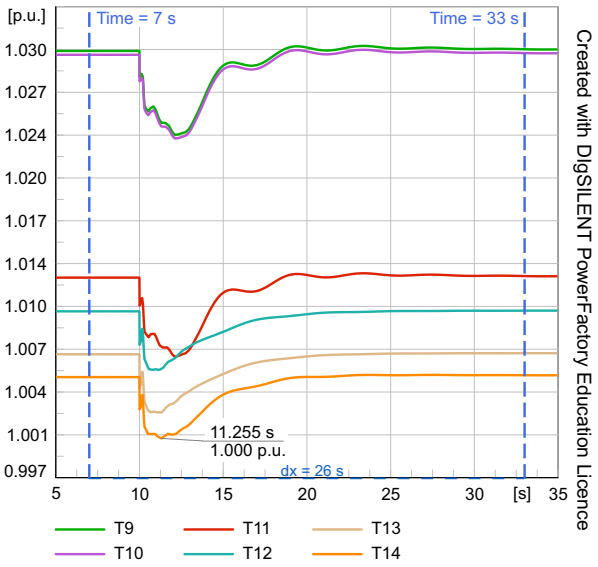

(b) Event 1: $G6_1$ outage

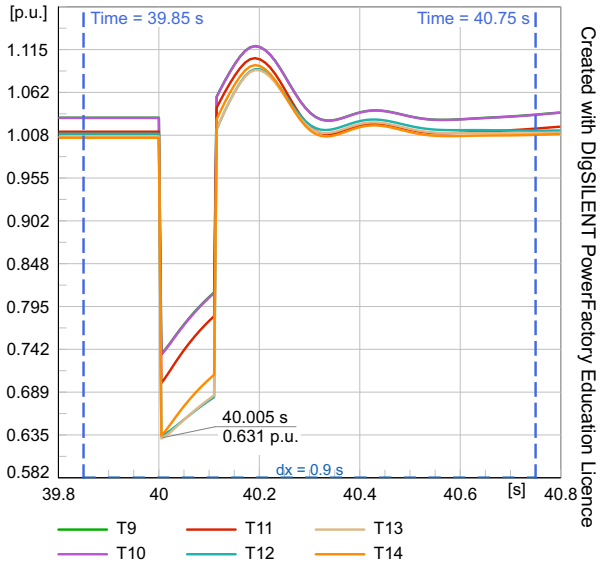

(c) Event 2: $L6_1$ short-circuit and clearance

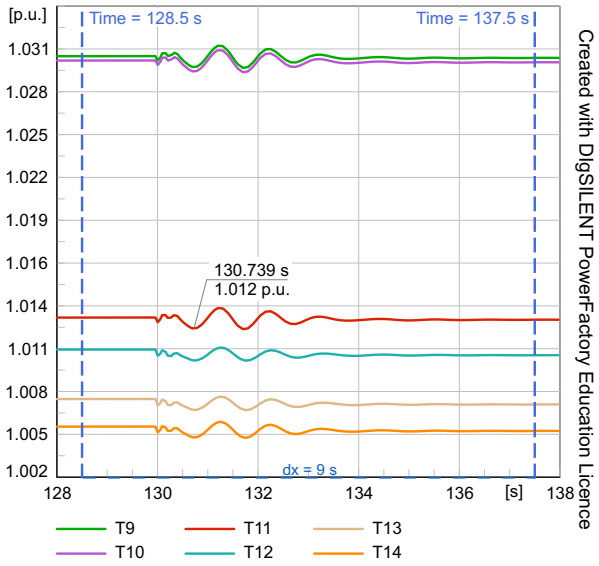

(d) Event 3: $L4_1$ switching

Figure D.2. Voltage response in zone 2 under the worst contingency state at peak condition for the M6 solution. Own work.

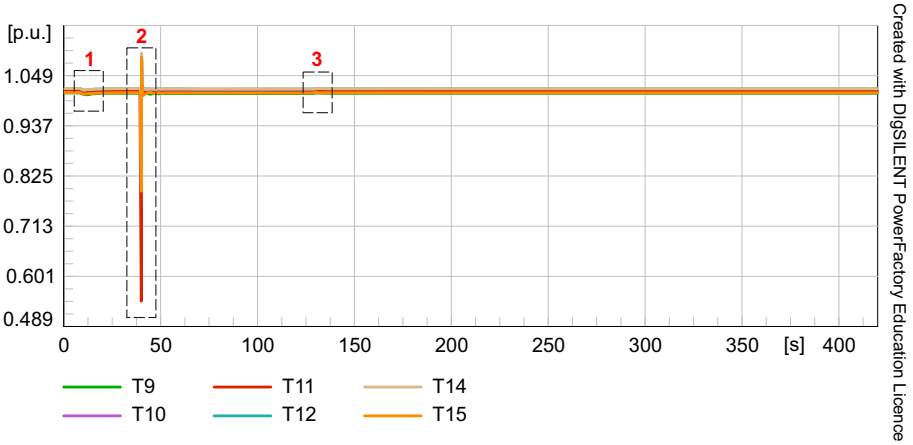

(a) Overall voltage profile in zone 3. Highlighted windows 1–3 correspond to the events below.

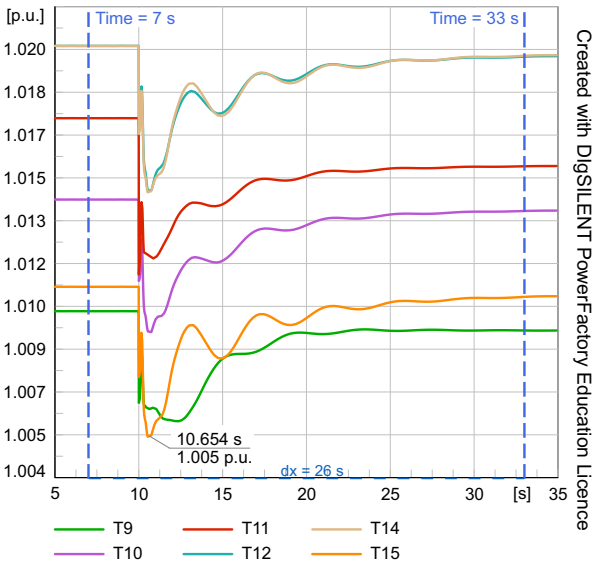

(b) Event 1: $G6_1$ outage

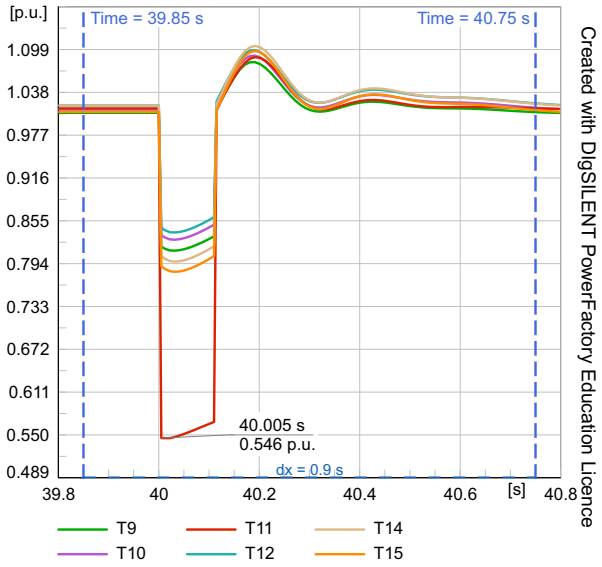

(c) Event 2: $L6_1$ short-circuit and clearance

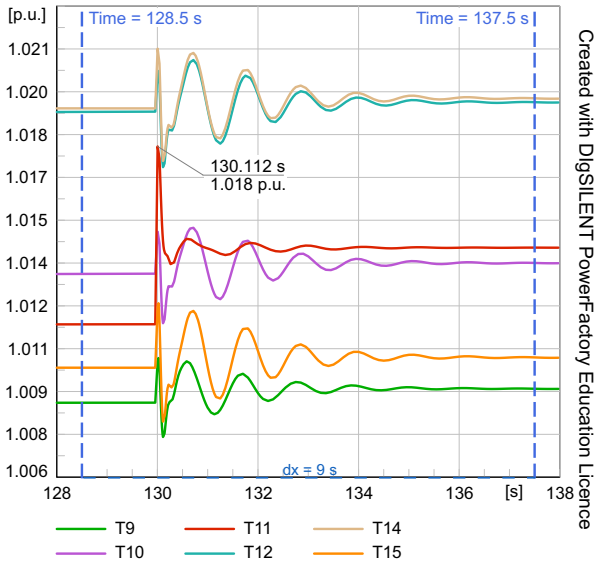

(d) Event 3: $L4_1$ switching

Figure D.3. Voltage response in zone 3 under the worst contingency state at peak condition for the M6 solution. Own work.

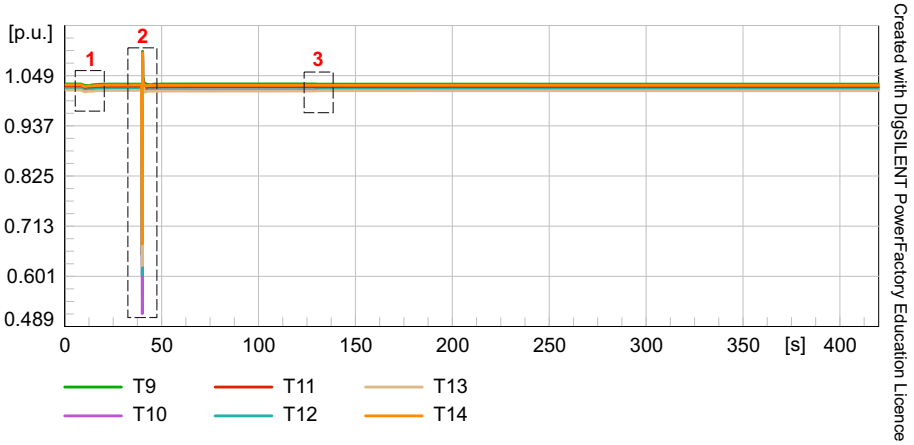

(a) Overall voltage profile in zone 4. Highlighted windows 1–3 correspond to the events below.

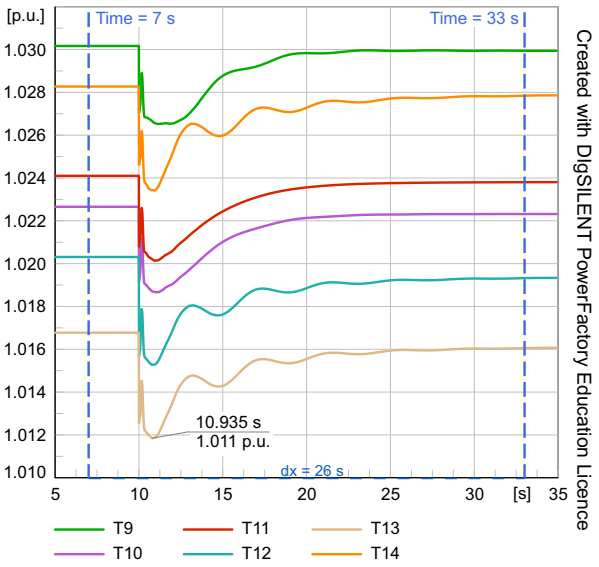

(b) Event 1: $G6_1$ outage

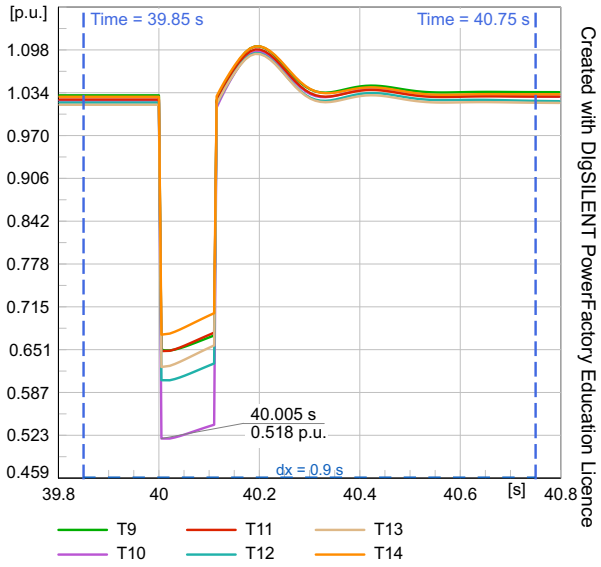

(c) Event 2: $L6_1$ short-circuit and clearance

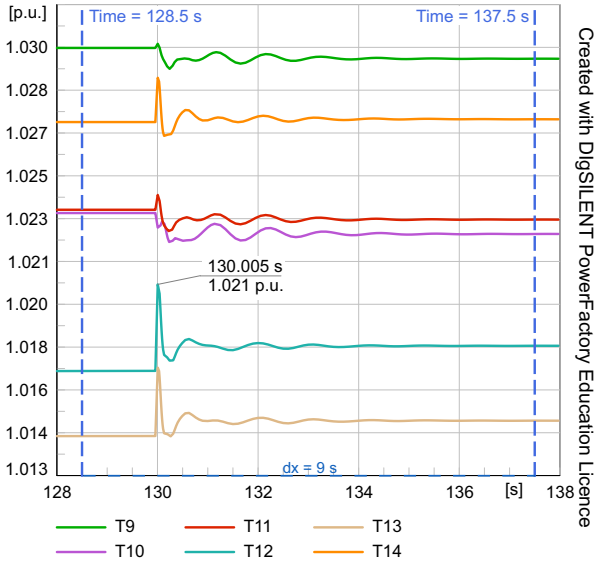

(d) Event 3: $L4_1$ switching

Figure D.4. Voltage response in zone 4 under the worst contingency state at peak condition for the M6 solution. Own work.

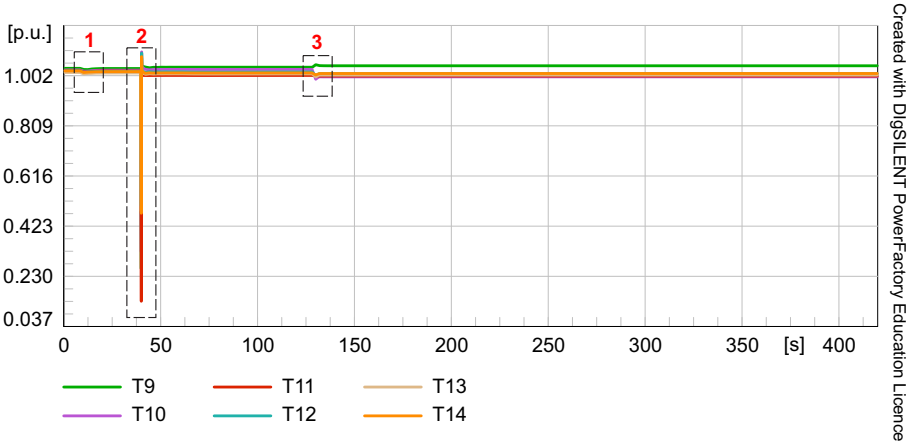

(a) Overall voltage profile in zone 4. Highlighted windows 1–3 correspond to the events below.

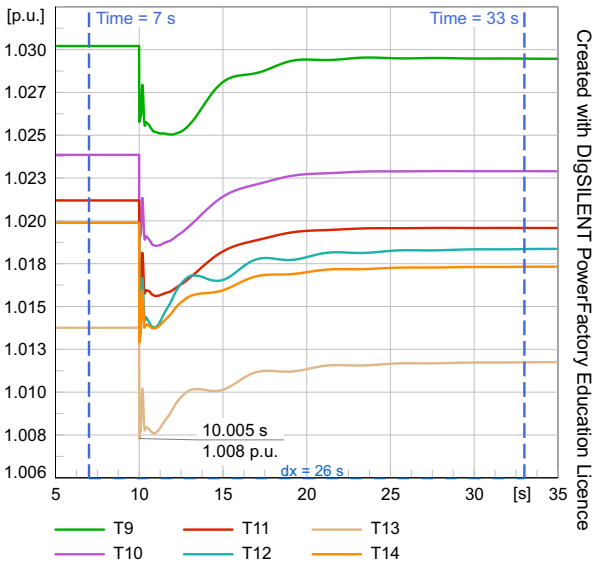

(b) Event 1: $G6_1$ outage

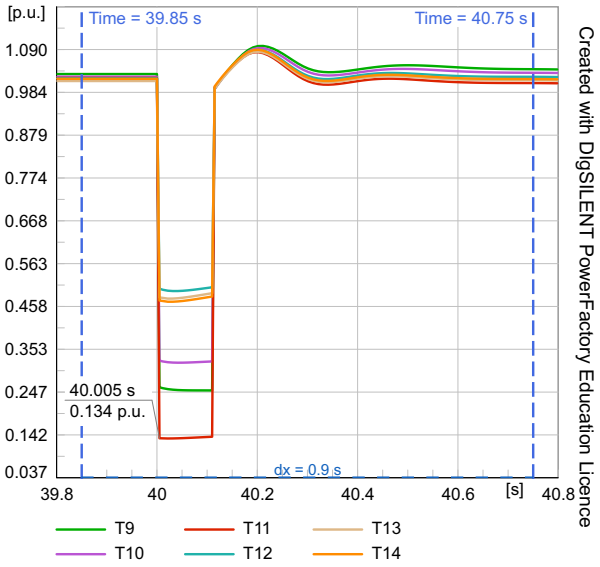

(c) Event 2: $L6_1$ short-circuit and clearance

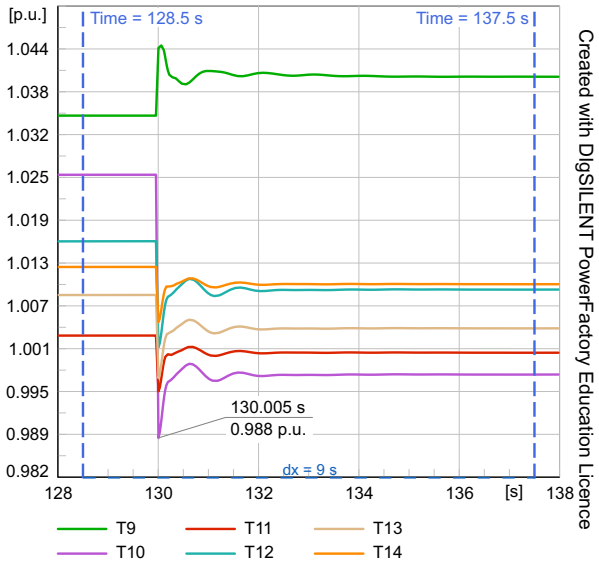

(d) Event 3: $L1_1$ switching

Figure D.5. Voltage response in zone 1 under the worst contingency state at shoulder condition for the M6 solution. Own work.

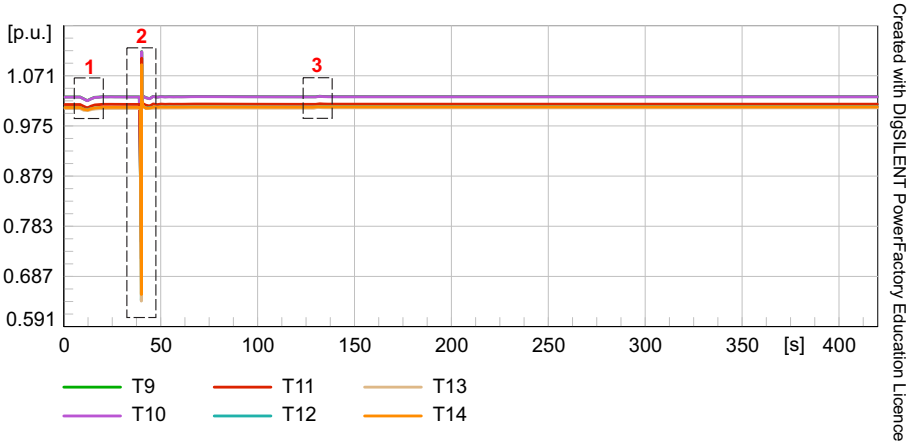

(a) Overall voltage profile in zone 4. Highlighted windows 1–3 correspond to the events below.

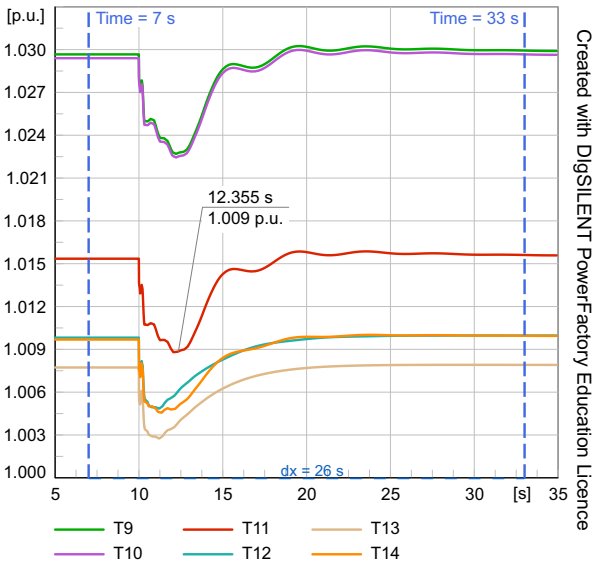

(b) Event 1: $G6_1$ outage

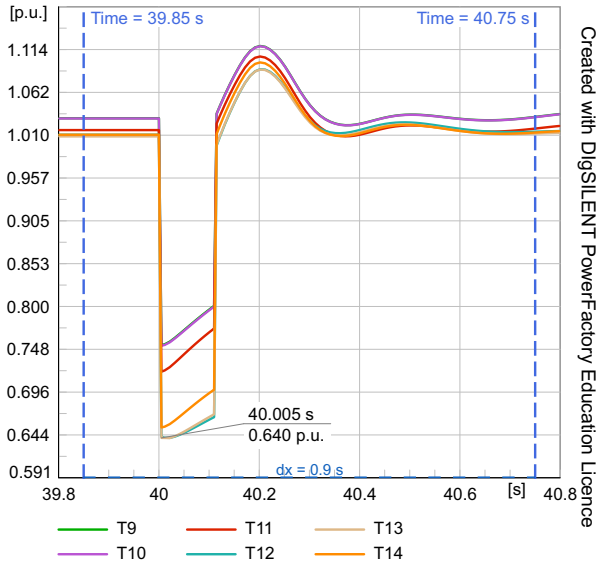

(c) Event 2: $L6_1$ short-circuit and clearance

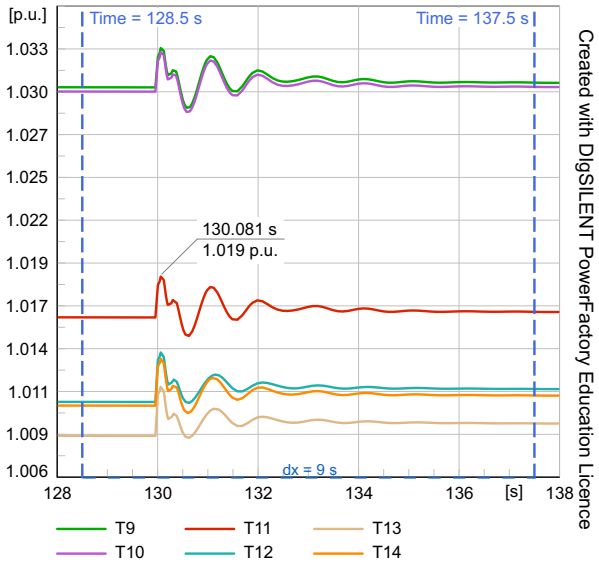

(d) Event 3: $L1_1$ switching

Figure D.6. Voltage response in zone 2 under the worst contingency state at shoulder condition for the M6 solution. Own work.

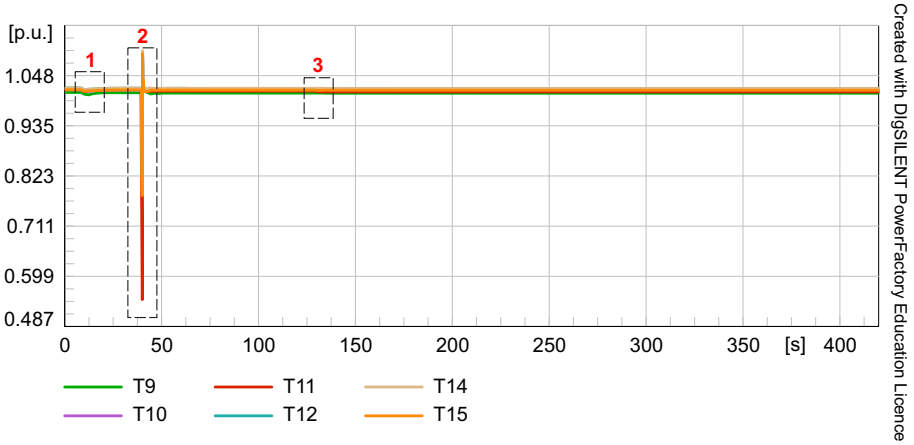

(a) Overall voltage profile in zone 4. Highlighted windows 1–3 correspond to the events below.

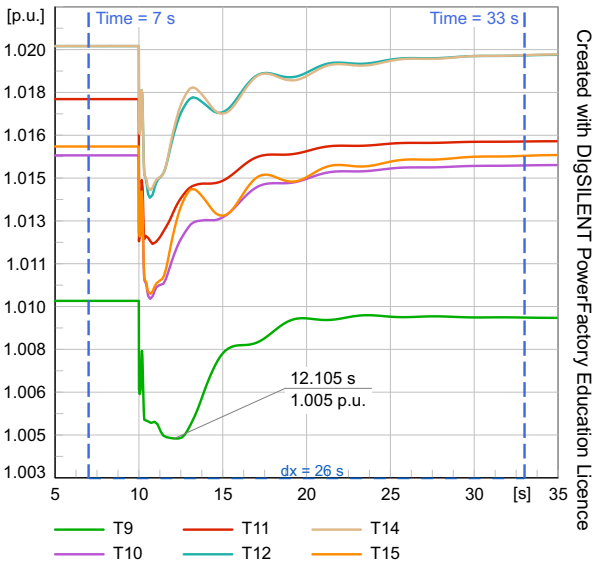

(b) Event 1: $G6_1$ outage

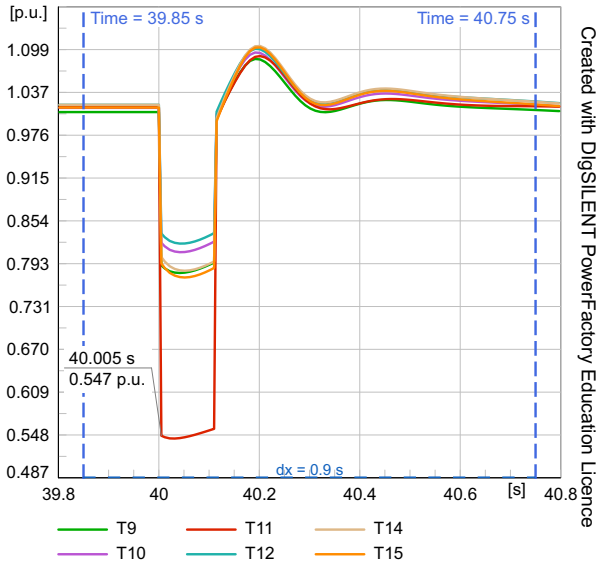

(c) Event 2: $L6_1$ short-circuit and clearance

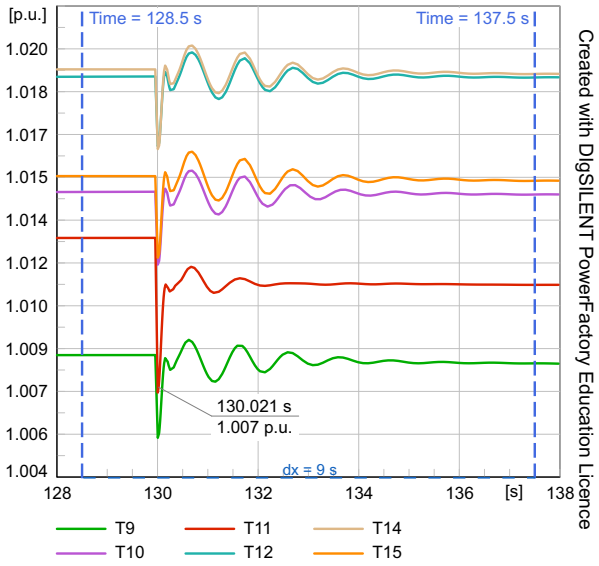

(d) Event 3: $L1_1$ switching

Figure D.7. Voltage response in zone 3 under the worst contingency state at shoulder condition for the M6 solution. Own work.

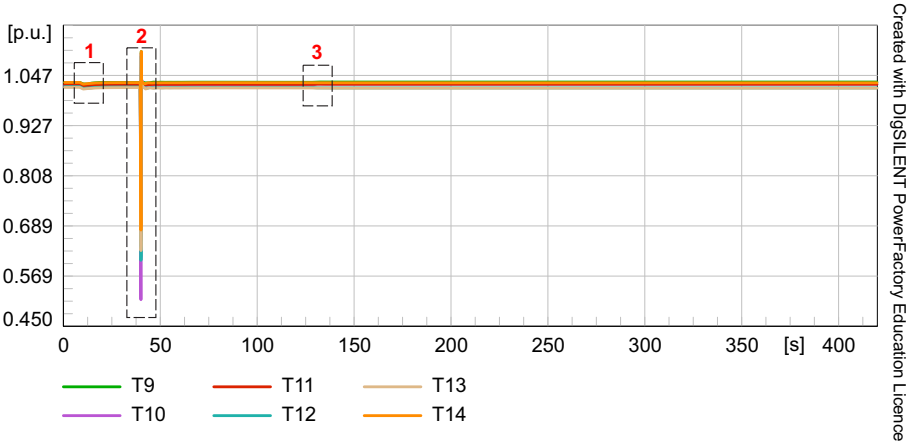

(a) Overall voltage profile in zone 4. Highlighted windows 1–3 correspond to the events below.

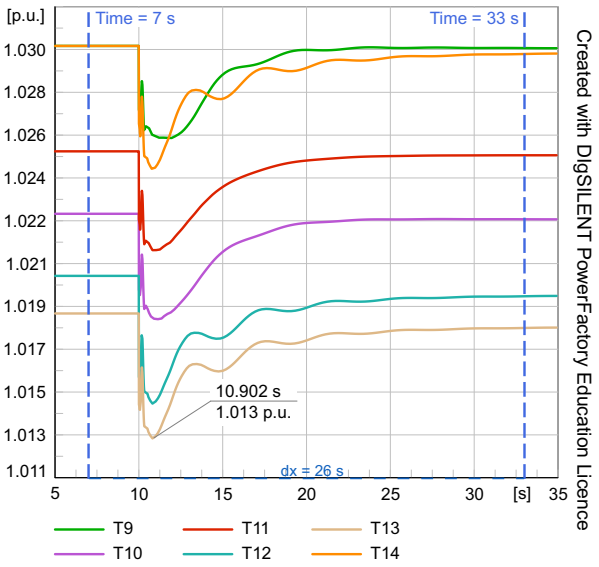

(b) Event 1: $G6_1$ outage

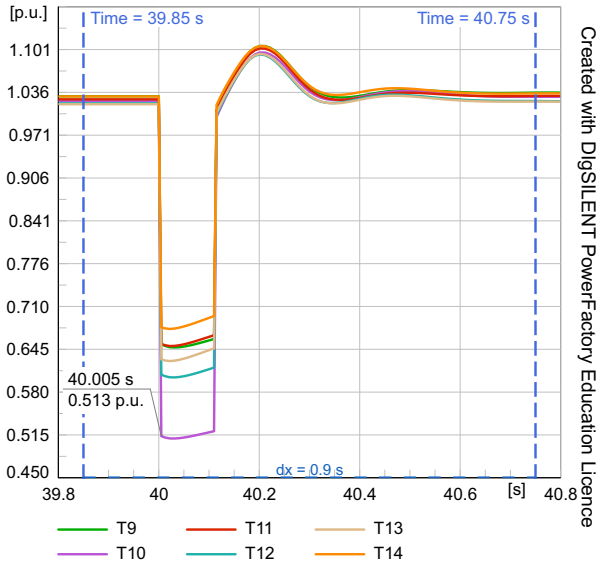

(c) Event 2: $L6_1$ short-circuit and clearance

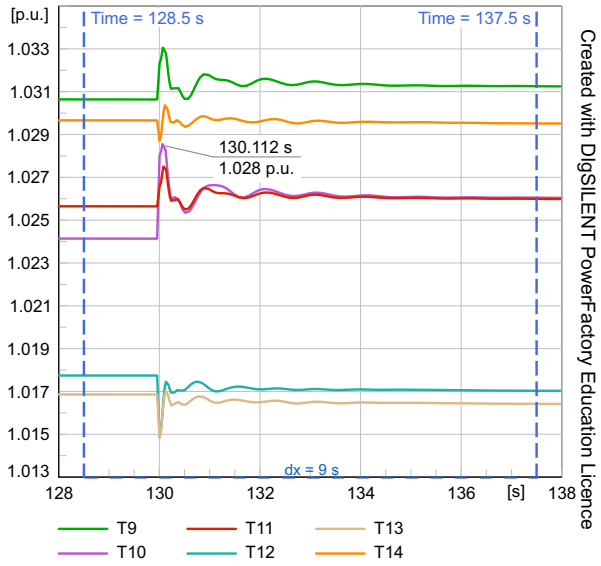

(d) Event 3: $L1_1$ switching

Figure D.8. Voltage response in zone 4 under the worst contingency state at shoulder condition for the M6 solution. Own work.

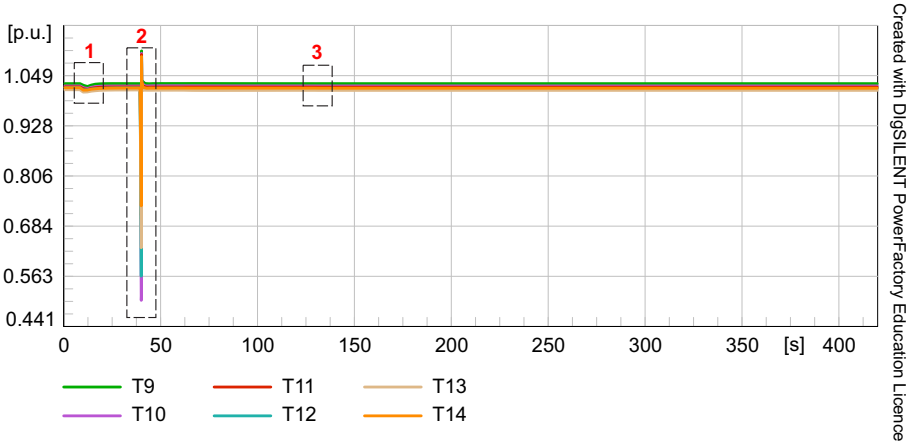

(a) Overall voltage profile in zone 4. Highlighted windows 1–3 correspond to the events below.

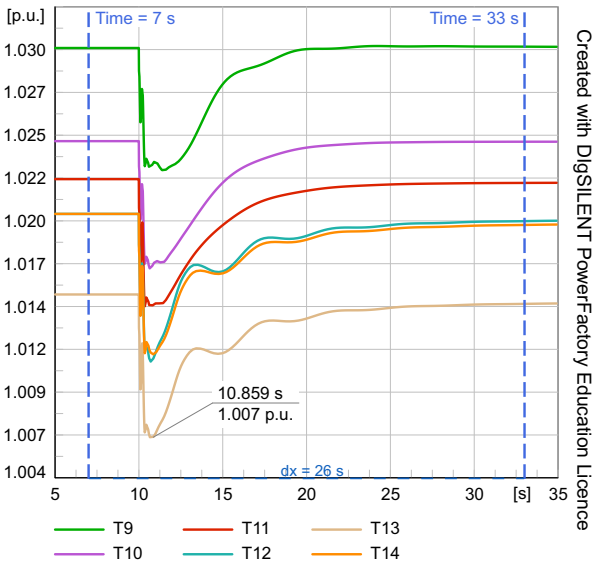

(b) Event 1: $G5_3$ outage

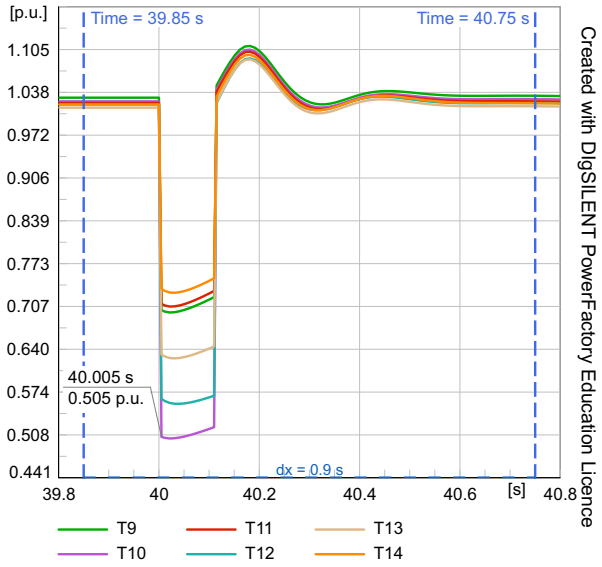

(c) Event 2: $L7_1$ short-circuit and clearance

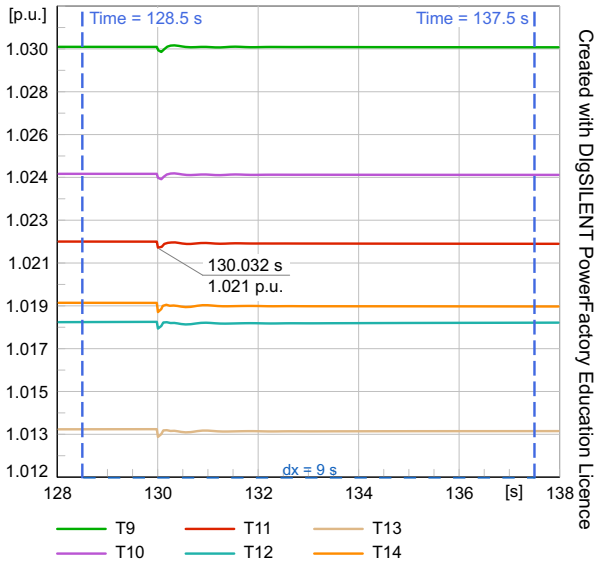

(d) Event 3: $L2_4$ switching

Figure D.9. Voltage response in zone 1 under the second-worst contingency state at off-peak condition for the M6 solution. Own work.

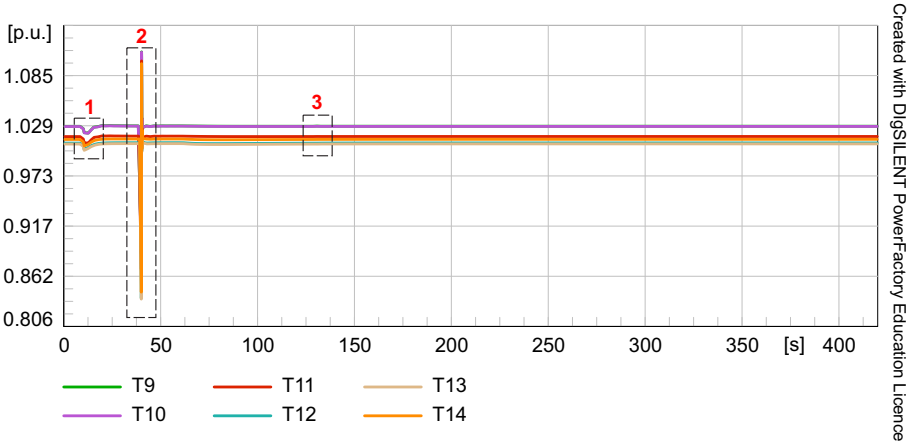

(a) Overall voltage profile in zone 4. Highlighted windows 1–3 correspond to the events below.

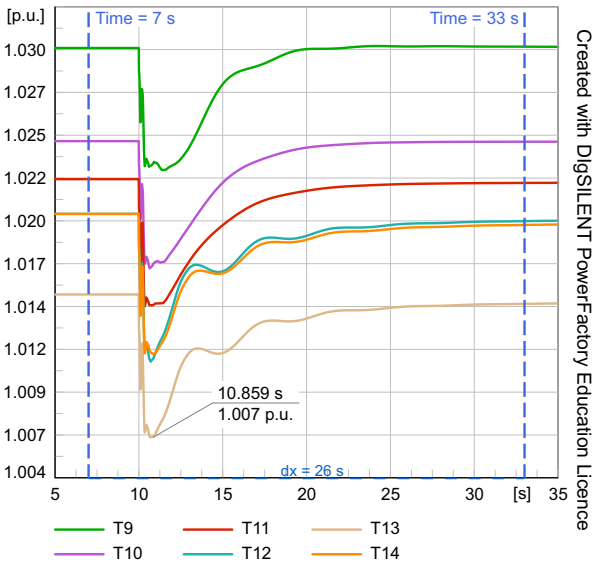

(b) Event 1: $G5_3$ outage

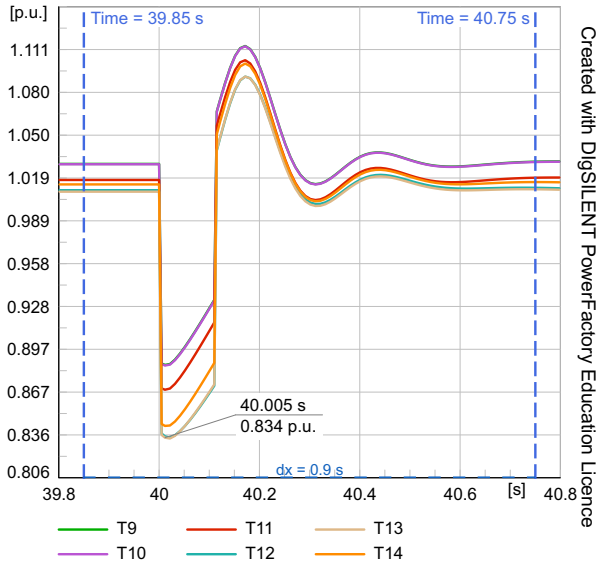

(c) Event 2: $L7_1$ short-circuit and clearance

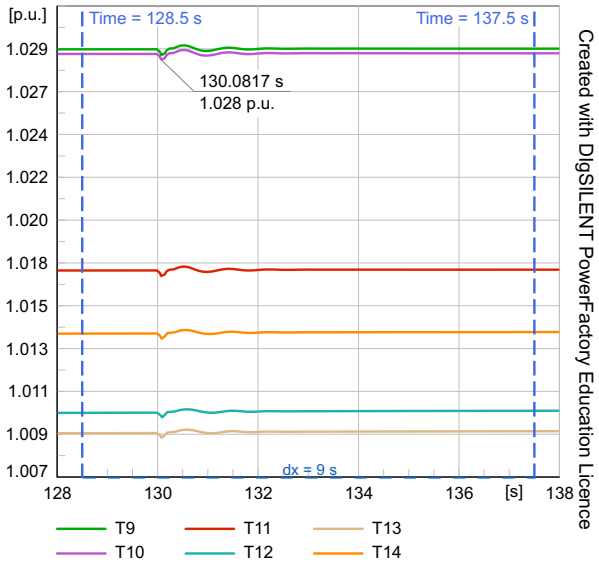

(d) Event 3: $L2_4$ switching

Figure D.10. Voltage response in zone 2 under the second-worst contingency state at off-peak condition for the M6 solution. Own work.

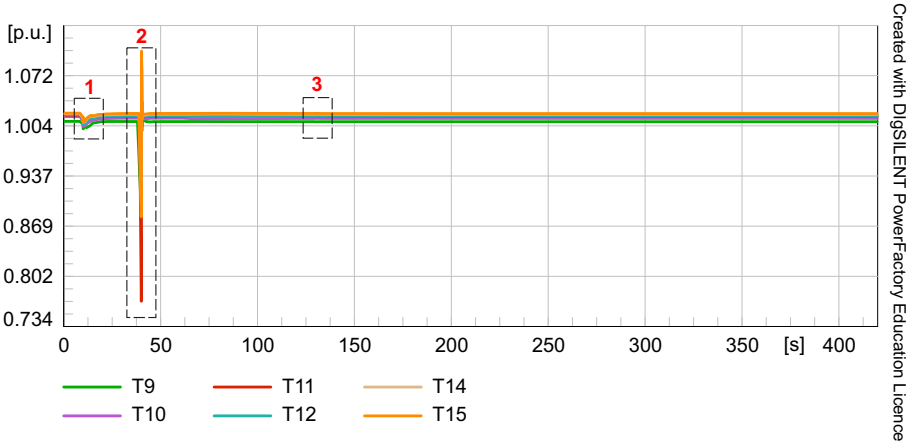

(a) Overall voltage profile in zone 4. Highlighted windows 1–3 correspond to the events below.

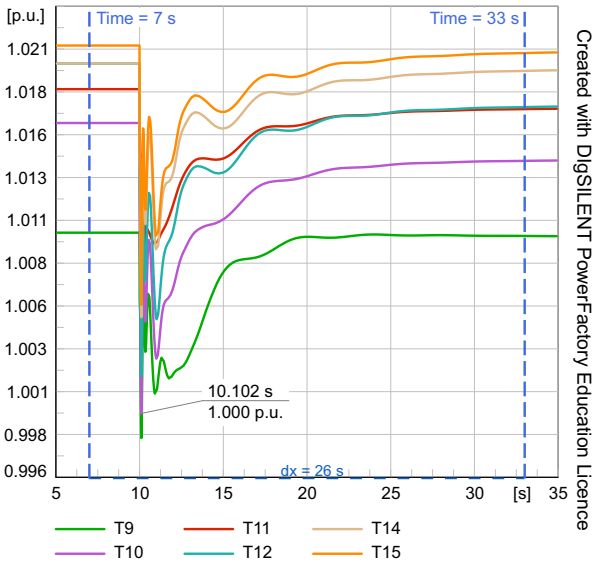

(b) Event 1: $G5_3$ outage

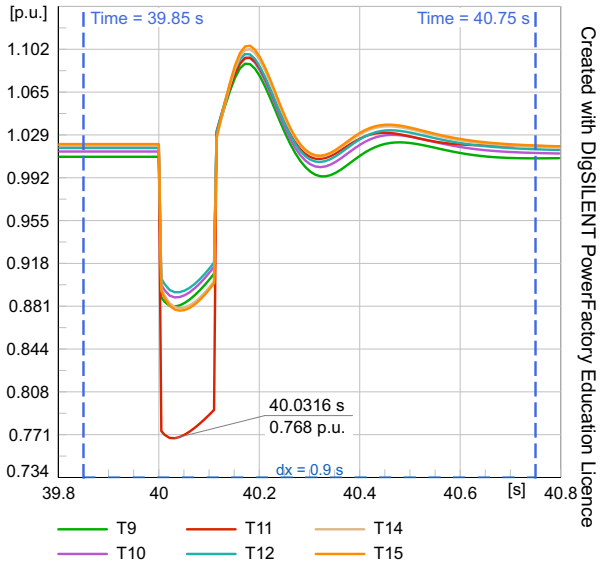

(c) Event 2: $L7_1$ short-circuit and clearance

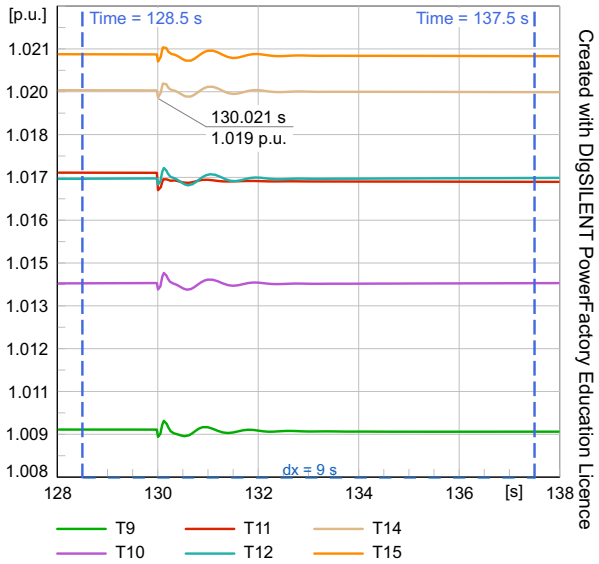

(d) Event 3: $L2_4$ switching

Figure D.11. Voltage response in zone 3 under the second-worst contingency state at off-peak condition for the M6 solution. Own work.

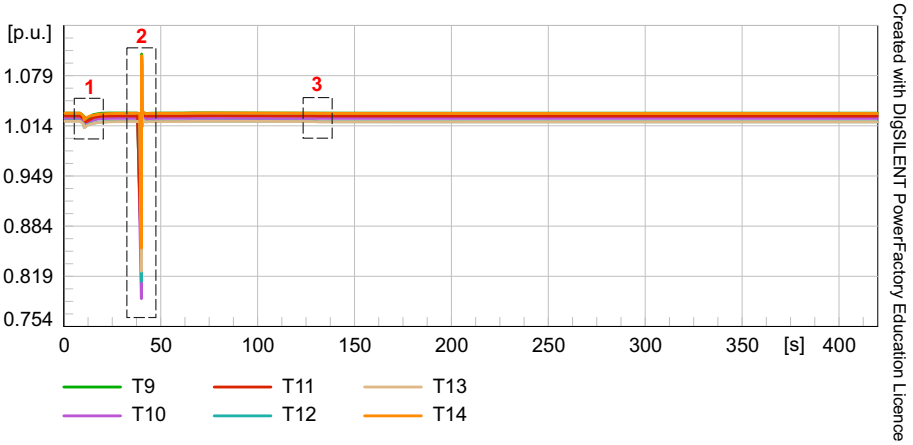

(a) Overall voltage profile in zone 4. Highlighted windows 1–3 correspond to the events below.

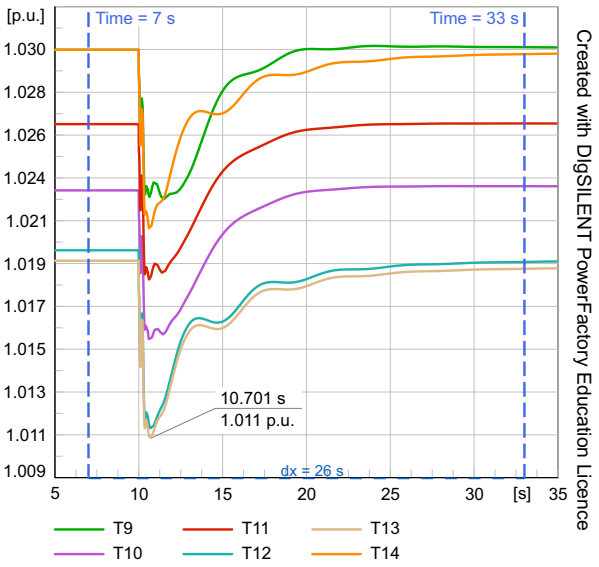

(b) Event 1: $G5_3$ outage

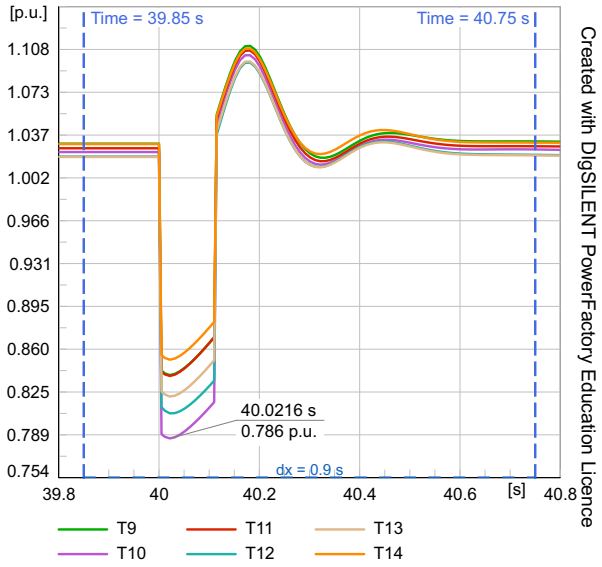

(c) Event 2: $L7_1$ short-circuit and clearance

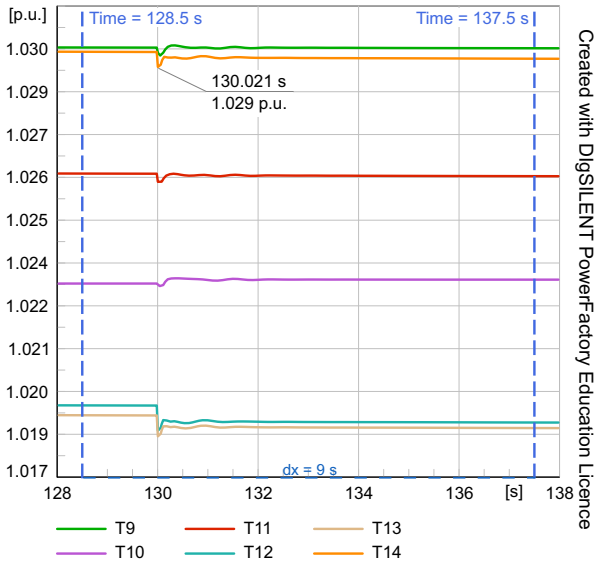

(d) Event 3: $L2_4$ switching

Figure D.12. Voltage response in zone 4 under the second-worst contingency state at off-peak condition for the M6 solution. Own work.